The work presented in this thesis was performed in the Life and Health Sciences Research Institute (ICVS), Minho University. Financial support was provided by FEDER funds through the Operational Programme Competitiveness Factors - COMPETE and National Funds through FCT - Foundation for Science and Technology under the project POCI-01-0145-FEDER-007038; and by the project NORTE-01-0145-FEDER000013, supported by Norte Portugal Regional Operational Programme (NORTE 2020), under the PORTUGAL 2020 Partnership Agreement, through the European Regional Development Fund (ERDF).

Ana Catarina Mesquita Azevedo **Influence of HOXA9 in the response of glioblastoma to immune checkpoint inhibitors** UMinho | 2019

Universidade do Minho
Escola de Medicina

Ana Catarina Mesquita Azevedo

Influence of HOXA9 in the response of glioblastoma to immune checkpoint inhibitors

setembro de 2019

Universidade do Minho
Escola de Medicina

Ana Catarina Mesquita Azevedo

Influence of HOXA9 in the response of glioblastoma to immune checkpoint inhibitors

Dissertação de Mestrado
Mestrado em Ciências da Saúde

Trabalho efetuado sob a orientação do
Doutor Bruno Marques Costa
e da
Doutora Cláudia Nóbrega

setembro de 2019

Acknowledgements

Começo por agradecer aos meus orientadores: Bruno Costa e Cláudia Nóbrega. Ao Bruno por me ter aceitado neste projeto, pela partilha de conhecimento e pelos momentos de aprendizagem. À Cláudia, por todo o apoio, ensinamentos, confiança e motivação.

À Céline e à Eduarda por todas as sugestões e ajuda para desenvolver o trabalho aqui apresentado. À Marta, que mesmo longe, sempre me apoiou e me ajudou a aumentar a minha capacidade de trabalho. Ao João, por ter dado literalmente o sangue e suor para me ajudar neste projeto; obrigada por todo o apoio e amparo.

Quero deixar também o meu agradecimento ao Agostinho Carvalho e à Cristina Cunha, assim como ao Cláudio, Samuel e Cláudia, por se prontificarem sempre para nos ajudar.

À Sónia, à Nathalia, à Carol e à Catarina pela boa disposição no laboratório e por toda a ajuda. A todos os SSRDs, NERDs e PopHealth por toda a partilha de conhecimento e ajuda sempre prestada.

À Andreia, Bruna, Joana, Marta, Sofia e Nuno: por todos os desabafos, pelo apoio, pela amizade, pela força e confiança depositada. Obrigada pela partilha dos piores e melhores momentos de sempre. Foram essenciais.

Às meninas: Ana, Anabela, Isabel e Marisa, obrigada pelas conversas, pelas alturas em que me obrigam a sair do "buraco" e por estarem sempre presentes. Obrigada pela vossa amizade.

Ao Hélder, por me fazer feliz. Por ter estado presente nos melhores e piores momentos. Por me ajudar a ultrapassar todos os obstáculos e me motivar a cada dia. Pela paciência e por me ouvir neste percurso, o que por vezes não foi fácil. Obrigada pelo carinho, incentivo, apoio, conversas e amor.

À minha família, por ser a melhor família de sempre. Aos meus pais pelo apoio e amor incondicional, por estarem sempre presentes e por me ampararem nos momentos menos bons e rirem comigo nos bons. Pela paciência, pelo incentivo e pelos sacrifícios que fizeram por mim. Por me ajudarem a crescer e fazerem de mim o que sou hoje. Devo-vos tudo. Ao meu irmão pelo apoio, paciência e por me acompanhar sempre.

Para a Paulinha, pela esperança...

STATEMENT OF INTEGRITY

I hereby declare having conducted this academic work with integrity. I confirm that I have not used plagiarism or any form of undue use of information or falsification of results along the process leading to its elaboration.

I further declare that I have fully acknowledged the Code of Ethical Conduct of the University of Minho.

Influence of HOXA9 in the response of glioblastoma to Immune Checkpoint Inhibitors

Glioblastoma (GBM) is the most common and malignant primary central nervous system (CNS) tumour in adults, characterized by high resistance to conventional therapies and a very poor outcome, with a median survival of 15 months. GBM is a highly immunosuppressive tumour, with mechanisms to promote tumour escape from the immune system. Its microenvironment is characterized by the presence of cytokines that inhibit the immune system by suppressing T-cell activation and proliferation, and skewing the immune cells towards a pro-tumour phenotype. Additionally, GBM cells frequently overexpress programmed cell death ligand 1 (PD-L1), an immune checkpoint ligand that binds to programmed cell death 1 (PD1) present in activated T-cells. Recently, immunotherapies using immune checkpoint inhibitors (ICIs) have gained importance by showing promising results in treatment of various cancers. Previous studies showed that HOXA9, a critical transcription factor deregulated in gliomas, is critical in resistance to standard chemotherapy, and global aggressiveness of GBM. Moreover, HOXA9 down-regulates mechanisms related to antigen processing and presentation, and to immune responses. This project aims to decipher the relevance of HOXA9 in the immune evasion in GBM, both in treatment-naïve conditions and under ICIs therapy. For this, *HOXA9* over-expression and silencing models of human GBM cell lines were used, to understand whether *HOXA9* expression modulates the expression of cytokines and of immune checkpoint ligands, and how it influences T-cell responses in the presence or absence of ICIs. Results with human GBM cell lines suggest that expression of *HOXA9* is associated with differential expression of immune related cytokines: namely inversely associates with *IL1B* expression; and with *IL8* expression in GL18 cell line; and also associated with *CCL2* expression in U251 cell line. At protein level, the silencing of HOXA9 leads to a decrease in PD-L1 expression and to an increase in the PD-L2 expression in the membrane of U251 cells. Moreover, a minor but significant increased sensitivity to anti-PD1 therapy is observed in U251 cells, but not in the other cell lines (U87 and U251). Regarding T-cell survival and subpopulations, namely Tregs, no significant differences were obtained. Overall, this work suggests that HOXA9 might increase immunosuppression in GBM, and that a partially effective immune response against GBM cell lines seems to exist. To further complement and clarify these results, it is essential to evaluate the secretion of these cytokines and chemokine; and to extend this study, *in vivo* GBM models could clarify the roles of HOXA9 in immune cells infiltration and in survival of mice in treatment-naïve conditions or upon treatment with ICIs.

Key words: Glioblastoma; HOXA9; Immunosuppression; Immune Checkpoint Inhibitors

Influência do HOXA9 na resposta do glioblastoma a Inibidores de "Checkpoints" Imunes

O glioblastoma (GBM) é o tumor primário mais comum e maligno do sistema nervoso central em adultos, caracterizando-se por uma elevada resistência às terapias convencionais e por um mau prognóstico, com uma sobrevivência mediana de 15 meses. O GBM é muito imunossupressor, com mecanismos para promover a evasão do sistema imunitário. O seu microambiente tumoral é caracterizado pela presença de citocinas que inibem o sistema imunitário, suprimindo a ativação e proliferação das células T e alterando as células imunes para um fenótipo pro-tumoral. Adicionalmente, as células de GBM sobre-expressam frequentemente o "programmed cell death ligand 1" (PD-L1), que se liga ao "programmed cell death 1" (PD1) presente nas células T. Recentemente, imunoterapias que usam inibidores de "checkpoints" imunes (ICIs) ganharam extrema importância, pois mostraram resultados promissores no tratamento de vários cancros. Estudos prévios mostram que o HOXA9, um crítico fator de transcrição desregulado em gliomas, é muito importante na resistência à terapia convencional e na agressividade global do GBM, regulando, ainda, negativamente mecanismos relacionados com o processamento e apresentação de antigénios e com respostas imunes. Este projeto tem como objetivo compreender a importância do HOXA9 na evasão do sistema imunitário no GBM, com e sem ICIs. Para tal, foram usados modelos de sobre-expressão e de silenciamento do *HOXA9* de linhas celulares de GBM humanas para perceber se a expressão do *HOXA9* modula a expressão de citocinas e de ligandos de "checkpoints" imunes e qual a sua influência na resposta das células T, com ou sem ICIs. Os resultados com as linhas celulares de GBM humanas sugerem que a expressão do *HOXA9* está associada a uma diferente expressão de citocinas relacionadas com o sistema imunitário. Assim, está inversamente associada à expressão de *IL1B* e de *IL8* na linha celular GL18 e diretamente associada à expressão de *CCL2* na linha celular U251. A nível proteico, o silenciamento do *HOXA9* leva à diminuição da expressão de PD-L1 e ao aumento da expressão de PD-L2 na membrana das células U251. Além disso, foi observado um pequeno, mas significativo, aumento da sensibilidade à terapia com anti-PD1 nas células U251, mas estes efeitos não foram observados nas linhas celulares U87 e GL18. Em relação à sobrevivência e subpopulações de células T, nomeadamente Tregs, não foram obtidas diferenças significativas. No geral, estes resultados sugerem que o HOXA9 pode aumentar a imunossupressão no GBM e que parece existir uma resposta imune parcial contra as linhas celulares de GBM. Para complementar e clarificar estes resultados, é essencial avaliar a secreção destas citocinas e da quimiocina. Os modelos *in vivo* podem clarificar o papel do HOXA9 na infiltração de células imunes e na sobrevivência dos ratinhos, com e sem ICIs.

Palavras chave: Glioblastoma; HOXA9; Imunossupressão; Inibidores de "Checkpoints" imunes

Table of contents

1. Introduction 1

1.1 An overview of cancer 1

1.2 Gliomas: classification and clinical significance 2

1.2.1 Glioblastoma: pathophysiology and clinical features 4

1.2.1.1 Classification and epidemiology of glioblastoma 4

1.2.1.2 Etiology of glioblastoma 5

1.2.1.3 Current therapies in glioblastoma 5

1.2.1.4 The HOXA9 gene 5

1.3 Immune surveillance and immune evasion in cancer 6

1.3.1 Immune-based anti-tumour therapies 12

1.4 Immune evasion in glioblastoma 13

1.4.1 Cytokines and chemokines in glioblastoma 15

1.4.2 Immune checkpoint inhibitors in glioblastoma 16

2. Objectives 17

3. Materials and Methods 18

3.1 Cell lines and culture conditions 18

3.2 Gene expression analysis 18

3.2.1 RNA extraction 18

3.2.2 Complementary DNA synthesis 19

3.2.3 Reverse transcriptase - quantitative polymerase chain reaction (RT-qPCR) 19

3.3 Flow cytometry stain and analysis 20

3.3.1 Surface staining 20

3.3.2 Intracellular staining 20

3.3.3 Annexin V/Propidium Iodide staining 21

3.3.4 Data acquisition and analysis 21

3.4 Co-cultures of tumour cells and activated T-cells 21

3.4.1 Activation and expansion of human peripheral blood mononuclear cells (hPBMCs) 21

3.4.2 Co-culture of human tumour cells with activated T-cells 22

3.4.3 Activation and expansion of mouse T-cells 22

3.4.4 Co-culture of mouse tumour cells with activated T-cells 23

3.5 HOXA9 silencing in mouse GBM cell line 23
3.6 Statistical analysis 23
4. Results 25
4.1 Influence of HOXA9 on the expression of immune related factors in tumour cells 25
4.1.1 HOXA9 affects the expression of cytokines and chemokines in human GBM cell lines 25
4.1.2 HOXA9 influences the expression of immune checkpoint ligands in tumour cells 28
4.2 Impact of HOXA9 in the sensitivity of glioblastoma cell lines to T-cell mediated cytotoxicity 32
4.3 Impact of HOXA9 in the sensitivity of glioblastoma cell lines to immune checkpoint inhibitors 34
4.4 Influence of HOXA9 in T-cell survival, in the presence or absence of Immune Checkpoint Inhibitors. 36
4.5 Impact of HOXA9 expression by glioblastoma cells in the percentage of T-cell subpopulations, independently of Immune Checkpoint Inhibitors' presence 38
4.6 Studies of HOXA9 impact in glioblastoma immune evasion in a murine model – preliminary data ... 40
4.6.1 Silencing of HOXA9 in a murine GBM cell line 40
4.6.2 Optimization of mouse T-cell activation and expansion protocol 41
5. Discussion 47
6. Conclusions and Future Perspectives 54
7. References 55
8. Supplementary Figures 68
9. Supplementary Tables 74

List of Abbreviations

APC – Antigen presenting cell

ANOVA – Analysis of variance

BBB – Blood-brain barrier

BCL-2 – B-cell lymphoma 2

BSA – Bovine Serum Albumin

CCL2 – Chemokine C-C motif ligand 2

CD – Cluster of Differentiation

cDNA – Complementary DNA

CNS – Central nervous system

CTLA-4 – Cytotoxic T lymphocyte-associated antigen 4

DC – Dendritic cell

DMEM – Dulbecco's modified eagle medium

DNA – Deoxyribonucleic acid

EGFR – Epidermal growth factor receptor

FBS – Fetal bovine serum

FDA – Food and Drug Administration

FMO – Fluorescence Minus One

GBM – Glioblastoma

HLA-G – Major histocompatibility complex, class I, G

HOX – Homeobox

hPBMC – Human Peripheral Blood Mononuclear Cell

IDH1/2 – Isocitrate dehydrogenase 1/2

ICIs – Immune checkpoint inhibitors

IL – Interleukin

IFNγ – Interferon - gamma

LAG-3 – Lymphocyte activation gene 3

LN – Lymph nodes

MFI – Mean fluorescence intensity

MGMT – O-6-methylguanine-DNA methyltransferase

MHC – Major histocompatibility complexes

mLN – mouse lymph nodes

NK – Natural Killer

PBMC – Peripheral Blood Mononuclear Cell

PBS – Phosphate buffered saline

PD-1 – Programmed cell death 1

PDGFRA – Platelet-derived growth factor receptor A

PD-L1/2 – Programmed cell death ligand 1/2

PI3K – Phosphoinositide 3-kinase

PTEN – Phosphatase and Tensin homolog

P53 – Tumour protein p53

RNA – Ribonucleic acid

RPMI – Roswell Park Memorial Institute

RT-qPCR – Reverse transcription - quantitative polymerase chain reaction

shRNA – short hairpin Ribonucleic acid

TAM – Tumour associated macrophages

TBP – TATA-box binding protein

TCGA – The Cancer Genome Atlas

TCR – T-cell receptor

Teff – Effector T cell

TGF-β – Transforming Growth Factor- beta

TIL – Tumour infiltrating lymphocyte

TMZ – Temozolomide

TNFα – Tumour necrosis factor alpha

Tm – Melting temperature

TP53 – Tumour protein 53

Treg – T regulatory

WHO – World Health Organization

List of Figures

Figure 1 – Cancer hallmarks. 2

Figure 2 – Glia progenitors' cells and the subsequent classification of gliomas. 3

Figure 3 – Cancer immunity cycle. 9

Figure 4 – Cancer immune evasion. 10

Figure 5 – Mechanisms for tumours to escape immune surveillance. 11

Figure 6 – Immune checkpoint blockade. 12

Figure 7 – Different factors secreted by tumour cells induce immunosuppression in GBM microenvironment. . 14

Figure 8– Expression of immune related genes in human GBM cell lines with differential levels of HOXA9 expression. 27

Figure 9 – Expression of immune checkpoint ligand genes in human GBM cell lines with differential levels of HOXA9 expression. 29

Figure 10 – Protein expression of immune checkpoint ligands in human GBM cell lines. 32

Figure 11 – Activated T-cells induced death of GL18 and U251 GBM cell lines at a T:E ratio of 1:5. 33

Figure 12 – T-cell mediated cytotoxicity in tumour cells, in treatment naïve conditions or in the presence of ICIs. 35

Figure 13 – HOXA9 and ICIs impact on T-cell survival. 37

Figure 14 – Influence of HOXA9 expression in tumour cells, in T-cells subpopulations, in the presence or absence of ICIs. 39

Figure 15 – The murine GBM cell line GL261 was not silenced for Hoxa9, though was transfected. 41

Figure 16 – Percentage of cells recovered after the activation and expansion of mLN cells protocol with the different conditions tested. 43

Figure 17 – Assessment of the activation profile of mLN cells activated and expanded, in vitro. 45

Figure 18 – Pre-activated mLN cells induce dead in tumour cells. 46

Supplementary figure 1 – Microarray data, regarding immune-related genes validated by RT-qPCR: cytokines, chemokines and immune checkpoint ligands. 68

Supplementary figure 2 – *IFNG* is not detected in human GBM cell lines. 69

Supplementary figure 3 – *IL10* is not detected in human GBM cell lines. 70

Supplementary figure 4 – *PD1* is not detected in human GBM cell lines. 71

Supplementary figure 5 – Positive controls for staining with CD80 and CD86. 72

Supplementary figure 6 – Expression of CD45 in human GBM cell lines. 73

List of Tables

Supplementary Table 1 – Primers used for RT-qPCR, with the respective Tm and the length of the products. ... 74

Supplementary Table 2 – Antibodies panel for the molecular analysis by Flow Cytometry. 75

Supplementary Table 3 – Relative expression of *IL1B* in human GBM cell lines, obtained by RT-qPCR. 76

Supplementary Table 4 – Relative expression of *TNFA* in human GBM cell lines, obtained by RT-qPCR. 77

Supplementary Table 5 – Relative expression of *TGFB1* in human GBM cell lines, obtained by RT-qPCR. 78

Supplementary Table 6 – Relative expression of *IL8* in human GBM cell lines, obtained by RT-qPCR. 79

Supplementary Table 7 – Relative expression of *IL6* in human GBM cell lines, obtained by RT-qPCR. 80

Supplementary Table 8 – Relative expression of *CCL2* in human GBM cell lines, obtained by RT-qPCR. 81

Supplementary Table 9 – Relative expression of *CD86* in human GBM cell lines, obtained by RT-qPCR. 82

Supplementary Table 10 – Relative expression of *CD80* in human GBM cell lines, obtained by RT-qPCR. 83

Supplementary Table 11 – Relative expression of *PDL1* in human GBM cell lines, obtained by RT-qPCR. 84

Supplementary Table 12 – Mean fluorescence intensities (MFIs) of CD86 in the human GBM cell lines, obtained by flow cytometry..... 85

Supplementary Table 13 – MFIs of CD80 in the human GBM cell lines, obtained by flow cytometry..... 85

Supplementary Table 14 – MFIs of PDL1 in human GBM cell lines, obtained by flow cytometry..... 86

Supplementary Table 15 – MFIs of PDL2 in human GBM cell lines, obtained by flow cytometry..... 86

1. Introduction

1.1 An overview of cancer

Cancer incidence and mortality is rapidly increasing and is expected to become the leading cause of death in the world, still in this century. In 2018, it was estimated that 18.1 million new cancer cases appeared and that 9.6 million deaths occurred due to this malignancy, worldwide (1). Despite the advances in cancer knowledge and its therapies, it is expected that these numbers continue to increase, with the prevision of about 26 million new cancer cases and 17 million deaths per year, in 2030 (2). This is mainly because of the populations aging and growth, but also due to environmental factors, life-style habits, genetic predisposition and acquisition of random mutations (1,3–5).

Cancer is characterized by an uncontrolled and abnormal growth of cells and invasion of surrounding tissues (6). Most often, a single mutation is not sufficient for the development of cancer. It is considered to be not only one disease, but an amount of various and distinct neoplasias, arising from multiple genetic and epigenetic alterations in oncogenes, tumour-suppressing genes and microRNA genes (7). Cancer progression is driven by cumulative mutations and clonal expansion, leading to a heterogeneous population of tumour cells (7,8). These mutations occur in proto-oncogenes, inducing cell growth, division and survival, and in tumour-suppressor genes, impairing DNA repair and cell cycle checkpoints, leading to uncontrolled cellular growth (9). Cells carrying such alterations have survival advantages, in a way that results in increased and uncontrolled proliferation and in a loss of cooperation (8).

Tumour cells acquire some capabilities, through a multistep process, to sustain their growth, proliferation and metastatic dissemination (7,10). These capabilities were summarized and called hallmarks of cancer, that involve: (i) sustained proliferative signalling; (ii) resistance to cell death; (iii) induced angiogenesis; (iv) enabling replicative immortality; (v) activated invasion and metastasis (vi) evading growth suppressors; (vii) induced genome instability and mutation; (viii) development of tumour-promoting inflammation; (ix) deregulated cellular energetics and (x) evasion to immune destruction (Figure 1) (10).

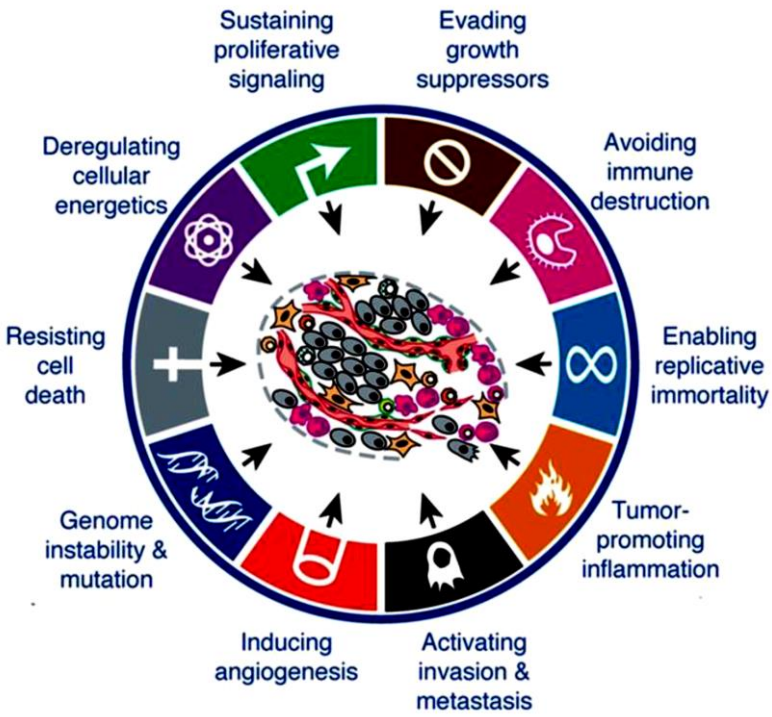

Figure 1 – Cancer hallmarks. The six hallmark and the four emerging hallmark capabilities that cancer cells acquire during tumour formation. Adapted from Hanahan and Weinberg, 2011 [8]

Since tumour cells rely on oncogenes for growth and survival, the identification of oncogenes involved in tumour initiation and progression provide new targets for therapies against cancer. However, as tumours arise from a sequential acquisition of mutations, different mutations will exist among tumour cells within a tumour and therefore, malignant cells will respond in distinct ways to a specific targeted therapy (7). Regarding this, new therapies are needed to face this problem.

1.2 Gliomas: classification and clinical significance

Malignant gliomas are the most common primary central nervous system (CNS) tumours in adults, accounting for approximately 75% of the primary malignant brain tumours (11,12). These cancers are most common to appear in the cerebral hemispheres and exhibit high invasion capacity within brain and destruction of normal brain tissues, leading to dead (13). The cell of origin of gliomas is still unknown, however there are two main hypotheses (Figure 2). One proposes that these tumours arise from mature glial cells that have the ability to became less differentiated and give arise to the tumour. The other suggests that this malignancy arrives from a less differentiated precursor (neural stem cell, astrocyte precursor or oligodendrocyte precursor) (11,14).

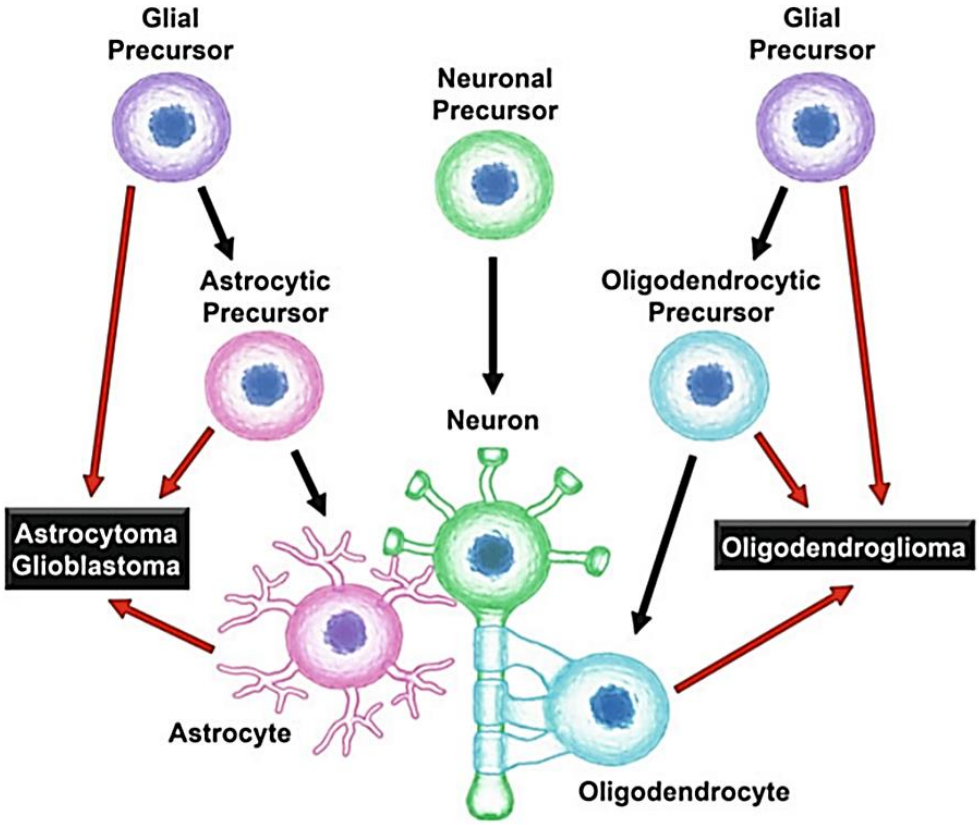

Figure 2 – Glia progenitors' cells and the subsequent classification of gliomas. Represented the glial progenitors' cells, the differentiated cells and the classification of gliomas. Adapted from Backos D., 2014 (15).

According to the World Health Organization (WHO) classification of 2016, gliomas are divided based on histological features taking into account the presumed cell of origin and the levels of differentiation, on their location and on molecular features, into 3 subtypes (16). Thus, histologically, gliomas are divided into astrocytomas, oligoastrocytomas, oligodendrogliomas, based on their similarity to the glial cells (17). Based on tumour malignancy, WHO also divides tumours in grades (grade I to IV), being grade I the ones associated to better prognosis and with slowest tumour growth and grade IV the most malignant with the worst prognosis (17,18). Astrocytomas are the most common type (75% of all gliomas) and can be further divided according to its grade into: grade I (pilocytic astrocytomas), grade II (diffuse astrocytomas, low grade), grade III (anaplastic astrocytomas) and the most common, grade IV (glioblastoma, GBM) (19,20). Moreover, since 2016, isocitrate dehydrogenase 1/2 (*IDH1/2)* mutational status, the co-deletion of the short arm of chromosome 1 and long arm of chromosome 19 (1p/19q) and other genetic parameters have been used to classify gliomas (17).

1.2.1 Glioblastoma: pathophysiology and clinical features

GBM, the most common, aggressive and malignant glioma, is characterized by uncontrolled cell proliferation, diffuse infiltration, necrosis, strong angiogenesis, high resistance to apoptosis and genomic instability (13,21).

GBMs have a hugely deregulated tumour genome, with amplification in oncogenes and deletion in tumour suppressor genes involved in several interconnected signalling pathways (22,23). The main signalling pathways deregulated in GBM are: i) p53 signalling pathway, implicated in processes such cell cycle arrest, cell death, cell differentiation, senescence, DNA repair and neovascularization; ii) tumour suppressor retinoblastoma (pRB) signalling pathway, also involved in cell cycle progression processes; iii) PI3K-PTEN-Akt-mTOR signalling pathway, involved in cellular proliferation, growth, apoptosis and cytoskeletal rearrangement; iv) and RAS/MAPK signalling pathway, related with apoptosis and cell transformation processes (22,24).

Additionally, other genes are frequently found mutated in GBM, namely: i) loss of tumour suppressor phosphatase and tensin homolog (PTEN); ii) activation of epidermal growth factor receptor (EGFR) and; iii) inactivation of platelet-derived growth factor receptor A (PDGFRA) (21,22,25). Moreover, O-6-methylguanine-DNA methyltransferase (*MGMT*) gene methylation status is being considered in treatment decisions, as a predictive biomarker for temozolomide (TMZ) (21).

1.2.1.1 Classification and epidemiology of glioblastoma

Regarding the 2016 WHO new classification of gliomas, GBM are now classified as Glioblastoma, *IDH*-mutant or Glioblastoma, *IDH*-wildtype (WT). The first one represents about 10% of the cases and corresponds normally to secondary GBM (the ones that arise from a lower-grade glioma previously diagnosed) with incidence mostly in younger patients. The *IDH*-WT is the most frequent (about 90% of the cases) and is called *de novo* or primary GBM, and predominates in older patients (17). When evaluation of the *IDH* gene cannot be performed, the tumour is classified as Glioblastoma, NOS (not otherwise specified) (17). Although they may occur at any age, GBM affects mostly people with 50 to 70 years-old (22).

Proposed by Verhaak *et al.*, using The Cancer Genome Atlas (TCGA), GBM are also divided based on molecular features into neural, proneural, classical and mesenchymal subtypes, although this classification is not used in diagnosis (21,25). In this way, the neural subtype is characterized by the

expression of neuron markers such as NEFL, GABRA1, SYT1 and SLC12A5; proneural subtype is distinguished by alterations/mutations on *PDGFRA* and *IDH1*, as well as in TP53; the classical subtype main feature is the high expression of EGFR and the lack of TP53 mutations, but also the amplification of chromosome 7 and the deletion of chromosome 10; and the mesenchymal subtype is associated with mutations in NF1 and PTEN and also with expression of MET that causes epithelial-to-mesenchymal transition (25).

1.2.1.2 Etiology of glioblastoma

The etiology of GBM is mostly unknown, being the only established risk factor the exposure to ionizing radiation (26). Studies associating head injuries, foods containing N-nitroso compounds, calcium or antioxidants, tobacco smoking, alcohol consumption and exposure to electromagnetic fields with development of GBM are inconclusive, though association with genetic syndromes (*e.g.* neurofibromatosis types 1 and 2, Li-Fraumeni syndrome and Turcot's syndrome) are reported (26,27). Knowing the risk factors underlying the development of this diseases might have an impact in the prevention and in patient's prognosis.

1.2.1.3 Current therapies in glioblastoma

Nowadays, the standard-of-care treatment for GBM patients consists in a multimodal approach, with surgical resection of the tumour (typically incomplete since GBM is a highly infiltrating tumour), followed by radiotherapy with concomitant and adjuvant chemotherapy, with temozolomide (TMZ), an alkylating agent (28–30). Besides such efforts, patient's overall survival is still very poor (median of approximately 15 months) (22). GBM presents a high heterogeneity and proliferation and high resistance to the conventional therapies, adding to the difficulty of drugs to cross the blood brain barrier (BBB) and the likelihood of damaging permanently the brain; for all this, it is very difficult to achieve an effective therapy to improve the quality of life and the overall survival of GBM patients (29).

1.2.1.4 The HOXA9 gene

Homeobox (HOX) genes are a family of homeodomain containing transcription factors that play a critical role during embryonic development (31,32). There are thirty-nine mammalian HOX genes grouped in four paralogous clusters (HOXA, HOXB, HOXC and HOXD) in different chromosomes (31,33). During

development, HOX genes follow both temporal and spatial pattern of expression, specific for each body region (31,34).

Several HOX genes are aberrantly expressed in various tumours (35). In particularly, HOXA9 expression has been shown to be associated with more than 50% of acute myeloid leukemias and associated with a poor prognosis (31,36–38). HOXA9 was also reported to be involved in some solid tumours oncogenesis, like colon carcinoma, breast cancer, epithelial ovarian cancer, glioblastoma and non-muscle invasive bladder cancer (39–41).

In ovarian cancer, HOXA9 was described to promote an inflammatory microenvironment that leads to tumour growth and allows tumours to escape to immune destruction, through up-regulation of some cytokines as interleukin 6 (IL-6) (37,42,43). Furthermore, HOXA9 induces macrophages to acquire M2-like phenotype, promoting immunosuppression in its microenvironment (44).

In GBM, HOXA9 is activated through epigenetic modifications, regulated by the PI3K pathway (45). Interestingly, *HOXA9* expression promotes resistance to TMZ, the chemotherapeutic agent used in the clinics, and is able to promote malignant transformation in orthotopic mice models (46). HOXA9 is also associated with a shorter overall survival, both in mice and in patients (45–47). Moreover, in GBM, HOXA9 was identified to have a role in cancer-related pathways, for example in cell proliferation, in DNA repair and in stem cell maintenance (46). HOXA9 also promotes cell viability, invasion and proliferation, increases stemness capacity and decreases apoptosis, establishing HOXA9 as an important oncogene in the GBM aggressiveness (45,46).

Interestingly, HOXA9 down-regulates genes involved in immune related pathways in GBM (e.g. immune response, inflammatory response and antigen processing and presentation) (46). HOXA9 is also able to increase the expression of PD-L1 in some GBM cell lines (46). Increasing evidences suggest that activation of some oncogenic pathways is associated with a non-responsive tumour microenvironment and with resistance to immunotherapies (48–50). Thus, HOXA9 is a candidate to be a predictive biomarker of the response to immunotherapies in GBM.

1.3 Immune surveillance and immune evasion in cancer

The idea that the immune system can have a role in cancer development and progression started early, in the 1950s, when Burnet and Thomas built their cancer immunosurveillance hypothesis (51–54). They postulated that the adaptive immunity act to recognize and eliminate tumour cells (51,54,55). In the next

years, numerous studies have established that immunodeficient mice are more susceptible to develop carcinogen-induced tumours than immunocompetent mice (51). In 2001, a study revealed that tumours formed in mice which lack a fully immune system were more immunogenic (with highly immunoreactive clones) than the ones formed in mice with an intact immune system, suggesting that the immune system shapes tumour immunogenicity, besides having a protective function against tumours (51,56). This theory was demonstrated through the transplantation of tumours developed in immunodeficient into immunocompetent mice, in which only half of the mice develop progressive growing tumour, comparing to the mice transplanted with tumours developed in immunocompetent mice, in which all mice developed progressive growing tumours (51). The concept of immunoprotection against tumour cells and the shape of tumour immunogenicity set the basis to understand the cancer immunoediting hypothesis that establish a dual role of immune system in cancer development: host-protective and tumour-promoting (51,55). The cancer immunoediting hypothesis postulates three sequential phases: "elimination" in which innate and adaptive immune system work together to eradicate the tumour growth; "equilibrium" when tumour cells are in a state of dormancy, also in this phase the tumour cells are shaped by the immune system; and "escape" in which the immune system cannot control the tumour cells and promote the tumour grow (51).

In ideal conditions (Figure 3), tumour cells release neo-antigens that are captured by dendritic cells (DC), an antigen presenting cell (APC) that migrates to the LN (lymph nodes) to present the antigen to T-cells. T-cells are a population of lymphocytes and can be divided into two populations based on their expression of cell surface markers ($CD4^+$ T-cells and $CD8^+$ T-cells). $CD4^+$ T-cells, also called of helper T-cells, are responsible for providing help to other immune cells, through cell to cell interactions or the secretion of cytokines (57). $CD8^+$ T-cells when effectively primed, mature to cytotoxic T lymphocytes (CTLs), which are the effector cells to eliminate "damaged" cells (57). In order to prime and activate the T-cells to specific cancer antigens, two signals are needed: the binding MHC-antigen complex to T-cell receptor (TCR) and a co-stimulatory signal (binding of CD80 and CD86 molecules to CD28 molecule). These T-cells recognize, using its TCR, the antigens presented by DCs in the context of major histocompatibility complexes (MHC) I and II molecules (only APCs express both MHC-I and MHC-II; all the other cells express only MHC-I) (57,58). DCs express also co-stimulatory molecules (CD80 and CD86) that are necessary to prime and activate T-cells (53,58). Without a co-stimulatory signal, T-cells are not activated and get into a state of anergy, and an anti-tumour immune response is not mounted (53). Then, T-cells traffic from the LN to and infiltrate the tumour microenvironment (tumour infiltrating lymphocytes – TILs), recognizing the tumour cells and killing them (58). The death of tumour cells leads to the release of more tumour-

associated neo-antigens that increases the anti-tumour immune response and leads to the resumption of the cycle (58). Despite this well-oiled process, tumours do develop in face of an immune system as tumour cells have acquired several mechanisms to evade this anti-tumour immune response.

Genetic instability, tumour heterogeneity and immune selection contribute to tumour cells to acquire the ability to evade the immune system. Tumour cells have different strategies to avoid anti-tumour immune responses (Figure 4). On one hand, tumour cells hide from the immune system, by decreasing the expression of a series of molecules in its membrane. Meaning, to prevent recognition by the immune system, tumour cells downregulate or lose the expression of MHC molecules, co-stimulatory molecules (CD80 and CD86) and adhesion molecules (CD54) (59,60). On the other hand, tumour cells also can scape to immune destruction by becoming resistant to apoptosis and expressing inhibitory molecules to prevent T-cells function (59). Resistance to apoptosis can be achieved by three different mechanism: inhibition of granzyme B, inactivation of death receptors (FAS and TRAIL-R) and BCL-2 overexpression (61,62). To inhibit immune function, tumour cells express in their membranes programmed cell death ligand 1 and/or 2 (PDL1/PDL2), MHC II molecules, CD80/CD86 and HLA-G that bind respectively to programmed cell death 1 (PD1), lymphocyte activation gene 3 (LAG-3), cytotoxic T lymphocyte-associated antigen 4 (CTLA-4) and immunoglobulin-like transcripts (ILT) present in T-cells (59,63). By expressing CD47, cancer cells give a signal to prevent being phagocyted by macrophages (58,59). Also, tumours create an immunosuppressive microenvironment: i) by the secretion of immunosuppressive cytokines [such as interleukin 10 (IL10) and transforming growth factor-beta (TGFβ)]; ii) by inducing immunosuppressive cells like T regulatory (Treg) cells (characterized by $CD4^{+}$, $CD25^{high}$, $CD127^{low}$ and $FOXP3^{+}$), M2-like macrophages and myeloid-derived suppressor cells (MDSC) and; iii) by inducing an exhausted phenotype in effector cells (58,59,64,65). Treg cells are responsible for maintaining self-tolerance and immune homeostasis and can supress anti-cancer immunity through CTLA-4, consumption of interleukin 2 (IL2) and production of immune inhibitory cytokines and molecules (66). They infiltrate the tumour microenvironment by chemotaxis: tumour cells and TAMs produce for example chemokine C-C motif ligand 2 (CCL2) that recruits Treg cells into tumour tissues (67). In several cancer types, high infiltration of Treg cells is associated with a poor prognosis, since they promote tumour progression (66,68,69).

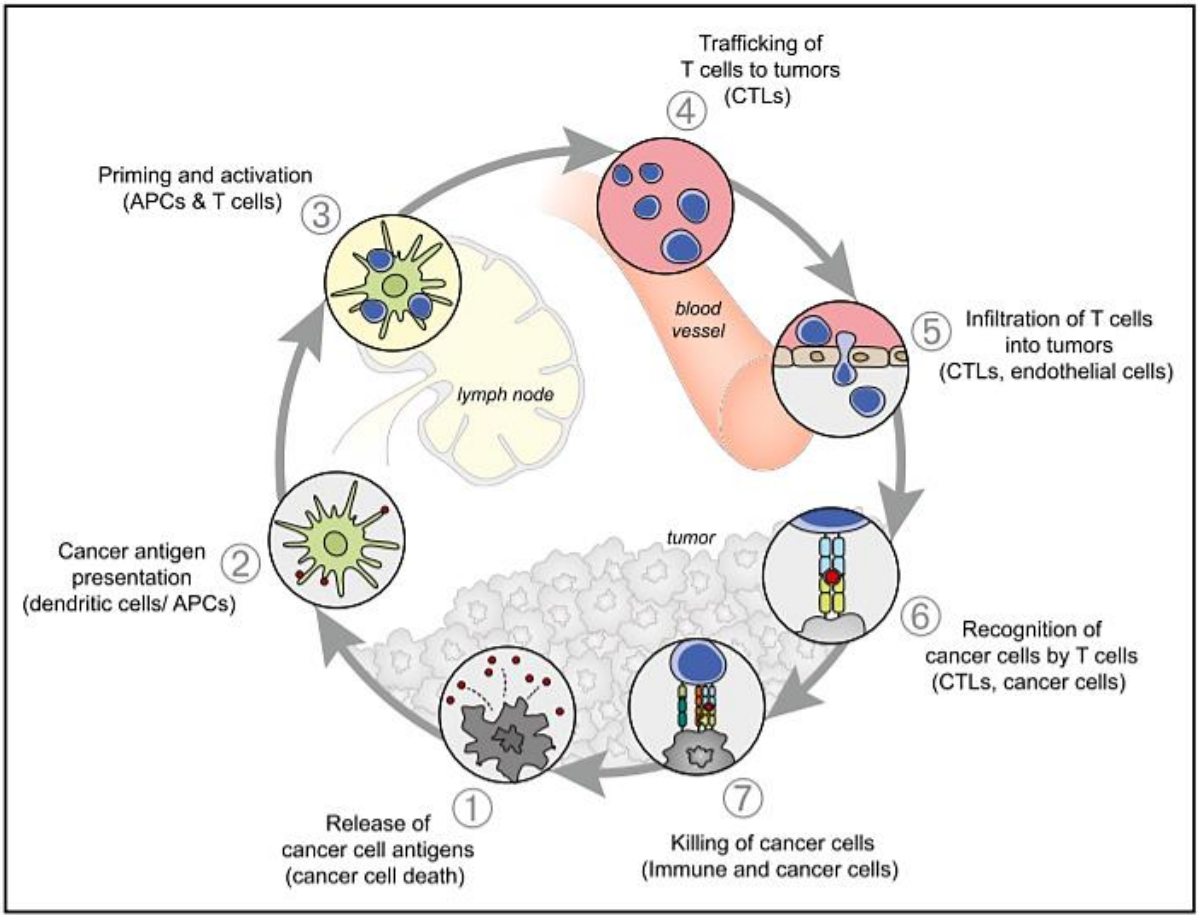

Figure 3 – Cancer immunity cycle. This cycle is divided in seven major steps, that starts with the release of antigens by the tumour cells (1), followed by the presentation of these antigens to T-cells by APCs (2), that results in T-cell priming and activation in the LN (3). Then, T-cells traffic to tumour site (4) and infiltrate into the tumour microenvironment (5). There, tumour cells are recognized (6) and killed by T-cells (7). This is a cyclic process that leads to the generation of amplified responses, by the release of neo-antigens by the tumour death cell (1) and ultimately to immunity to cancer, in ideal conditions. From Chen *et al.*, 2013 (58).

The immune system has mechanisms to control the immune response to maintain immune homeostasis, relying on immune checkpoint proteins to control the function of immune cells. These immune checkpoint proteins present in the surface of T-cells [CTLA-4, PD-1, T-cell immunoglobulin and mucin domain containing protein 3 (Tim-3), LAG-3] are responsible for the regulation of T-cell activation and promote immune tolerance (70). As CTLA-4 and PD-1/PD-L1 axis are two big regulators of the immune response (co-inhibitory molecules) and trigger immunosuppressive responses, their role in cancer is vital. So, understanding their mechanism of action and their function allows to comprehend their roles in cancer and the purpose for an anti-CTLA-4 and an anti-PD-1/anti-PD-L1 therapies.

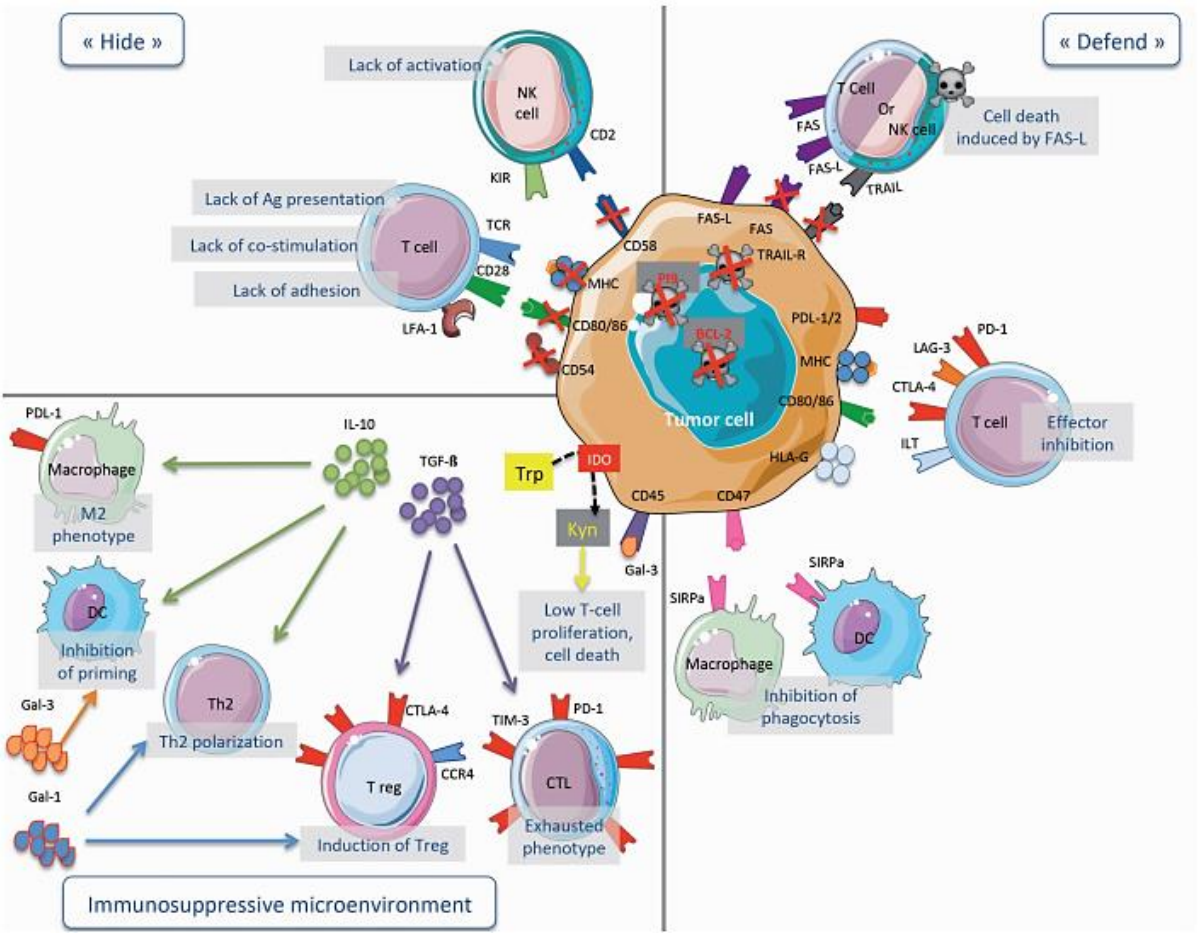

Figure 4 – Cancer immune evasion. Tumour cells have acquired several mechanisms to hide and defend themselves from the immune system and to generate an immunosuppressive microenvironment in order to evade the immune response. Tumour cells hide from the immune system by inducing the down-regulation of MHC molecules (*i.e.* leading to limited antigen presentation), of co-stimulatory molecules (*e.g.* CD80 and CD86) and of adhesion molecules (*e.g.* CD54). Also, tumour cells develop mechanisms to defend themselves from immune surveillance by resisting to immune cells-induced apoptosis (*e.g.* upon down-regulation of FAS and TRAIL receptors), by promoting T-cell inhibition (*e.g.* upon expression of inhibitory molecules such as PD-L1, PD-L2, CD80, CD86, HLA-G in tumour cells that bind to immune checkpoint proteins present in T-cells), and by inhibiting macrophage's phagocytosis (*e.g.* up-regulation of CD47). Moreover, tumour cells interact with their microenvironment to make it immunosuppressive, by secreting immunosuppressive factors (*e.g.* IL-10 and TGF-β) that inhibit the immune system and promote an exhausted phenotype of CTL, polarization of macrophages into M2 phenotype and recruitment of Treg cells. From M. de Charette, 2018 (59).

CTLA-4 is involved in early stages of T-cells activation and regulates their response (71). During T cell priming, co-stimulatory signals are needed through the interaction of CD28, present on T-cell surface, with CD80 or CD86, present in APC's. This interaction drives TCR signal amplification and T-cell activation (72,73). This co-stimulatory signal leads to the expression of CTLA-4 on T-cells membrane, which has a higher affinity towards CD80 and CD86 than CD28, leading to the inhibition the activation signal, and regulation of T cell activation (74). It has also been described that CTLA-4 signalling inhibits $CD4^+$ T-cells

and enhances the function of Treg cells (75). CTLA-4 is overexpressed on activated $CD4^+$ T-cells and $CD8^+$ T-cells in tumour microenvironment and can supress T-cell activation by interrupting the co-stimulatory signal (76,77).

In the same way, PD-1/PD-L1 axis regulates T-cell immune responses in peripheral tissues during inflammatory processes, mostly to avoid autoimmune diseases (71). PD-1 is present on activated T-cells, B-cells and natural killer (NK) cells, and modulates TCR signalling. It has two ligands (PD-L1 and PD-L2) that are expressed on APC's surface, but can also be expressed on tumour cells' membrane (77,78). PD-L1 supresses the function and proliferation of CTLs and promotes Treg cells activity by binding to its ligand (PD-1), and decreases the production of some immunostimulatory cytokines, for example interferon gamma (IFNγ) (76,79,80). PD-1/PD-L1 axis is a mechanism for tumours to escape immune surveillance by inducing T-cell disfunction and preventing an effective anti-tumoral immune response (Figure 5) (81). In addition, this mechanism can also stimulate IL10 production in peripheral T-cells, suppress DCs and induce Treg cells differentiation (82). T-cell disfunction is achieved by inducing T-cell anergy, exhaustion and apoptosis (81,82).

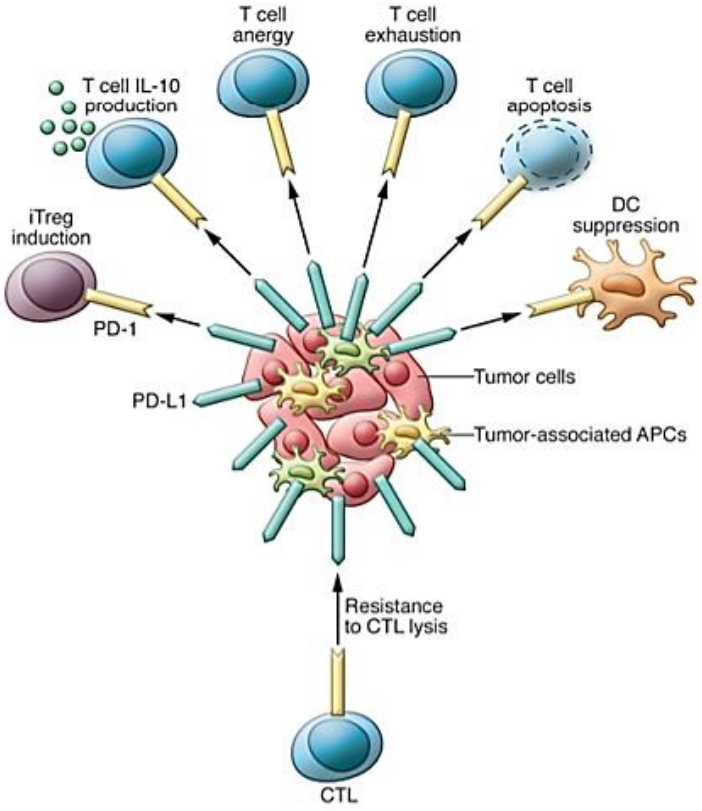

Figure 5 – Mechanisms for tumours to escape immune surveillance. Tumour cells can express high levels of PD-L1 in its membrane, which leads to several mechanisms to evade immune response: induction of Treg cells, induction of T-cells to produce IL10, T-cell anergy, T-cell exhaustion, T-cell apoptosis, DC suppression and resistant to CTL activity. From Chen *et al.*, 2015 (82).

1.3.1 Immune-based anti-tumour therapies

For a long time, the strategy for cancer treatment relied solely on surgery and on radio- and chemotherapy, with no significant benefits for patients (83,84). In recent years, therapeutic agents that modulate the immune system to induce or potentiate anti-tumoral responses have shown successful improvements in cancer treatment. Cancer immunotherapies include cytokine treatment (e.g. IFNγ and IL2), adoptive T-cell therapies and T-engineering (e.g. chimeric antigen receptor (CAR) T-cell therapy), cancer vaccines (e.g. dendritic cell therapy and preventive vaccines) and immune checkpoint blockade therapies (85).

Expression of the ligands for immune checkpoints by tumour cells lead to tumour immune escape. Thereby, these immune checkpoints and its ligands are attractive as targets for an immunotherapy (Figure 6) (85). As this therapy has successful results in pre-clinical and clinical studies, the US Food and Drug Administration (FDA) have approved a few Immune checkpoint inhibitors (ICIs) for the treatment of these malignancies (85). Nowadays, anti-CTLA-4, anti-PD1 and anti-PD-L1 are the ICIs with more clinical relevance. The FDA has approved the use of the following ICIs for treatment of cancer patients: ipilimumab (anti-CTLA-4) for the treatment of melanoma; pembrolizumab and nivolumab (anti-PD-1) for treatment of metastatic melanoma; nivolumab for treatment of previously treated, advanced or metastatic squamous lung cancer, small cell lung cancer and Hodgkin lymphoma; and atezolizumab (anti-PD-L1) for bladder cancer (86–89).

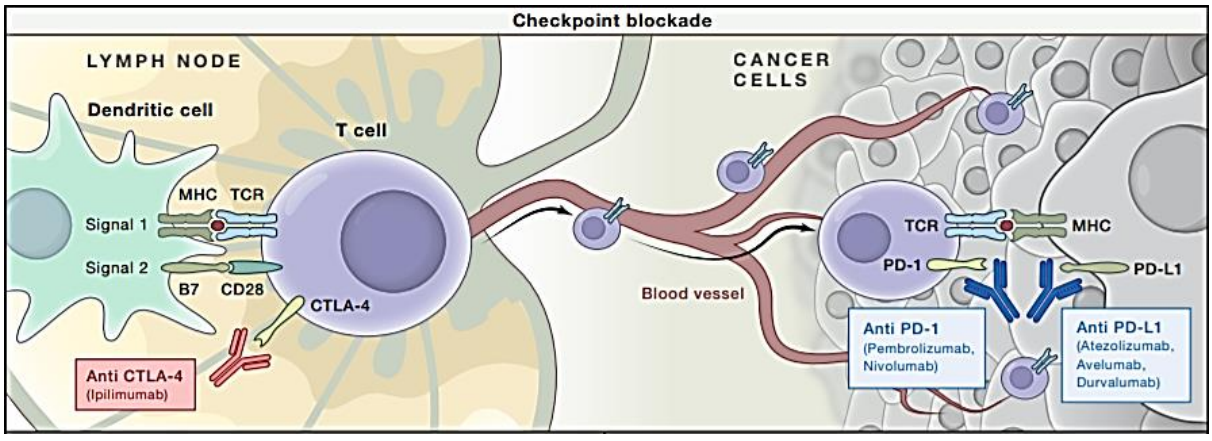

Figure 6 – Immune checkpoint blockade. Representation of the different immune checkpoint inhibitors and their acting site. Anti-CTLA-4 (ipilimumab) act in the LN during T-cell activation, to prevent the inhibition of T-cell activation by CTLA-4. On the other hand, anti-PD1 (pembrolizumab and nivolumab) and anti-PDL1 (atezolizumab, avelumab and durvalumab), act on tumour site to enhance the anti-tumour immune activity. From Abril-Rodriguez, 2017 (90).

1.4 Immune evasion in glioblastoma

Traditionally, the CNS was considered an "immune privileged" organ (91). The presence of an intact blood-brain barrier (BBB), the absence of a conventional lymphatic system (brain is drained by a classical lymphatic conduits within the meninges), the down-regulation of MHC molecules and the seldom infiltration of APCs and T-cells limit the immune responses in the brain (76,92). Nowadays, it is well established that the immune system interacts with the CNS, even more in the case of injury, inflammation and tumour, in which the BBB is somewhat disrupted and more permeable (76).

The immune system has an important role in killing/eliminating GBM cells through a series of steps that allow the recognition and elimination of GBM cells (58). However, GBM cells are able to avoid and take advantage of the immune system, as they can defend from its attack, promoting a pro-tumoral microenvironment (58).

GBM induces an immunosuppressive microenvironment that is characterized by the presence of immunosuppressive cytokines secreted by tumour cells, microglia, TAMs and Treg cells (92). Immunosuppressive factors (Figure 7) such as interleukin 6 (IL6), IL10, interleukin 1 (IL1), TGFβ, vascular endothelial growth factor (VEGF), prostaglandin-E and CCL2, secreted by tumour cells could inhibit the activity of effector cells (92–94). Globally, these factors inhibit both the innate and adaptive immune system, by suppressing NK activity, T-cell activation and proliferation, inducing T-cell apoptosis and promoting a M2 phenotype of TAMs (79,92). It is important to note that depending on the context, some of these factors can have a pro-inflammatory or an anti-inflammatory role (93).

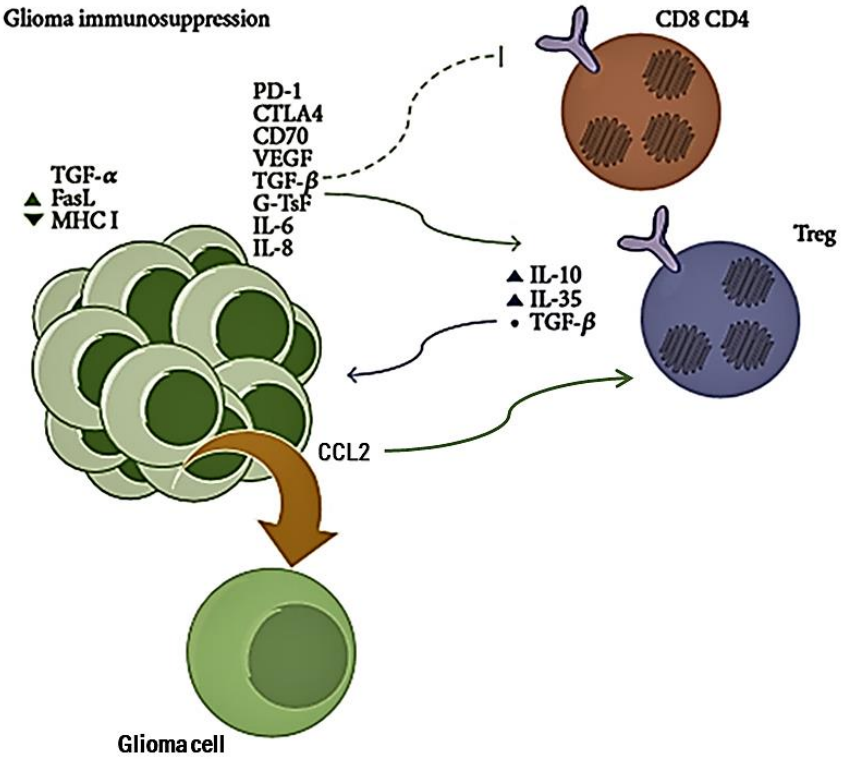

Figure 7 – Different factors secreted by tumour cells induce immunosuppression in GBM microenvironment. GBM cells (green) secrete molecules that recruit Treg cells (blue) and inhibit helper and cytotoxic T-cells (brown). These factors promote an immunosuppressive microenvironment in GBM. Adapted from Magaña-Maldonado *et al.*, 2016 (94)

Besides secreted immunosuppressive factors, the GBM microenvironment is also characterized by the presence of immunosuppressive cells, of which Treg cells (92). In fact, GBM patients are found to be highly immunosuppressed, with a decrease in $CD4^+$ T-cells and an increase in Treg cells, both systemically and in the tumour microenvironment (95). The presence of high numbers of Treg cells among TILs, adding to decreased numbers of $CD8^+$ T-cells (decrease Teff/Treg ratio) is associated with poor prognosis (67,96). CTLs are considered critical in anti-tumour immune response, but in the tumour microenvironment, they are frequently found with impaired effector functions and with an exhausted phenotype (97). Some of the factors secreted by GBM cells, like CCL2, can recruit Treg cells into the tumour microenvironment; these Treg cells secrete some cytokines as TGF-β and IL10 that downregulate other lymphocytic populations (Figure 7) (93,98,99). Treg cells express co-inhibitory molecules such as CTLA-4 and PD-1 and its expression is significantly higher in Tregs within the tumour microenvironment when compared with the ones from peripheral blood (64,92,100). Moreover, accumulation of TILs has been proposed to correlate with survival of GBM patients, and T-cells that express PD-1 are found in a significant proportion of glioma samples, which highlights the importance of T-cells in modulating the

GBM microenvironment (101–103). Globally, secretion of immunosuppressive factors and the recruitment of immunosuppressive cells, like Treg cells, seem to contribute to immune evasion of GBM cells (80,81).

Immune checkpoint molecules, like CTLA-4 and PD1, are also known to be implied in GBM immunosuppression. In fact, the majority of GBMs express PD-L1 and its correlated with increasing tumour grade and poor survival (79,92,101,104,105).

1.4.1 Cytokines and chemokines in glioblastoma

The release of cytokines and chemokines by tumour cells and also by immune cells are highly implied in GBM. Interleukin 1β (IL1β) and tumour necrosis factor α (TNFα), two inflammatory cytokines, play an essential role in inflammation driven tumour growth and progression and are found in large quantities in GBM (106,107). They can stimulate the expression of other inflammatory cytokines and promote tumour invasion, angiogenesis and survival (106). On the other side, they also can have anti-tumour effects, by mobilizing leukocytes (108). IFNγ is described to be up-regulated in GBM cells and for instance, up-regulates the expression of PDL1 in GBM cells. However, it has been associated with induction of adaptive immune response, and when secreted by $CD4^+$ T-cells, leads to decrease of GBM cells growth through the increase of antigen processing and presentation (108). TGFβ has an immunosuppressive role in cancer, in particularly it suppresses tumour-infiltrating T-cells activity and down-regulates MHC-II expression on $CD4^+$ T-cells. Also, TGFβ promotes migration, angiogenesis and growth of GBM (108). Interleukin 8 (IL8) is highly expressed in GBM cells and promotes angiogenesis and invasion and is considered to be highly immunosuppressive. Indeed, IL8 lead to immunosuppressive and pro-tumorigenic leukocyte infiltration into the tumour (108,109). IL10, other immunosuppressive (and anti-inflammatory) cytokine highly expressed in GBM, inhibit T-cell proliferation through downregulation of MCH-II molecules to enhance tumour progression. Other effects of IL10 include the suppression of $CD4^+$ T-cells responses and consequently the production of some cytokines, and the suppression of antigen presentation. Additionally, secretion of IL10 by microglia and macrophages leads to the inhibition of patient's immune responses and therefore to tumour progression; and secretion of IL10, together with TGFβ, by Treg cells, inhibit T-cells response, inducing anergy (94,108,110). Il6 has a dual effect in GBM, it can have a pro-tumoral or an anti-tumoral effect. Regarding the pro-tumoral effect, IL6 promotes tumour cell proliferation, survival, metastasis, angiogenesis and resistance to apoptosis and also helps to immune suppression. In what concerns the anti-tumoral effect, IL6 enhances T-cell proliferation and survival and increases $CD8^+$

T-cell trafficking to lymph nodes and tumours (108,111). CCL2 is a chemokine secreted by GBM cells and promotes Treg cells recruitment and migration into the tumour microenvironment (94).

1.4.2 Immune checkpoint inhibitors in glioblastoma

The remarkable success of immunotherapies in cancers, other than GBM, and the knowledge that the CNS interacts with the immune system provide a rational for the use of immunotherapies, namely of ICIs, in GBM (80). Preclinical *in vivo* mouse models using to study the effect of ICIs in the GBM treatment show that the combination of anti-PD1 and anti-CTLA4 induce long-term survivals, with a 75% of cure rate. Anti-CTLA4 as a monotherapy only show a cure rate of 25% and anti-PD1 monotherapy have 50% of survival. Moreover, they show that the success of anti-PD1 monotherapy rely on the dosage levels of the antibody, being the best result reported (50% of survival as previously referred) with a systemic administration of 8 cycles (500 ug per mouse first dose then subsequent 250ug per dose 3 days apart for the next 7 doses). This treatment is described also to increase the Teff/Treg ratio (112).

Currently, there are numerous ongoing clinical trials testing anti-CTLA-4, anti-PD1 and anti-PD-L1 in GBM patients, in combination with surgery, radiotherapy or/and chemotherapy or even with other ICIs (92). There are, for example, a phase II trial of anti-PD1 as a neoadjuvant therapy; a phase III trial of anti-PD1 with TMZ and with radiation in newly diagnosed GBM patients and; a randomized phase II recurrent GBM trial of pembrolizumab (anti-PD1) with or without bevacizumab. Other ongoing trials aims to investigate the effect of nivolumab (anti-PD1) or TMZ in a newly diagnosed GBM with unmethylated MGMT status (CheckMate-494) and the effect of nivolumab with radiotherapy and TMZ, followed by adjuvant TMZ with nivolumab in a newly diagnosed GBM with methylated MGMT promotor (CheckMate-548) (113). For instance, a finished clinical trial (Checkmate 143 trial) concluded that anti-PD1 (nivolumab) does not improve the survival of patients with relapsed GBM, although a small subset of these patients presents a robust response (92,114). Thus, it is mandatory to analyse their immune responses and find predictive biomarkers of this particular immunotherapy (92). Regarding HOXA9, in GBM, nothing is known about its putative role in immune evasion and in response to immunotherapies with ICIs.

2. Objectives

The central hypothesis of this research work is that HOXA9 may have a key functions in immune evasion and in the response of GBM to ICIs, namely to anti-CTLA4 and anti-PD1 therapies. Curiously, previous studies showed that HOXA9 is associated with some immune related pathways; however, how HOXA9 may help GBM to evade the immune system is still to be elucidated (46). Furthermore, as there are no established predictive biomarkers for the efficacy of immunotherapies with ICIs, studies are needed to evaluate new molecules, such as HOXA9, as potential novel biomarkers.

The goal of this project is to investigate if HOXA9 has a role in immune evasion and its predictive value as a biomarker for ICIs efficacy, in GBM. More specifically, the mains approaches are to:

1. Determine the influence of HOXA9 in the expression of immune related factors, such as immune checkpoints and its ligands and some cytokines and chemokines, in GBM.
2. Evaluate, the effect of HOXA9, both in the immune system modulation and in the sensitivity to T-cell mediated cytotoxicity, in naïve treatment conditions or in the presence of ICIs, *in vitro*.

Globally, this thesis work might contribute to elucidate the relevance of HOXA9 in the modulation of the immune microenvironment of GBM.

3.1 Cell lines and culture conditions

Three distinct human GBM cell lines were used during this work: two established human GBM cell lines, U87MG and U251 (kindly provided by Dr. Joseph Costello, University of California, San Francisco), and one primary GBM cell line, GL18, previously established in our laboratory. U251 and GL18 cell lines were previously transfected with HOXA9 gene-specific short hairpin RNA (shRNA) sequences or a non-effective shRNA cassette in pGFP-V-RS plasmid (scrambled negative control) [74]. U87MG was previously retrovirally transfected with MSCV neo vectors containing HOXA9 cDNA [74]. All cell lines were maintained in Dulbecco's Modified Eagle Medium (DMEM; Gibco®) supplemented with 10% Fetal Bovine Serum (FBS; Biochrom) or in RPMI 1640 Medium (Gibco®) supplemented with 10% FBS and 1 mM sodium pyruvate (Gibco®). All of these cell lines grow in DMEM, but in order to perform the co-culture assays, they have to be cultured also in RPMI, since hPBMCs only grow in RPMI.

One mouse glioma cell line, GL261, was purchased from DSMZ (Germany) and maintained in DMEM supplemented with 10% FBS or RPMI 1640 Medium supplemented with 10% FBS and 1mM sodium pyruvate.

All cell lines were maintained in a humified incubator, at 37°C with 5% CO_2.

3.2 Gene expression analysis

To evaluate the expression of *Hoxa9* and *HOXA9* and of immune related genes: *TNFA*, *IL10*, *TGFB1*, *IFNG*, *IL1B*, *IL6*, *IL8*, *CCL2*, *PDL1, PD1*, *CD80* and *CD86*, was used quantitative reverse transcriptase - polymerase chain reaction (RT-qPCR).

3.2.1 RNA extraction

RNA was extracted from each cell line using Trizol Reagent (Invitrogen) according to manufactures' instructions. Briefly, 0.5 mL of Trizol Reagent were added to lyse the cells by homogenising the samples by up and down and incubating at room temperature (RT) for 3 minutes. Next, 0.1 mL of chloroform was added and shaked vigorously, incubated at RT for 15 minutes and centrifuged at 12 000 g for 15 minutes at 4°C. After centrifugation, three phases were formed and RNA was found at the upper aqueous phase,

which was transferred to a new tube. Right after, 0.5 mL of isopropanol was added to precipitate RNA; samples were incubated for 10 minutes and centrifuged at 12 000 g for 10 minutes at 4°C. Supernatant was decanted and the RNA pellet washed with ethanol 75% and centrifuged at 7 500 g for 5 minutes, twice. RNA pellet was resuspended in RNase free water and the RNA was left for 10 minutes at 55°C before being stored at -80°C until being used.

3.2.2 Complementary DNA synthesis

One µg of total RNA (quantified by a nanodrop Spectrophotometer ND-1000) was used to be reverse transcribed into complementary DNA (cDNA) using High Capacity cDNA Reverse Transcription Kit (Applied Biosystems), according to manufacturer's recommendations. This Kit uses RT buffer 1x, dNTPs (0.04 mM), random primers 1x, reverse transcriptase (2,5 U/µL) and water (DNase and RNase free). Synthesis was performed on a thermocycler (Bio Rad) using the following protocol: 25°C for 10 minutes, 37 °C for 120 minutes, 85°C for 5 minutes and at 4°C until samples were stored at -20°C.

3.2.3 Reverse transcriptase - quantitative polymerase chain reaction (RT-qPCR)

Primers for the RT-qPCR were designed using the online tool "Primer3Plus". A table with the primers used and the relative melting temperature (Tm) can be found in the Supplementary Table 1.

The expression levels of immune related genes and of *HOXA9* or *Hoxa9* were determined by RT-qPCR, using the *TATA-binding protein* (*TBP, Tbp*) as reference gene. Depending on the gene and the cell line to be assessed, as depicted in Supplementary Table 1, the KAPA SYBR® FAST qPCR Master Mix (2X) Universal or the PowerUp™ SYBR™ Green Master Mix (Applied Biosystems), were used. Briefly, 1 µL of cDNA, KAPA SYBR® FAST qPCR Master Mix or PowerUp™ SYBR™ Green Master Mix, 0.2 µM of each primer and RNase free H_2O was used to prepare the RT-qPCR mix.

The reactions were performed in duplicate and ran on a Thermal cycler CFX96 (Bio-Rad) using the program Bio-Rad CFX Manager version 3.1. The conditions of RT-qPCR were as follows: 3 minutes at 95°C; followed by 40 cycles of denaturation, annealing and extension: 3 seconds at 95°C for denaturation, 30 seconds at respective Tm for annealing (supplementary table 1) and 30 seconds at 72°C for extension, for the RT-qPCR performed with KAPA SYBR® FAST qPCR Master Mix; and as follows: 2 minutes at 50°C and 2 minutes at 95°C; followed by 40 cycles of denaturation, annealing and extension: 15 seconds at 95°C for denaturation, 60 seconds at respective Tm for annealing and extension

(supplementary table 1), for the RT-qPCR performed with PowerUp™ SYBR™ Green Master Mix. For the melting curve, the dissociation was performed by 5 seconds at 65°C with increasing the temperature by 1°C from 65°C to 95°C. RT-qPCR products weights were confirmed on 2% agarose gels.

Data from the relative expression of the RT-qPCR was analysed using the ΔΔCT method for the analysis of gene relative expression in the cell lines (control ones and the ones with manipulated levels of HOXA9) (115).

3.3 Flow cytometry stain and analysis

In this section were described the staining protocols for flow cytometry: surface staining, intracellular staining and annexin v/propidium iodide (Ann/PI) staining. For that, were used the antibodies and dyes depicted in supplementary table 2.

3.3.1 Surface staining

The expression of the immune checkpoint ligands, PDL1, PDL2, CD80 and CD86, on the cells' surface of human GBM cell lines was determined using monoclonal antibodies (supplementary table 2). Cells were detached with trypsin, and total cell numbers were determined using a Neubauer chamber in an inverted microscope (Olympus CKX41). Half million cells were added to each U-shaped well of a 96-well plate, and washed twice with FACS buffer [phosphate buffered saline (PBS) supplemented with 0.3% bovine serum albumin (BSA), 0.01% sodium azide], for 2 minutes, 1 200 rpm, 4 °C. After incubation of tumour cells with Fc Block (1:50 dilution; eBioscience), cells were incubated with prediluted antibodies for 20 minutes, in the dark and on ice; cells were washed twice with PBS. Live/dead fixable dye (supplementary table 2) was added to the cells, incubated for 30 minutes in the dark, on ice, and washed once with PBS. The samples were acquired on the same day, unless they proceeded for intracellular stain.

3.3.2 Intracellular staining

Cells were surface stained (as described in section 5.1) with antibodies directed to CD45, CD3, CD4, CD8, CD127 and CD25. Afterwards, cells were incubated with Fixation/Permeabilization buffer (eBiosciences) for 30 minutes in the dark, on ice and then, washed once with FACs buffer, and once with

Permeabilization buffer (eBiosciences). Afterwards, the cells were incubated for 30 minutes in the dark, at room temperature with FoxP3 (diluted in Permeabilization buffer) and then washed twice with Permeabilization buffer and resuspended in PBS 1% BSA. The samples were acquired in the cytometer on the next day.

3.3.3 Annexin V/Propidium Iodide staining

After a surface stain with anti-CD45 (section 3.4.1; supplementary table 2), to be able to distinguish tumour cells from leukocytes, cells were washed twice with binding buffer (HEPES 100mM, NaCl 140mM, $CaCl_2 \cdot 2H_2O$ 2.5 mM). 50 µL of a mix of Ann and PI was added and incubated in the dark, for 15 minutes at room temperature. Acquisition on the cytometer was performed in the following 15 minutes.

3.3.4 Data acquisition and analysis

Single stains for CD80, CD86, PD-L1, PD-L2, CD25 and CD127 were performed using compensation beads (Invitrogen) to obtain clearly defined positive and negative populations for compensation. The samples were acquired on the same day on a BD LSRII flow cytometer (equipped with a blue 488nm, a red 633nm and a violet 405nm lasers), using the FACS Diva Software (Becton Dickinson, Franklin Lakes, NJ, USA). Data were analysed as described in the results section using the FlowJo Software version 10 (Tree Star, Ashland, OR, USA).

3.4 Co-cultures of tumour cells and activated T-cells

The cytotoxicity mediated by T-cells was evaluated by co-culture of tumour cells with previously activated T-cells, followed by evaluation of live and dead cells by flow cytometry. The same way, T-cells' subsets were evaluated after co-culture of tumour cells and activated T-cells.

3.4.1 Activation and expansion of human peripheral blood mononuclear cells (hPBMCs)

Ten million fresh hPBMCs from healthy donors, from Hospital de Braga (kindly provided by Dr. Agostinho Carvalho and Dra. Cristina Cunha, ICVS, University of Minho) were cultured in complete RPMI medium (RPMI-1640 with 10% FBS, 1 mM pyruvate and 100 U/mL penicillin and 100 mg/mL streptomycin) supplemented with 30U/mL of human recombinant IL-2 (ImmunoTools), in a T25 flask previously coated

for 2h at 37 °C, with 5 µg/mL of anti-human CD3 (ImmunoTools) and 2.5 µg/mL of anti-human CD28 (ImmunoTools). After 72h, cells were washed and resuspended in fresh complete medium with 30 U/mL of human recombinant IL-2 and cultured for more 24h in a new T25 flask. In the next day, the cells were washed and resuspended in medium without IL-2.

3.4.2 Co-culture of human tumour cells with activated T-cells

U87-MSCV/-HOXA9, GL18-shCTRL/-shHOXA9 and U251-shCTRL/-shHOXA9 cell lines, cultured in RPMI medium, were plated at an initial density of $2x10^5$ cells per well in 12-well plates, and incubated overnight. Next day, activated T-cells were added at a ratio of 1:5 of target cells: effector cells (T: E), with or without ICIs [10 µg/mL of anti-CTLA4 (clone BN13; BioXCell) or anti-PD1 (clone J116; BioXCell)]. For each cell line there were 4 conditions: i) tumour cells only; ii) tumour + T-cells + IgG isotype control (10 µg/mL; Sigma Aldrich); iii) tumour cells + T-cells + anti-CTLA4 and; iv) tumour cells + T-cells + anti-PD1. The cells were co-cultured for 48h at 37°C in 5% CO_2 atmosphere. Afterwards, cells in suspension were removed from the well and placed immediately in ice; tumour cells were detached from the wells using trypsin and added to the previously removed cells in suspension, to be counted and stained for flow cytometry.

3.4.3 Activation and expansion of mouse T-cells

C57BL/6J mice were euthanized by a lethal dose of anaesthesia and the inguinal, axillary and superficial cervical LN were aseptically removed. Single cell suspension was obtained by gentle disrupting the LN between two notched slide glasses, and, after washing, LN cells were resuspended in complete RPMI medium [RPMI + 10% FBS + 100 U/mL penicillin and 100 mg/mL streptomycin + 1mM sodium pyruvate + 50 µM β-mecaptoethanol (β-me; Sigma)]. After this, the number of cells extracted was obtained using trypan blue exclusion dye in a proportion 1:5, using a Neubauer chamber.

For the activation and expansion of T cells, a T25 flask was coated, for 2h at 37°C, with anti-mouse CD3 (5 µg/mL; clone 145-2C11; BioLegend). After thoroughly washing the flask with PBS, $1x10^7$ million LN cells were cultured with complete RPMI medium. Supplemented with recombinant mouse IL-2 (30U/mL; Invitrogen) and with anti-mouse CD28 (2µg/mL; clone 37.51; BioLegend). After 72h of T-cell activation, cells in suspension were collected, centrifuged at 1 200 rpm, for 10 minutes at 4°C, and the pellet resuspended in complete RPMI medium supplemented with IL2; cell suspension was transferred to a new T25 flask and cultured for more 24h. Afterwards, cells in suspension were collected, viable counted,

washed resuspended in complete RPMI medium. Activation profile of these T-cells was confirmed by flow cytometry, as described above.

3.4.4 Co-culture of mouse tumour cells with activated T-cells

GL261 cells, cultured in complete RPMI medium, were plated at an initial density of $5x10^4$ cells per well in a 12-well plate, and incubated overnight; activated mouse T-cells were added to the wells at different ratios of T: E (1:5; 1:10; 1:20). After 48h of culture, cells in suspension were collected and placed on ice; adherent cells were detached from the wells using cell dissociation media (Sigma Aldrich) and added to the first suspension of cells. Total cells were counted and stained for Ann/PI.

3.5 HOXA9 silencing in mouse GBM cell line

The GL261 cell line was manipulated to silence HOXA9 with *Hoxa9* gene-specific shRNA vector insert (TR500979; clones TR500979A, TR500979B, TR500979C and TR500979D; Origene) or non-effective shRNA (scrambled negative control) inserted in a pRS plasmid (TR30012; Origene). For that, $1.5x10^5$ cells were plated per well in a 12-well plate and when reaching 70-90% confluence the cells were transfected. First, Lipofectamine™ 3000 reagent was diluted in Opti-MEM™ Medium (Diluted Lipofectamine 3000) and vortex for 2s. Then, was prepared the master mix of DNA, by diluting DNA (0.5µg) in Opti- MEM™ Medium and added P3000 reagent (2 µL/µg) – Diluted DNA. Next, was added the Diluted DNA to the tube of Diluted Lipofectamine 3000 reagent (in 1:1 ratio) and incubated for 15 minutes at room temperature. Finally, the medium was removed from the wells and was added fresh medium (DMEM + 10% FBS) and DNA-lipid complex to the cells and maintained for 48h. The transfected cells were selected with 1 µg/mL of puromycin, since these plasmids present a resistance gene to puromycin.

3.6 Statistical analysis

When normality was assumed, unpaired t-test or One-Way ANOVA was performed, but when normality assumptions were not satisfied, the equivalent non-parametric Mann Whitney U test or Kruskal-Wallis test, respectively, was applied. To determine statistical differences between groups was used, first, the Levene's test to check for equality of variances. If the Levene's test revealed differences among the homoscedasticity of both groups, Welch's correction was applied.

Overall, the results were expressed as group means ± standard deviation, when the parametric test was used; and as group median ± distance between the first and third quart. Differences were considered statistically significant for p-values below 0.05. The results were analysed using GraphPad Prism version 7 (GraphPad Software, La Jolla, CA, USA).

4.1 Influence of HOXA9 on the expression of immune related factors in tumour cells

The development of an inflammatory microenvironment has long been considered important in the initiation and progression of GBM (116) however, the role of HOXA9 on the modulation of the expression and release of some cytokines has yet to be elucidated. Ligands of immune checkpoints are wildly described to be upregulated in several cancer types, including GBM (91). For this reason, it is important to assess also if HOXA9 can modulate the expression of these proteins. Although there are previous microarray data on the expression of some cytokines and immune checkpoint ligands (117), it was necessary to validate this data through a technique with greater sensitivity, such as RT-qPCR. This work was focused on the expression of the following genes: *IL1B*, *TNFA*, *IFNG*, *TGFB1*, *IL8*, *IL10*, *IL6*, *CCL2*, *CD86*, *CD80, PDL1* and *PD1*.

The expression of these genes was assessed in three different human GBM cell lines: U87-MSCV/HOXA9 (an overexpression model for *HOXA9,* in which U87-MSCV is the control cell line with low levels of *HOXA9* and U87-HOXA9 is the manipulated cell line to express high levels of *HOXA9*); GL18-shCTRL/-shHOXA9 and U251-shCTRL/-shHOXA9 (two silencing models for *HOXA9,* in which -shCTRL are the control cell lines with high levels of *HOXA9,* and -shHOXA9 are the ones silenced for *HOXA9*). All of these cells grow preferentially in DMEM, but in order to perform the co-cultures of tumour cells with hPBMCs (which only grow in RPMI), in this work, tumour cells were cultured also in RPMI. As gene expression can change with the culture conditions (118–120), for RT-qPCR evaluation, the expression of immune related genes was assessed in human GBM cell lines, cultured both in DMEM and RPMI.

4.1.1 HOXA9 affects the expression of cytokines and chemokines in human GBM cell lines

Numerous cytokines have a role in tumour growth and in the promoting of an immunosuppressive tumour microenvironment. For instance, IL1β and TNFα are the main drivers of inflammation in GBM, promoting tumour growth (106,121), and IFNγ is correlated with the expression of PD-L1 (122); TGFβ1 promote tumour growth and immunosuppression; IL8 and IL6 promote invasion; CCL2 is evolved in Treg cells recruitment and IL10 inhibits T-cell function (94). In order to understand if some immune related genes were altered in the presence of *HOXA9*, RT-qPCR were performed directed a set of genes: *IL1B*, *TNFA*

and *IFNG* that are pro-inflammatory genes and *TGFB1*, *IL8*, *IL6*, *CCL2* and *IL10* that are anti-inflammatory genes.

Regarding the pro-inflammatory genes, for *IL1B*, and for both culture media, the expression of this gene decreased in the U87 cell line (i.e. upon *HOXA9* over-expression), but for the silencing models these differences were not significant (Figure 8A and B; supplementary table 3). For *TNFA*, no consistent differences were seen on its expression for the different cell lines (Figure 8C and D; Supplementary Table 4), and in all the cell lines, *IFNG* expression was is not detected (Supplementary Figure 2). Concerning the anti-inflammatory genes, a decrease of *TGFB1* expression was observed in both *HOXA9* silencing models when cultured in DMEM, but not in RPMI; additionally, no differences were seen for the U87 cell line overexpressing *HOXA9* (Figure 8E and F; Supplementary Table 5). Regarding *IL8* expression, an increase of its expression was observed when *HOXA9* expression was silenced, though these differences were not consistent in the two silencing models and in the two culture media, but in the overexpression model, U87 cell line, there was no significant differences (Figure 8G and H, Supplementary Table 6). No *IL10* expression was detected in any cell line (Supplementary Figure 3). Concerning *IL6* expression, in the silencing model GL18 cultured in DMEM, a significant decrease in its expression was observed, but not in the other cell lines tested (Figure 8I and J, Supplementary Table 7). *CCL2* expression was significantly decreased in the U251 cell line (silencing model), in both cell culture media, but no differences were seen in other cell lines (Figure 8k and L, Supplementary Table 8).

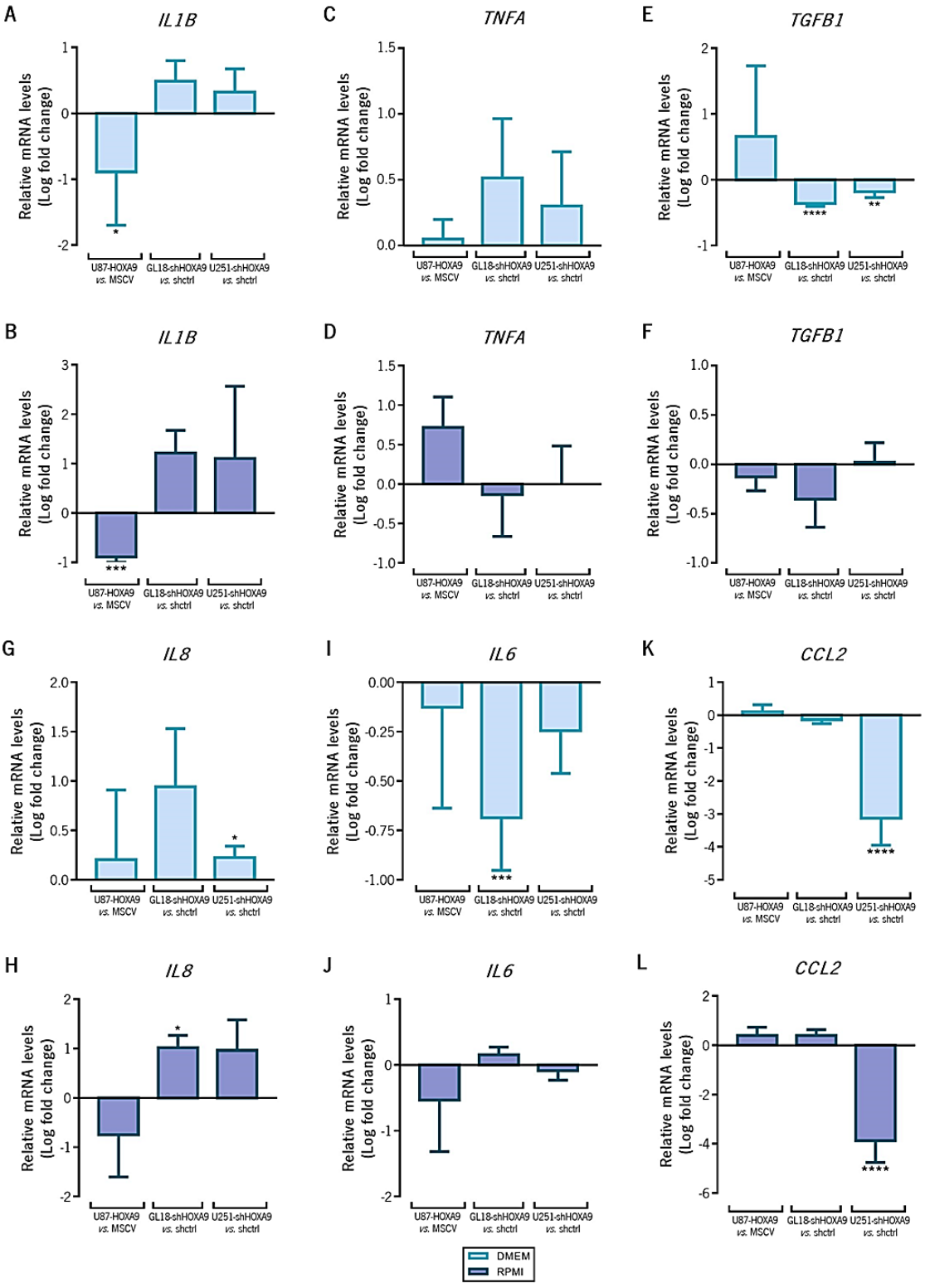

Figure 8– Expression of immune related genes in human GBM cell lines with differential levels of HOXA9 expression. Expression of *IL1B* **(A, B)**, *TNFA* **(C, D)**, *TGFB1* **(E, F)**, *IL8* **(G, H)**, *IL6* **(I, J)** and *CCL2* **(K, L)**, in human GBM cell lines. Gene relative quantification, by RT-qPCR, was performed in cell lines cultured in DMEM **(A, C, E, G, I, K)** and in RPMI **(B, D, F, H, J, L)**. In each graph is represented the logarithm of the fold change of the relative expression of the transformed cell line (*i.e.* U87-HOXA9, GL18-shHOXA9 and U251-shHOXA9) to the respective control (*i.e.* U87-MSCV, GL18-shCTRL and U251-shCTRL) for each cell line. Each gene's relative expression is depicted in supplementary tables 3 to 8. T-test was used to compare the fold change logarithm of the expression of immune related genes between the transformed cell line with the respective control.

Each column represents the mean ± standard deviation of 3 independent biological samples. * $p < 0.05$; ** $p < 0.01$; *** $p < 0.001$; **** $p < 0.0001$

4.1.2 HOXA9 influences the expression of immune checkpoint ligands in tumour cells

CD80 and CD86 are the ligands for CTLA4 and PD-L1 and PD-L2 are the ligands for PD1, and these ligands are upregulated in tumour microenvironment to promote immune evasion (91). Besides expressing ligands for PD1 and CTLA4, tumour cells can also express the PD1 itself, and depending on the cancer type can promote tumour growth, by binding to its ligand in tumour cells or can block PD1, inhibiting tumour proliferation (123).

The expression of *PD1* was evaluated by RT-qPCR, though the expression of these gene was not detected in the tested cell lines (Supplementary Figure 4). Besides the presence of bands of interest, the RT-qPCR was contaminated by several unspecific links, make it impossible to quantify the expression of *PD1* in these cell lines.

By RT-qPCR was observed that silencing of *HOXA9* expression, leads to significant decrease in the expression of *CD86* only when culture in RPMI (Figure 9A and B; Supplementary Table 9); in the same conditions, and also in the GL18 silencing model cultured in DMEM, an increased expression of *CD80* was observed (Figure 9C and D; Supplementary Table 10). Regarding CD80 and CD86 protein expression at the cell surface (assessed by flow cytometry), all the human cell lines analysed were negative for these markers (Figure 10; Supplementary Tables 12 and 13); importantly, and as expected, these antibodies were able to stain human PBMCs or activated T-cells (as positive controls for CD80 and CD86, respectively; Supplementary Figure 5), reinforcing that these tumour cell lines are truly negative for CD80 and CD86.

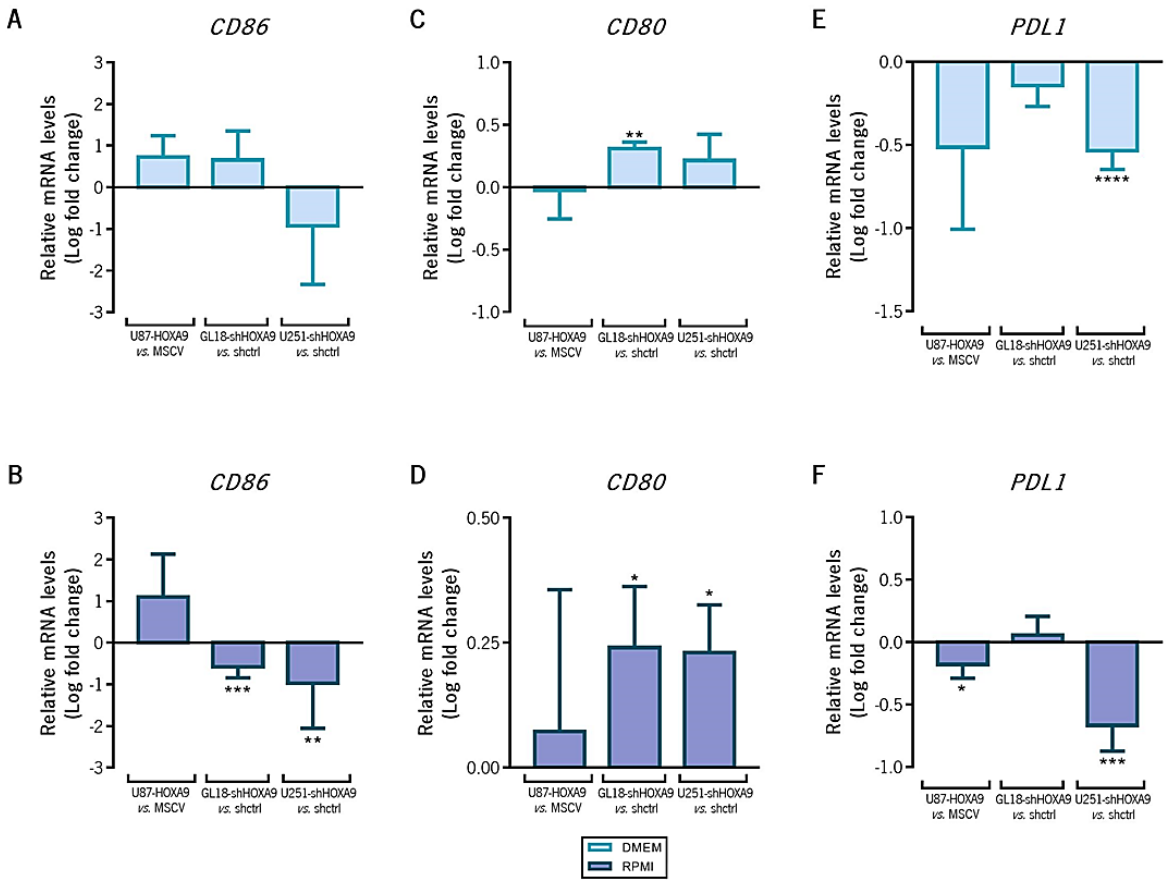

Figure 9 – Expression of immune checkpoint ligand genes in human GBM cell lines with differential levels of HOXA9 expression. Expression of *CD86* **(A, B)**, *CD80* **(C, D)** and *PDL1* **(E, F)**, in human GBM cell lines. Gene relative quantification, by RT-qPCR, was performed in cell lines cultured in DMEM **(A, C, E)** and in RPMI **(B, D, F)**. In each graph is represented the logarithm of the fold change of the relative expression of the transformed cell line (*i.e.* U87-HOXA9, GL18-shHOXA9 and U251-shHOXA9) to the respective control (*i.e.* U87-MSCV, GL18-shCTRL and U251-shCTRL) for each cell line. Each gene's relative expression is depicted in supplementary tables 9 to 11. T-test was used to compare the fold change logarithm of the expression of immune checkpoint ligand genes between the transformed cell line with the respective control. Each column represents the mean ± standard deviation of 3 independent biological samples. * $p < 0.05$; ** $p < 0.01$; *** $p < 0.001$; **** $p < 0.0001$

The expression of *PDL1* was significantly decreased in the U87 cell line overexpressing *HOXA9*, cultured in RPMI and in the U251 cell line silenced for *HOXA9* expression, in both culture media, but not altered for the other silencing model (Figure 9E and F; Supplementary Table 11). Concerning PD-L1 and PD-L2 protein expression at the cell surface, all cell lines were positive (Figure 10, Supplementary Tables 14 and 15). Additionally, when comparing the expression of these markers between the control cell line and the respective transformed cell line, a significant decrease in the expression of PD-L1 was observed in the U251 cell line silenced for *HOXA9* (Figure 10B). No differences were observed in the other cell lines and, specifically in the GL18 cell line, the relative PD-L1 protein expression [*i.e.* the relative mean fluorescence intensity (MFI)] were not consistence between biological samples (Supplementary Table 14),

data corroborated by the RT-qPCR data (Figure 9E and F; Supplementary Table 11). Regarding PD-L2, an increased protein expression was observed with the silencing of *HOXA9*, in the U251 subexpression model, but no differences were observed in the other cell lines (Figure 10C; Supplementary Table 15).

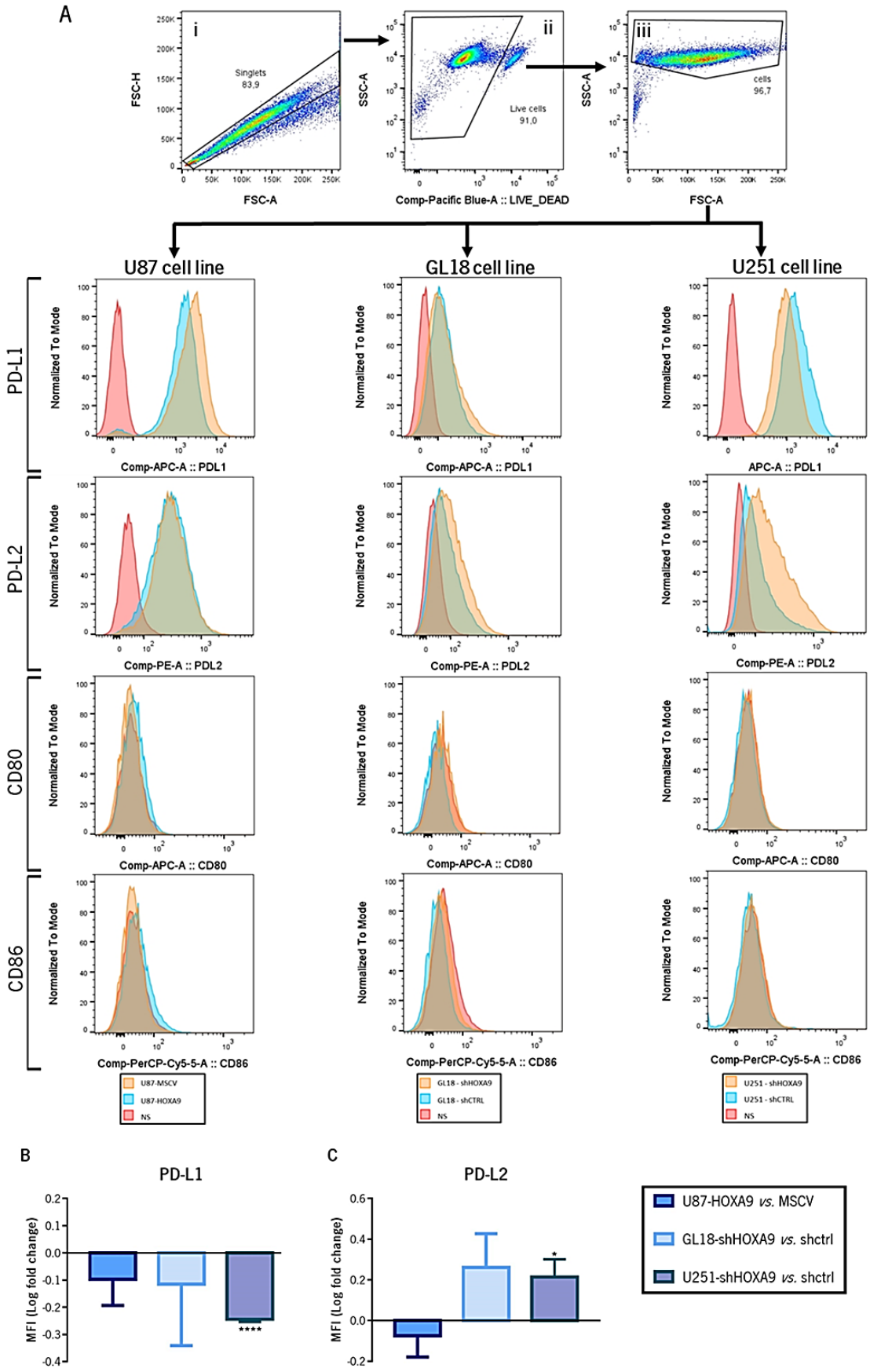
A
i
Singlets
83,9
FSC-H
FSC-A
ii
Live cells
91,0
SSC-A
Comp-Pacific Blue-A :: LIVE_DEAD
iii
cells
96,7
SSC-A
FSC-A
U87 cell line
GL18 cell line
U251 cell line
PD-L1
PD-L2
CD80
CD86
Normalized To Mode
Comp-APC-A :: PDL1
APC-A :: PDL1
Comp-PE-A :: PDL2
Comp-APC-A :: CD80
Comp-PerCP-Cy5-5-A :: CD86
U87-MSCV
U87-HOXA9
NS
GL18 - shHOXA9
GL18 - shCTRL
U251 - shHOXA9
U251 - shCTRL
B
PD-L1
MFI (Log fold change)
****
C
PD-L2
*
U87-HOXA9 vs. MSCV
GL18-shHOXA9 vs. shctrl
U251-shHOXA9 vs. shctrl

Figure 10 – Protein expression of immune checkpoint ligands in human GBM cell lines. A) For the analysis of PD-L1, PD-L2, CD80 and CD86 by flow cytometry, doublets were excluded (i), followed by the selection of the live cells (ii) and the population of interest was selected based on the FSC/SSC profile (iii) and representative histograms of the expression of PD-L1, PD-L2, CD80 and CD86, in human GBM cell lines (U87-MSCV/HOXA9; GL18-shCTRL/shHOXA9 and U251-shCTRL/shHOXA9). **B)** Relative protein expression of PD-L1 in the membrane of human GBM cell lines. **C)** Relative protein expression of PD-L2 in the membrane of human GBM cell lines. In each graph is depicted the fold change logarithm of the mean fluorescence intensity (MFI) of the transformed cell line (*i.e.* U87-HOXA9, GL18-shHOXA9 and U251-shHOXA9) to the respective control (*i.e.* U87-MSCV, GL18-shCTRL and U251-shCTRL). Each antibody MFI, for each cell line is presented in supplementary tables 12 to 15. T-test was used to compare the MFI of PD-L1 and PD-L2 between the transformed cell line (*i.e.* U87-HOXA9, GL18-shHOXA9 and U251-shHOXA9) with the respective control (*i.e.* U87-MSCV, GL18-shCTRL and U251-shCTRL). Each column represents the mean ± standard deviation of 3 independent biological samples. * $p < 0.05$; **** $p < 0.0001$.

4.2 Impact of HOXA9 in the sensitivity of glioblastoma cell lines to T-cell mediated cytotoxicity

The co-cultures consist in cultures of tumour cells (adherent) and T-cells (in suspension), and its aim is to study the interaction between these two populations, evaluating the effect of T-cells in the tumour cells and vice-versa. The first step for the optimization of the co-culture (tumour cells with activated T-cells) assays was to evaluate whether activated human T-cells (protocol already optimized in the laboratory) were able to induce tumour cells death, and at what ratio of target: effector cells (T: E; *i.e.* tumour cells: activated T-cells) this effect could be seen. To obtain the percentages of induced death in the tumour cells by activated T-cells, tumour cells viability was assessed by flow cytometry upon staining for Annexin V/Propidium Iodide (Ann/PI; Figure 11A). The T:E ratios (1:5; 1:10 and 1:20) were optimized for the co-cultures of GL18 and U251 GBM cell lines (Figure 11B and C); as for the U87 GBM cell line, this was already established in the laboratory at a 1:5 ratio. In the GL18 and U251 co-cultures a T: E ratio of 1:5 was chosen, because a lower percentage of live cells was observed at this ratio in comparison to tumour cells cultured in the absence of activated T-cells (Figure 11B and C).

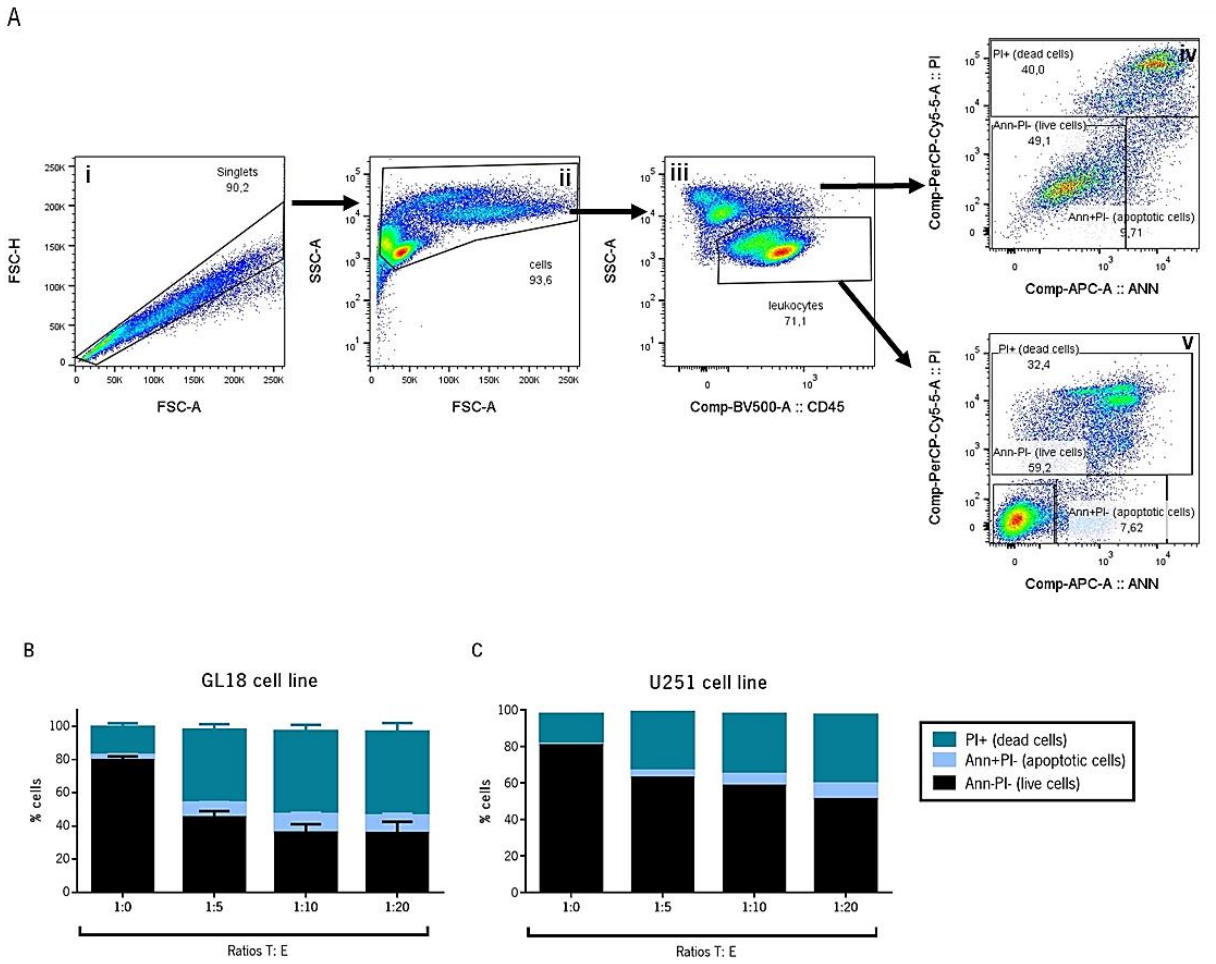

Figure 11 – Activated T-cells induced death of GL18 and U251 GBM cell lines at a T:E ratio of 1:5. A) For the assessment of cells viability, doublets were excluded (i) and tumour cells ($CD45^-$; Supplementary Figure 6) or activated hPBMCs ($CD45^+$; leukocytes) were selected (ii); dead (PI+), apoptotic (PI-Ann+) and live (PI-Ann-) cells were analysed in tumour cells (iii) and in activated human T-cells (iv). **B)** GL18 co-culture optimization. **C)** U251 co-culture optimization. Three different T: E ratios (1:5; 1:10 and 1:20) were tested and the percentages of live, apoptotic and dead cells were obtained by flow cytometry, using Ann/PI stain. For GL18, 3 replicates per condition were performed, and for U251, 1 replicate per condition was performed.

For each assay, it was confirmed that the percentage of dead in the control conditions (basal death) was lower than 20%, which is approximately the death seen for the cell lines (Figure 12A, D and G); only assays in this condition were considered valid and considered for the analysis. Were analysed the percentages of live, apoptotic and dead cells, but no differences were observed regarding the percentages of apoptotic and death cells; in the percentages of live cells some differences were observed and these ones are referred in this results section. No differences were observed in the basal death in the U87 cell line, between U87-MSCV and U87-HOXA9, neither in the GL18 cell line, between GL18-shCTRL and GL18-shHOXA9 (Figure 12A and D). But, in U251 cell line a significant decrease in the percentage of live cells were found in U251-shHOXA9 comparing to its control (Figure 12G). In order to evaluate the effect of

HOXA9 in T-cells induced death of tumour cells, the fold change of the percentage of viable cells at the control condition to the condition of tumour cells with activated T-cells was calculated. In the U87 cell line, the overexpression of *HOXA9* leads to a decrease in the fold change of live cells upon adding activated T-cells (Figure 12B). *HOXA9* expression did not impact the fold change of live cells upon adding activated T-cells in the silencing models (Figure 12E and H). These data suggest that in these conditions, *HOXA9* expression on tumour cells in the overexpression model can increase T-cells mediated cytotoxicity but does not affect T-cell mediated cytotoxicity in the silencing models.

4.3 Impact of HOXA9 in the sensitivity of glioblastoma cell lines to immune checkpoint inhibitors

Immune checkpoint ligands (such as PD-L1) expression levels can affect and predict the efficacy of ICIs (124,125). Also, some oncogenic pathways are associated with a non-responsive tumour microenvironment and with resistance to immunotherapies (48–50). In the U251 human GBM cell line, silencing of *HOXA9* leads to a significant decrease in the expression of PD-L1 and to a significant increase in the PD-L2 protein expression in the membrane of GBM cells. Next, was hypothesized whether ICIs (anti-CTLA4 and anti-PD1) could increase this effect and whether HOXA9 expression could affect the response of tumour cells to ICIs, using the co-culture system. Comparing the conditions of tumour cells with T-cells and anti-CTLA4 or anti-PD1 with isotype control, within the same cell line, it was observed that the presence of anti-CTLA4 or anti-PD1 did not affect T-cell induced death of tumour cells (Figure 12A, D and G). To assess the effect of *HOXA9* expression in tumour cells response to ICIs, the fold change of the percentage of viable cells, from the condition without ICIs (tumour cells and activated T-cells with isotype control) to the conditions with ICIs (i.e. tumour cells and activated T-cells with anti-CTLA4 or with anti-PD1) was calculated (Figure 12C, F and I). For the U87 (*HOXA9* overexpression model) and for the GL18 (*HOXA9* silencing model) cell lines, no differences were seen regarding the effect of *HOXA9* in the response of ICIs (Figure 12C and F), but regarding the U251 cell line (*HOXA9* silencing model), there was a minor, but significant, decrease in sensitivity of tumour cells death to anti-PD1, with the silencing of *HOXA9* (Figure 12I). These data suggest that, at these conditions and at these ICIs concentrations, *HOXA9* expression does not affect the response to anti-CTLA4 and slightly increases the sensitivity to anti-PD1 therapy, but only in one of the GBM silencing models.

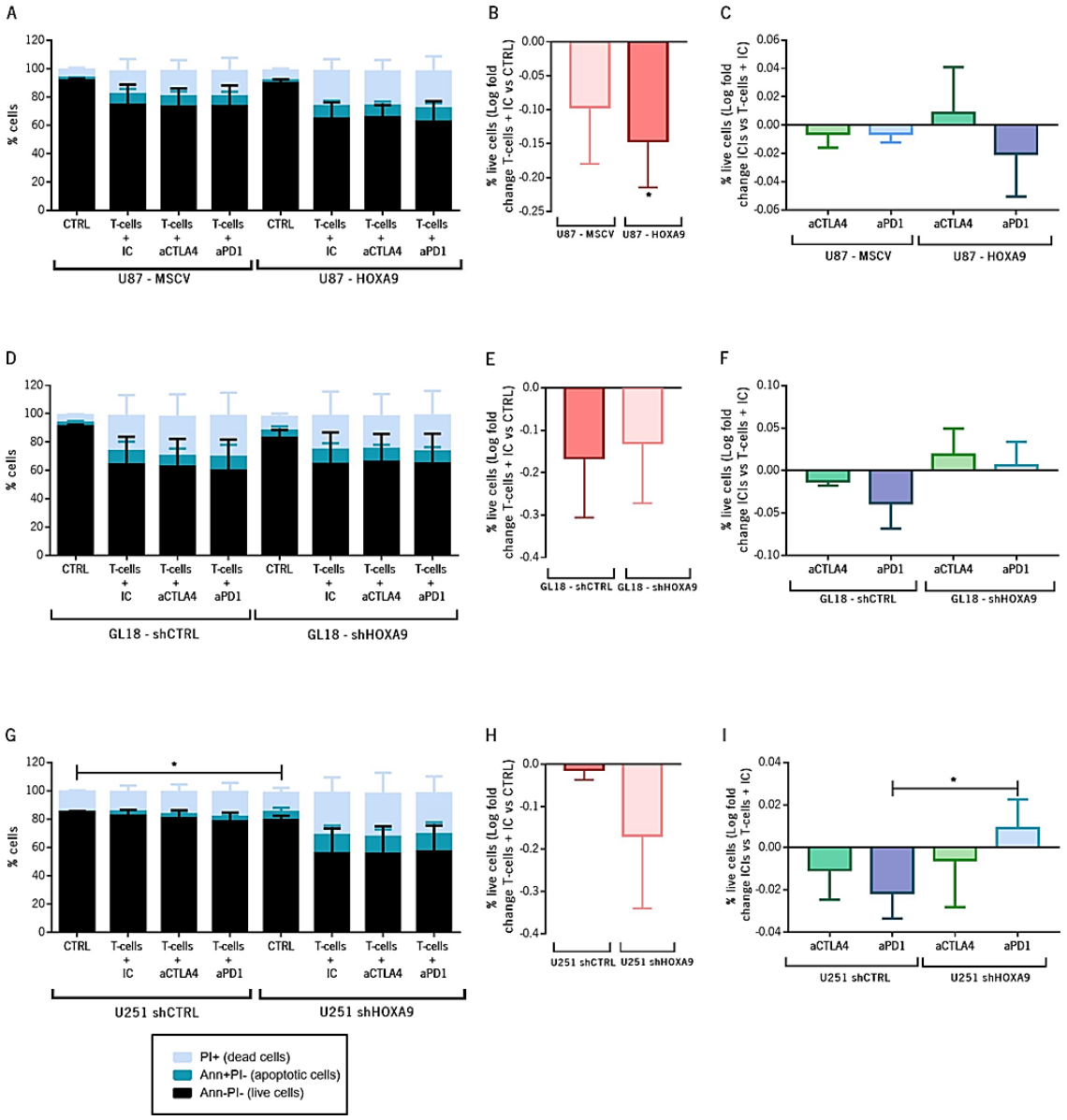

Figure 12 – T-cell mediated cytotoxicity in tumour cells, in treatment naïve conditions or in the presence of ICIs. A, D, G) Depicts the percentage of live (Ann-PI-), apoptotic (Ann+PI-) and dead cells (PI+), in tumour cells only (CTRL), tumour cells with activated T-cells and isotype control (IgG; IC) or in face of anti-CTLA, or of anti-PD1 of U87 (**A**), GL18 (**D**) and U251 (**G**) cell lines. One-way ANOVA was used to compare the percentage of live, apoptotic and dead cells between the conditions with isotype control, anti-CTLA4 and anti-PD1 in the transformed cell lines (*i.e.* U87-HOXA9, GL18-shHOXA9 and U251-shHOXA9) and in the control cell lines (*i.e.* U87-MSCV, GL18-shCTRL and U251-shCTRL). **B, E, H)** Represents the fold change logarithm of live cells from tumour cells only condition to tumour cells with activated T-cells (with IC), of U87 (**B**), GL18 (**E**) and U251 (**G**) cell lines. T-test was used to compare the fold change logarithm of the percentage of live, apoptotic and dead cells between the transformed cell line (*i.e.* U87-HOXA9, GL18-shHOXA9 and U251-shHOXA9) and the respective control (*i.e.* U87-MSCV, GL18-shCTRL and U251-shCTRL). **C, F, I)** Represents the fold change logarithm of live cells form the tumour cells with activated T-cells (with IC) condition to the conditions with anti-CTLA4 or with anti-PD1, of U87 (**C**), GL18 (**F**) and U251 (**I**) cell lines. T-test was used to compare the fold change logarithm of the percentage of live, apoptotic and dead cells in the conditions with anti-CTLA4 and anti-PD1 between the transformed cell line (*i.e.* U87-HOXA9, GL18-shHOXA9 and U251-shHOXA9) with the respective control (*i.e.* U87-MSCV, GL18-shCTRL and U251-shCTRL). The average ± standard deviation is represented from 3 independent assays. * $p < 0.05$.

4.4 Influence of HOXA9 in T-cell survival, in the presence or absence of Immune Checkpoint Inhibitors

One of the mechanisms of immunosuppression in GBM is the induction of T-cell apoptosis (79). Therefore, it is important to evaluate the effect of *HOXA9* expression on T-cell survival in the co-culture assays, and the impact of adding ICIs. For this, the $CD45^+$ population (*i.e.* leukocytes) of the co-cultures was analysed (Figure 11A). When comparing co-cultures, without ICIs, of control tumour cell with tumour cells overexpressing (Figure 13A) or with tumour cells silenced for *HOXA9* (Figure 13C and E), no differences were observed in the percentage of live, apoptotic and death leukocytes. Also, within the same cell lines, ICIs had no effect on the survival of T-cells, when comparing co-cultures of tumour cells and activated T-cells with isotype control with the same conditions with anti-CTLA4 or anti-PD1 (Figure 13A, C and E). To assess the effect of *HOXA9* in the response to ICIs, the fold change of the percentage of viable cells at the control of tumour cell and T-cells with isotype control to the conditions of tumour cell and T-cells with ICIs (anti-CTLA4 or anti-PD1) was calculated. No significant differences were found on the survival of activated T-cells in response to ICIs, when comparing co-cultures of control tumour cells with tumour cells overexpressing (Figure 13B) or silenced for *HOXA9* (Figure 13D and F). With this analysis, was demonstrated that *HOXA9* expression and ICIs do not influence the T-cell survival in co-cultures of GBM cell lines.

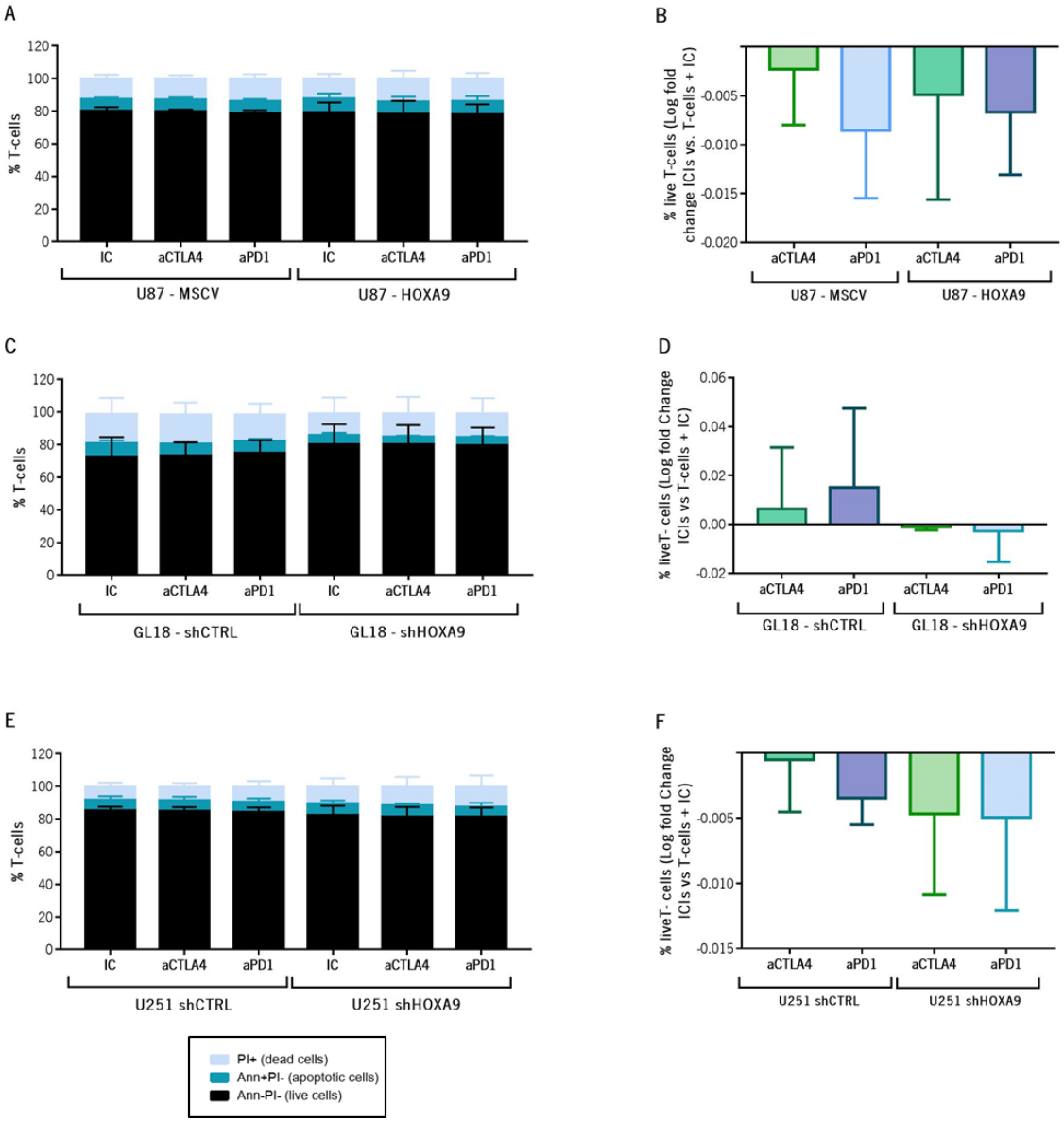

Figure 13 – HOXA9 and ICIs impact on T-cell survival. A, C, E) Represents the percentage of live (Ann-PI-), apoptotic (Ann+PI-) and dead cells (PI+) in tumour cells with T-cells and isotype control (IgG; IC) or in face of anti-CTLA, or of anti-PD1 of U87 (**A**), GL18 (**C**) and U251 (**E**) cell lines. One-way ANOVA was used to compare the percentage of live, apoptotic and dead cells between the conditions with isotype control, anti-CTLA4 and anti-PD1 in the transformed cell lines (*i.e.* U87-HOXA9, GL18-shHOXA9 and U251-shHOXA9) and in the control cell lines (*i.e.* U87-MSCV, GL18-shCTRL and U251-shCTRL); and no significant differences were observed. **B, D, F)** Represents the fold change logarithm of live T-cells from the condition of the tumour cells and T-cells with isotype control to the condition with anti-CTLA4 or with anti-PD1, of U87 (**B**), GL18 (**D**) and U251 (**F**) cell lines. T-test was used to compare the fold change logarithm of the percentage of live cells in the conditions with anti-CTLA4 and anti-PD1 between the transformed cell line (*i.e.* U87-HOXA9, GL18-shHOXA9 and U251-shHOXA9) with the respective control (*i.e.* U87-MSCV, GL18-shCTRL and U251-shCTRL). The average ± standard deviation is represented from 3 independent assays.

4.5 Impact of HOXA9 expression by glioblastoma cells in the percentage of T-cell subpopulations, independently of Immune Checkpoint Inhibitors' presence

GBM is characterized for being an immunosuppressive tumour, with a high percentage of immunosuppressive cells, like Treg cells, and low percentage of effector cells (79,95). For this reason, assess if HOXA9, in treatment-naïve condition or with ICIs treatment, could have an impact in the modulation of the immune system, *in vitro*, is very important. For this, in the co-culture system, the T-cell profile was further analysed, assessing the percentages of $CD4^+$ T-cells, $CD8^+$ T-cells and Treg cells, by flow cytometry, in the silencing of *HOXA9* GBM cell lines models (Figure 14A).

In terms of percentage of total T-cells ($CD3^+$), all conditions present about 97% of T-cells as a result of the *in vitro* activation and expansion of T-cells protocol. Comparing the silenced for *HOXA9* expression cell lines (*i.e.* GL18-shHOXA9 and U251-shHOXA9) with the respective control cell lines (*i.e.* GL18-shCTRL and U251-shCTRL), no differences were observed in the percentages of $CD8^+$ T-cells, $CD4^+$ T-cells and Treg cells in naïve-treatment conditions (Figure 14B-E). Also, when was compared the silenced for *HOXA9* expression cell lines (*i.e.* GL18-shHOXA9 and U251-shHOXA9) with the respective control cell lines (*i.e.* GL18-shCTRL and U251-shCTRL) in the presence of anti-CTLA4 or anti-PD1, no differences were observed regarding in the percentages of $CD8^+$ T-cells, $CD4^+$ T-cells and Treg cells (Figure 14B-E). However, to conclude about the impact of HOXA9 and ICIs (anti-CTLA4 and anti-PD1) in the modulation of the T-cells subpopulations, is mandatory to increase the number of assays, since its represented data just from 2 independent assays.

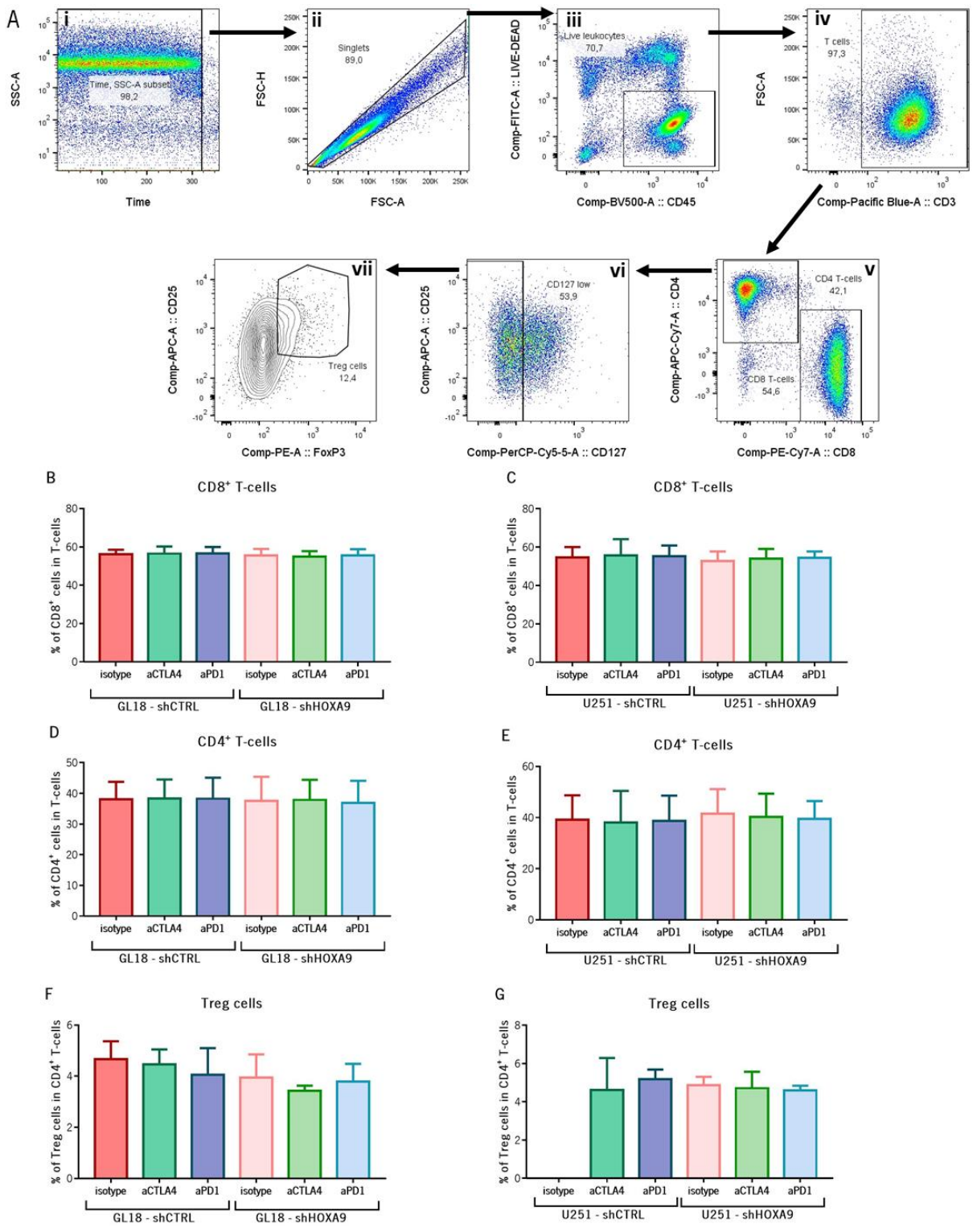

Figure 14 – Influence of *HOXA9* expression in tumour cells, in T-cells subpopulations, in the presence or absence of ICIs. A) Representative gating strategy of the T-cells populations on a GL18 co-culture. Selection of a homogeneous sample acquisition over time, plotted for SSC-A *vs.* time (i). Doublets were excluded (ii), the live leukocytes selected (iii), and then the T-cell population ($CD3^+$). $CD4^+$ T-cells and $CD8^+$ T-cells were selected (v), and inside the $CD4^+$ T-cells, the population of cells expressing low CD127 was selected (vi), followed by the selection of the $CD25^+Foxp3^+$ (vii). Tregs were characterized as $CD3^+CD4^+CD127^-CD25^+FoxP3^+$. T-cell subpopulations were analysed in co-cultures in GBM cell lines with silencing of *HOXA9* models: GL18 (**B, D, F**) and U251 (**C, E, G**). Represents the percentage of **B, C**) $CD8^+$ T-cells; **D, E**) $CD4^+$ T-cells and **F, G**) Treg cells, in the

condition of the tumour cells and T-cells with isotype control (IC), with anti-CTLA4 or with anti-PD1. The average ± standard deviation is represented from 2 independent assays.

4.6 Studies of HOXA9 impact in glioblastoma immune evasion in a murine model – preliminary data

As the studies with human GBM cell lines, was next, proposed to perform the same studies but with a murine GBM model and additionally, perform *in vivo* studies with this model. However, as described in the next section, the silencing of the murine GBM cell line was not successful. Still, the protocol of the T-cell activation and expansion of mouse T-cells was optimized to proceeded with these assays as soon the murine GBM cell line is stablish.

4.6.1 Silencing of HOXA9 in a murine GBM cell line

To evaluate the effect of *Hoxa9* expression in a murine GBM cell line, on the cytotoxicity mediated by T-cells, *Hoxa9* expression in the GL261 cell line had to be modulated. Since the GL261 cell line has high endogenous levels of this gene (mean relative expression of 201.19), the expression of *Hoxa9* needed to be silenced. This process would generate a control cell line with high levels of *Hoxa9,* and its paired silenced cell line with low levels of *Hoxa9*. For this, 4 different shRNA constructs were used to stably silence this gene. To confirm the success of the transfection, cells were selected with puromycin, since the constructs used present a resistance gene: tumour cells that were not transfected would die, and transfected cells would survive. It was possible to efficiently transfected the GL261 cell line with each of the 4 constructs (represented a significant example in Figure 15A). *Hoxa9* expression was evaluated by RT-qPCR. However, despite being transfected, cells were not successfully silenced, since *Hoxa9* relative expression of the cells with the constructs of interest were similar to the cells with the control construct (Figure 15B). To overcome this issue other shRNA construct, with other sequence or a different plasmid, should be tested.

As the GL261 cell line was not efficiently silenced, it was not possible to move forward with the experiments *in vitro* and *in vivo* in the murine model.

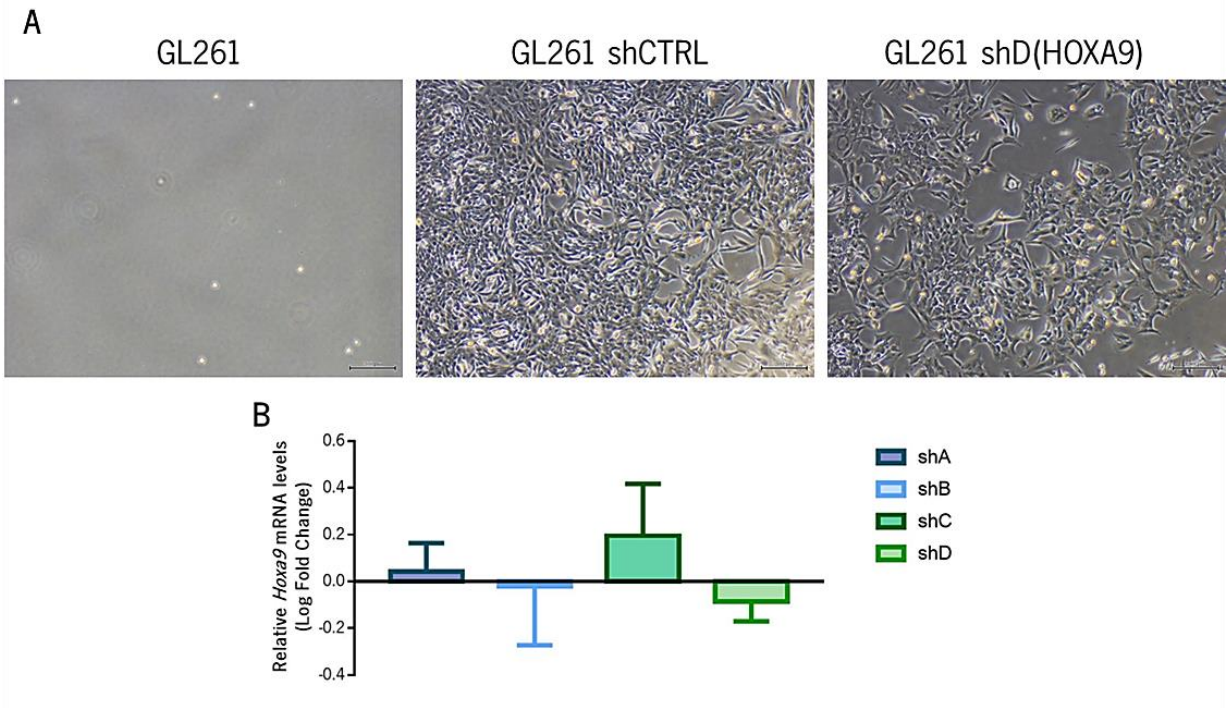

Figure 15 – The murine GBM cell line GL261 was not silenced for *Hoxa9*, though was transfected. A) Photos of GL261 cell line after 9 days with selection medium containing 1µg/mL puromycin, to confirm the efficient transfection of this cell line. From the left to the right, depicted are the parental cell line (GL261; not submitted to a transfection), then the line cell transfected with the control plasmid (GL261 shCTRL), and the GL261 cell line transfected with one of the tested constructs to silence the *Hoxa9* expression (GL261 shD). **B)** Fold change logarithm of the *Hoxa9* relative expression in cell line transfected with each of the 4 different constructs to silence *Hoxa9* expression to the cell lines transfected with control vector (shCTRL), evaluated by RT-qPCR. Each column represents the mean ± the standard deviation, from 3 independent biological samples, run in duplicate.

4.6.2 Optimization of mouse T-cell activation and expansion protocol

In vivo, T-cell activation is initiated with the interaction of the T-cell receptor (TCR)/CD3 complex with peptide present on the cell surface of APC; interaction of CD28 on the T-cells with CD80 and CD86, on APC, provides the co-stimulatory signal (126). The *in vitro* activation protocol mimics this process using antibodies that target CD3 and CD28, which have the ability to induce T-cell activation through these molecules' signalling. IL2 was used to induce T-cell expansion.

To perform the co-cultures with murine cells, it was necessary to adjust the T-cell activation and expansion protocol available for hPBMCs to mouse lymph nodes (mLN) cells. Mouse lymph nodes cells were used since this organ presents a similar percentage of T-cells in comparison to hPBMCs (about 60-70%). The use of mouse PBMCs, would require a high number of mice and, since mLN are enriched in T-cells, this reduces the number of mice used per assay.

The murine GBM cell line, GL261 grows in DMEM. Because of the co-culture assays to be performed afterwards, the activation and expansion protocol of mLN cells was performed in DMEM; also, in the literature are described some protocols in DMEM (127,128). In a first approach, wells of a 24-well plate were coated with anti-CD3 (5 μg/mL) and anti-CD28 (2 μg/mL) for 2h at 37°C; afterwards, $2x10^6$cells/mL was added per well, in complete DMEM supplemented with IL-2 (30 U/mL). The mLN cells were maintained in culture for 72h (activation), followed by 24h with complete DMEM and IL-2 in a new, uncoated 24-well plate (expansion). Viable cells were counted, and a very low percentage of the initial number of cells cultured was recovered. As for hPBMCs, the yield is usually around 100%, it was hypothesized that cells were not being properly activated and, due to lack of stimulus, they were dying (129).

Co-stimulation with anti-CD28 enhances the proliferative expansion and promotes cell survival during activation (129). In this sense, it would be expected that, by decreasing cell density, and adding soluble anti-CD28, instead of plate bounded anti-CD28, would favour the interaction between T cells and anti-CD28, thus enhancing a strong co-stimulatory signal to properly activate T-cells. First, the cell density was decreased from $2x10^6$ cells/mL to $1x10^6$ cells/mL, and soluble CD28 (0.4 μg/mL) was added in the medium. With this alteration on the protocol, a modest increase in the recovery of viable cells was obtained in comparison with the first protocol tested (from 1.48% to 7.00%). Thus, a cell density of $1x10^6$ cells/mL and soluble CD28 was used. Still, the obtained yield was far from the obtained for hPBMCs.

The usage of complete DMEM *vs.* complete RPMI was next tested. Importantly, RPMI was further supplemented with 1mM sodium pyruvate since it is the main source of energy for the cells. Supplementation with β-mercaptoethanol (β-me; 50 μM) was also tested since β-me is a reducing agent, that helps to prevent toxic levels of oxygen radicals and is necessary for the *in vitro* growth and activation of lymphocytes (130). In the absence of β-me, mLN cells cultured in RPMI presented higher percentages of recovered viable cells in comparison to DMEM (6.63% *vs.* 1.88%). The presence of β-me increases the percentage of cells recovered, especially for mLN cells cultured in RPMI (6.63% without β-me *vs.* 92.88% with β-me), but also for cells cultured in DMEM (1.88% without β-me *vs.* 11.75% with β-me). At this point, it was concluded that culturing mLN cells in RPMI supplemented with β-me is required to properly expand cells and achieve the expected cell recovery.

Although the previously results with DMEM were not promising, it was highly desirable to optimize this protocol using DMEM, in order to not to change the growth media of the tumour cell line. A new test, using DMEM and RMPI was performed, using different concentrations of anti-CD3 and anti-CD28. With

the same rational that co-stimulation with anti-CD28 enhances the proliferation and promote cell survival during activation, and based on previously described protocols (129,131,132), the concentration of anti-CD28 was increased from 0.4 µg/mL to 2 µg/mL. Additionally, it was shown that, with 2.5 µg/mL of anti-CD3 there is more proliferating T-cells ($CD4^+$ and $CD8^+$ cells), and with higher doses (*e.g.* 5 µg/mL) the expression of CD3 decreases in $CD4^+$ and $CD8^+$ T-cells (127). Based on this, the stimulation and expansion protocol for mLN cellss was tested in DMEM and RPMI, with 0.4 µg/mL or 2 µg/mL of soluble anti-CD28, and with 2.5 µg/mL or 5 µg/mL of plate-bounded anti-CD3. Results show that in DMEM, the recovery of viable mLN cells was below 20%, irrespectively of the tested condition (Figure 16). Regarding to the mLN cells cultured in RPMI, with 5 µg/mL of anti-CD3 there was an increased recovering of viable mLN cells especially with 0.4 µg/mL of anti-CD28, but also with 2 µg/mL, when compared with 2.5 µg/mL of anti-CD3 (Figure 16). Since the percentage of recovered live cells using RPMI was highest, and although there were better results with the lower concentration of anti-CD28 (*i.e.* 0.4 µg/mL), understanding if T-cells were effectively activated was the next step. To this, the activation profile was evaluated, by flow cytometry of the mLN cells cultured in RPMI, in the presence of 5 µg/mL of anti-CD3 and with both concentrations of CD28 (0.4 µg/mL and 2 µg/mL).

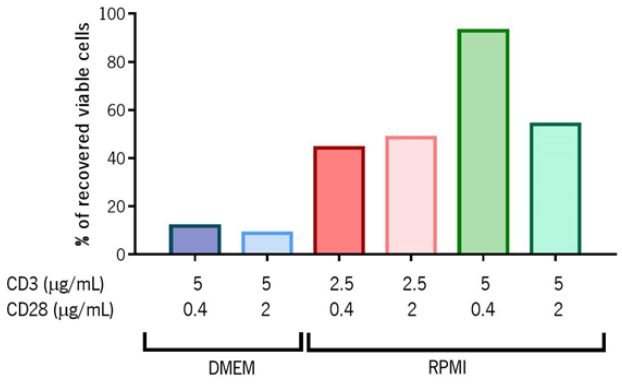

Figure 16 – Percentage of cells recovered after the activation and expansion of mLN cells protocol with the different conditions tested. Different mediums were tested (DMEM and RPMI with β-me), with different concentrations of plate-bounded anti-CD3 (2.5 µg/mL and 5 µg/mL) and soluble anti-CD28 (0.4 µg/mL and 2 µg/mL), at a cell density of $1x10^6$ cells/mL. The cells were plated in a 24-well plate and were counted using trypan blue. The results presented are referred to an activation and expansion period of 96h (72h + 24h). The percentage of recovered cells was calculated based on the initial number of cells cultured per well.

The T-cell activation profile was evaluated using CD44 and CD62L, that allow to distinguish 3 subpopulations [naïve ($CD44^{int}CD62L^{+}$), effector memory ($CD44^{hi}CD62L^{-}$) and central memory ($CD44^{hi}CD62L^{+}$)], CD69 and PD1, which are markers of activation and PD1 also known as an exhaustion marker. A marker to exclude dead cells was used in this stain. A relevant percentage of $CD4^{+}CD8^{+}$ T-cells were found on the mLN cells stimulated with 0.4 µg/mL of anti-CD28; these percentages were minor when cells were stimulated with 2 µg/mL of CD28 (Figure 17A). Moreover, it has been described that *in vitro* T-cell stimulation can lead to the generation of $CD4^{+}CD8^{+}$ T-cells (133) and these may also be found in the mLN, though at low percentages (1 – 10% of total T-cells) (133). Regarding CD44/CD62L expression, in both concentrations of anti-CD28, most of the $CD4^{+}$ and of the $CD8^{+}$ T-cells presented a central memory phenotype ($CD44^{hi}CD62L^{+}$; Figure 17B). In the same way, for both anti-CD28 concentrations tested, the majority of the $CD4^{+}$ T-cells were positive for the activation markers, CD69 and PD1. Regarding $CD8^{+}$ T-cells, these present a less activated phenotype when stimulated with 2 µg/mL of anti-CD28 in comparison to 0.4 µg/mL, as seen by the lower percentage of $PD1^{+}$ and of $CD69^{+}$ cells (Figure 17C). Overall, there was a higher number of recovered cells using 0.4 µg/mL of anti-CD28, but these presented higher percentages of $CD4^{+}CD8^{+}$ T-cells. For this reason, the condition with 2 µg/mL of anti-CD28 was chosen for future assays, despite $CD8^{+}$ T-cells were not as activated as the ones in 2 µg/mL of anti-CD28.

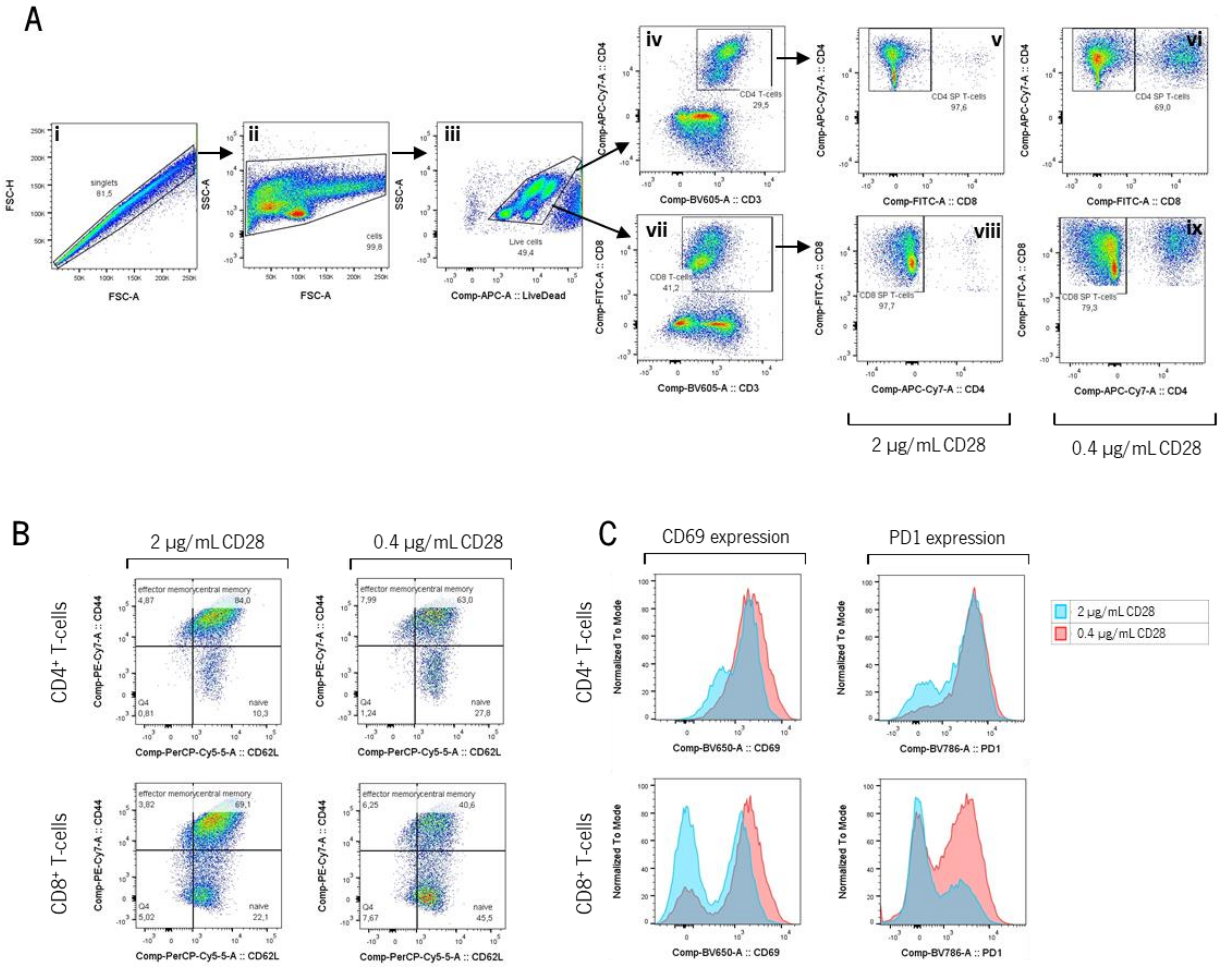

Figure 17 – Assessment of the activation profile of mLN cells activated and expanded, in vitro. A) Gating strategy of the mLN cells activated: doublets were excluded (i), and population of interest was selected based on the FSC/SSC profile (ii) followed by the selection of the live cells (iii), $CD4^+$ T-cells (iv) and $CD8^+$ T-cells (vii). Selection of the cells $CD4^+$ $CD8^-$ (v and vi), and of cells $CD8^+$ $CD4^-$ (viii and ix). Representative dot plots for the conditions: with 5 µg/mL of anti-CD3 and 2 µg/mL of anti-CD28 (v and viii) or with 5 µg/mL of anti-CD3 and 0.4 µg/mL of anti-CD28 (vi and ix). **B)** Plots of CD44/CD62L that allows to distinguish the naïve ($CD44^{int}CD62L^+$), effector memory ($CD44^hCD62L^-$) and central memory ($CD44^hCD62L^+$) populations in $CD4^+$ T-cells and in $CD8^+$ T-cells for each concentration of CD28. **C)** Histograms of the expression of activation markers, CD69 and PD1 (also an exhaustion marker), in $CD4^+$ T-cells and $CD8^+$ T-cells with both conditions: 2 µg/mL of anti-CD28 (blue) and 0.4 µg/mL of anti-CD28 (red).

The murine GBM cell line, GL261, grows preferably in complete DMEM media. However, the T-cell activation and expansion protocol could not be optimized using complete DMEM, so to perform the co-culture assays, GL261 cells had to be adapted to RPMI medium. The first step for the optimization of the co-culture assays was to evaluate whether activated T-cells, derived from mLN cells, were able to kill tumour cells (using the GL261 parental cell line), and at what ratio of T: E this effect could be seen. The 1:5; 1:10 and 1:20 ratios of T:E were tested in a co-culture assay; tumour cells (*i.e.* $CD45^-$ cells;

Supplementary Figure 6) viability, by flow cytometry upon staining for Ann/PI, was assessed. Results show that activated T-cells could efficiently induce tumour cell dead at T:E ratio of 1:5 (Figure 18).

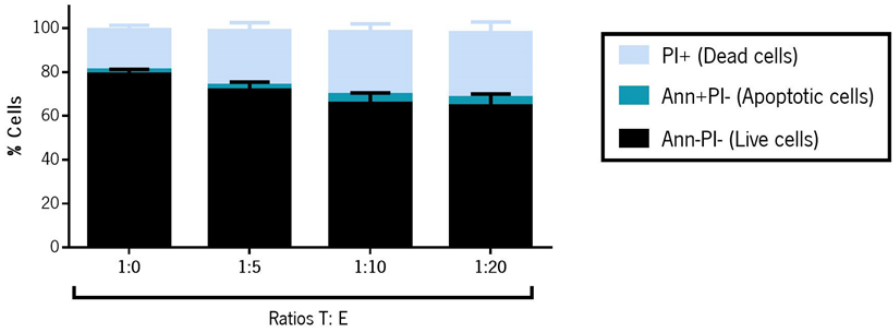

Figure 18 – Pre-activated mLN cells induce dead in tumour cells. mLN cells were activated and expanded in vitro, as previously described. Afterwards, activated T-cells were co-cultured with tumour cells (parental GL261cell line) at different T:E ratios (1:5; 1:10 and 1:20). Upon 48h of co-culture, cells were harvested, counted, and their viability analysed by flow cytometry by Ann/PI stain. CD45 was used to discriminate activated T-cells ($CD45^+$) from tumour cells ($CD45^-$; Supplementary Figure 6). The average ± standard deviation depicted is from a single assay: with each condition performed in triplicate.

5. Discussion

Glioblastoma is the most common primary malignant brain tumour in adults, with a very poor prognosis (21,134). Despite considerable progress in understanding the biological characteristics of GBM, and the efforts to find new effective therapies, survival has not improved. GBM is a highly immunosuppressive tumour, with the ability to change the phenotype of immune cells and to supress the adaptive immune responses (135). Therefore, it is important to know how tumours modulate the immune response, in order to provide new strategies towards an anti-tumour response. Increasing evidences suggest that activation of some oncogenic pathways is associated with a non-responsive tumour microenvironment and resistance to immunotherapies (48–50). HOXA9 is a transcription factor deregulated in GBM, described to down-regulate pathways associated with immune and inflammatory responses and antigen processing and presentation (46). Also, microarray data suggest that some cytokines and chemokines and also molecules involved in the immune checkpoint may suffer some changes in its expression due to HOXA9 (46). Therefore, this study aimed to understand the relevance of *HOXA9* expression in GBM immune evasion, both in treatment-naïve conditions and in response to immunotherapies with ICIs.

In this work were used human GBM cell lines [U87-MSCV/-HOXA9 (an overexpression of *HOXA9* model); GL18-shCTRL/-shHOXA9 and U251-shCTRL/-shHOXA9 (two silencing of *HOXA9* models)] and one murine GBM cell line (GL261). All these cell lines display different genetic profiles and characteristics, including different basal levels of *HOXA9*, raising the importance of using paired cell lines and not distinct cell lines with different basal levels of *HOXA9*. Nevertheless, the silencing between the two subexpression models is also different, leading to different levels of expression of *HOXA9*, and the *HOXA9* expression in U87 cell line overexpressing *HOXA9* is much higher that what is observed in patients (46).

Several immune-related genes (pro-inflammatory and anti-inflammatory genes) were analysed in human GBM cell lines with differential levels of expression of *HOXA9*. Based on previous results from a micro-array analysis (46) and from the literature regarding the expression of cytokines and chemokines in GBM (94,108,116), genes were selected and validated by RT-qPCR, which is a more sensitive technique (117). These genes were evaluated in human GBM cell lines cultured in DMEM (to validate the microarray data (46)) and also in RPMI (to assess the characteristics of these cells in the medium used for the co-cultures assays). Interestingly, different results of gene expression for GBM cells cultured in DMEM and in RPMI were obtained, suggesting that culture conditions might affect mRNA expression of some genes. In fact, it has been described that different culture conditions, for example growth factors present in serum-

containing media, among other changes, can affect the expression of some genes (118–120). Importantly, *HOXA9* relative expression levels were not affected by the alteration in culture conditions (data not shown).

Focusing on gene expression of the cell lines cultured in DMEM, as the ones evaluated in the microarrays, in *TNFA* no significant differences were obtained in none of the assays, and *CCL2* presents, in U251 cell line, a significant decrease in its expression when silencing for *HOXA9*, with both techniques (microarray and RT-qPCR). *IL1B* and *IL8* show the same tendency in the RT-qPCR with the microarray data in all cell lines. Concerning *TGFB1*, both in microarray and in RT-qPCR, significant and consistent results were obtained in GL18 cell line, although in the U251 cell line different and opposite results were obtained. What concerns the expression of *PDL1*, U251 silencing model presents a similar profile of expression. Overall, these two techniques showed concordant results (gene expression in same direction between cell lines that express and cell lines that do not express *HOXA9*), except for the *TGFB1* expression in U251 cell line, validating by RT-qPCR the results obtained by microarray.

A lot of cytokines and chemokines are secreted by the GBM cells to promote their growth and proliferation. *IL1B* is an inflammatory cytokine and is highly activated in GBM cells (116,136). Inflammation is a helpful response triggered to restore tissue injury, however, if inflammation is unregulated, it can become chronic and induce malignant cell transformation in the surrounding tissue (128). Cancers exhibit wide amounts of inflammatory infiltrates with high levels of cytokine expression in the tumour microenvironment, even though do not arise as consequence of chronic inflammation (107). Aberrant expression of *IL1B* in GBM cells plays an important role in inflammation drivring tumour growth and progression, by the upregulation of other pro-inflammatory cytokines, such as *TNFA* and *IL6* (121). This data suggests that *HOXA9* attenuates the inflammation in the GBM microenvironment, by reducing the expression of *IL1B*, but no association was observed with the expression of *TNFA* and of *IL6*. *TGFB1* and *IL8* are anti-inflammatory cytokines, and particularly, are involved in the suppression of the effector T-cells activity and are considered to be immunosuppressive factors in the tumour microenvironment (94,108,137). CCL2, a chemokine described to be produced by GBM cells, is specially involved in the recruitment of Treg cells (94). This work suggests that *HOXA9* can suppress the effector T-cell activity and promote an immunosuppressive microenvironment, composed by Treg cells through CCL2 recruitment. Globally, *HOXA9* seems to decrease inflammation in the GBM microenvironment, but increase the immunosuppression. This is in agreement with the notion that GBM is a highly immunosuppressive tumour (138). Overall, these results suggest that the effect of HOXA9 in the expression of these genes is

dependent on the cell lines and on their culture conditions. Next, would be important to evaluate the production of these cytokines, by western blot or Multiplex ELISA Array to confirm if the mRNA is being translated to protein, to further complementing these results.

Increasing evidences show that immunosuppression in GBM is not only due to intrinsic proprieties of GBM cells, but from the interaction of several cell types and the ability of GBM cells to coordinate these other cells and signalling pathways in its tumour microenvironment (138). To try to mimic the interaction that occurs between GBM cells and T-cells in a cancer patient, human GBM cell lines were placed in direct contact with activated T-cells, in *in vitro* co-cultures. These experiments showed that *HOXA9* expression does not affect T-cell mediated cytotoxicity and that T-cells were not able to significantly kill GBM cells, except for the U87 cell line. Although a partially effective immune response against GBM cell lines exists, GBM cells still manage to escape. On the T-cells side, no significant differences were observed regarding their survival and apoptosis. It is described that besides inducing apoptosis of T-cells, tumour cells can also promote exhaustion and anergy (82). Anergic T-cells are characterized by low production of IL2 and exhausted T-cells are characterized by the expression of multiple regulatory receptors (such as PD1, CTLA4 and LAG3) and loss of cytokines expression (such as TNFα, IFNγ) (139). Several immunosuppressive cytokines (such as TGFβ and IL6) are secreted by GBM cells and reduce the anti-tumour immune response, for example by blocking T-cell activation and proliferation (79). Therefore, evaluating the T-cell phenotype in terms of activation, anergic state or exhaustion would be an interesting approach. Using flow cytometry to evaluate the expression of regulatory markers and the production of cytokines can also give information about the T-cells state. As was observed the secretion of some immunosuppressive cytokines by GBM cells in basal conditions, is expected that in the co-cultures these cytokines secreted by GBM cells might decrease the anti-tumour immune response. Thus, a proteomic analysis of the co-cultures' medium can give important insights about the factors secreted in these co-cultures with differential levels of *HOXA9* expression and how it may influence T-cells state. Nevertheless, the use of healthy PBMCs donors, adds a lot of variability to the assays. In fact, it was observed a high variability within the assays in what concerns the effect of the T-cells on tumour cells. This means that the three independent assays performed might be scarce and more assays are required to make more reliable associations.

The presence of immunosuppressive cells, like Treg cells, contributes to the immunosuppressive microenvironment in GBM (93). A study with *in vitro* co-cultures of liver cancer cells with hPMBCs from healthy donors showed an increase in the number of Treg cells during the co-culture and suggested that

cancer-derived soluble factors result in the expansion of Treg cells (140). Also, studies with human GBM cell lines, *in vitro*, showed that these tumour cells can suppress T-cell proliferation and pro-inflammatory responses, and promote, survival, expansion and chemoattraction of Treg cells, by the release of soluble factors, such as CCL2 and TGFβ1 (99,141). A different expression pattern of some cytokines in the GBM cell lines due to *HOXA9* expression was observed, particularly in *CCL2* expression, that significantly decreases with the silence of *HOXA9* in U251 GBM cell line. Thus, through the expression of different cytokines, HOXA9 might modulate the immune system and promote Treg cells survival and proliferation. However, no differences were observed in Treg cells percentages, in the co-culture assays, but the results showed are very preliminary.

GBM cells are able to upregulate surface immunosuppressive molecules, as immune checkpoint ligands, inhibiting the immune response dependent on cell-to-cell interaction (142). These immunosuppressive molecules bind to immune checkpoints in T-cells, namely to PD1 and CTLA4, inhibiting T-cell activation and inducing their apoptosis (93). CD80 and CD86, besides binding to CTLA4 to provide an inhibitory signal, can also bind to CD28 to provide a co-stimulatory signal, although with less affinity. Hereupon, tumour cells can down-regulate the expression of these two molecules to limit the co-stimulation in T-cells (59,143). At the mRNA level, was observed that, irrespectively of the cell line tested and of its *HOXA9* expression, these human GBM cell lines have low expression of *CD80* and *CD86* (seen by the late amplification in the RT-qPCR), but do not express these molecules in their surface. In fact, it has been described, in a Kaposi's sarcoma cell line, that the expression of *CD80* leads to T-cell activation and proliferation, supporting that the down-regulation of these two molecules is a mechanism of immune evasion (144).

PD-L1 and PD-L2 are described to be expressed by GBM cells and are also associated with an unfavourable prognostic (105,145). Both PD-L1 and PD-L2 can induce T-cell apoptosis or anergy by binding to PD1, present in activated T-cells, that affects the anti-tumour immune response (91). In the U251 human GBM cell line, silencing of *HOXA9* leads to a significant decrease in the protein expression of PD-L1 and to a significant increase in the protein expression of PD-L2 in the membrane of GBM cells, but this result was not consistent with the other cell lines. These results suggest that HOXA9 might have an effect on the modulation of the expression of the PD1 ligands, and consequently in the modulation of the GBM microenvironment, namely in T-cell responses. It would be interesting to evaluate the expression of PD-L1 and of other immune checkpoint ligands in the co-culture assays, to see if in response to a stimulus (such as T-cell mediated cytotoxicity), there is a change in the expression of these molecules. It

is described that tumour cells can release tumour-derived exosomes expressing FAS ligand and also PD-L1 that blocks T-cell activation and proliferation and promote T-cell apoptosis (146,147). It would be important to look at these tumour-derived exosomes, and evaluate the expression of PD-L1 and PD-L2, that could be achieved by western blot, after a differential centrifugation to isolate the exosomes. Evaluating the exosomes released by GBM cells with high and low expression of *HOXA9*, could give more information about the expression of these markers in GBM. Moreover, anti- and pro-inflammatory cytokines can serve as growth and survival factors to stimulate tumour progression (107). Together, in the presence of *HOXA9*, the expression of PD-L1, with the expression of anti-inflammatory genes (*TGFB*, *IL6* and *CCL2*) in GBM cells, may contribute to the immunosuppressive microenvironment of GBM.

A study in breast cancer shows that blockade of IL1β leads to an increase in $CD8^+$ T-cells and to its infiltration in the tumour microenvironment, that consequently, leads to tumour regression. Moreover, they show that blocking of IL1β, previous to anti-PD1 therapy, increases the response to this immunotherapy and abrogated tumour progression (148). In the present study, using the U251 silencing model, it was observed an increased PD-L1 expression and a decreased *IL1B* expression in the presence of HOXA9. This goes along with the observation, for this same cell line (U251), that, an increase expression of *HOXA9* is related with an increased sensitivity to anti-PD1 therapy.

Immune checkpoint inhibitors have achieved remarkable success in cancer treatment; however, not all patients show clinical benefit. Several factors can affect and predict the efficacy of ICIs, as tumour mutation burden, immune checkpoint ligands (such as PD-L1) expression levels, density of TILs and mismatch-repair deficiency in some cancers (124,125). Nevertheless, it is still needed to find new reliable predictive biomarkers of ICIs response, to allow a precision immunotherapy and to better understand and overcome resistance mechanisms. One study already tried to evaluate the above-mentioned predictive biomarkers in the response of GBM patients to ICIs therapy, using TCGA, but found inconsistent patterns (either suggesting resistance or susceptibility to ICIs), raising the need to find other predictive biomarkers for ICIs in GBM (149). Therefore, in this work was study the HOXA9 predictive value for ICIs therapy. Regarding the immunotherapy with anti-CTLA4, no significant differences were found, neither in the response to ICIs, neither in the effect of HOXA9 to this therapy, consistent with the results from the expression of CD80 and CD86 in the GBM cells. About anti-PD1 therapy, it did not increase the T-cell mediated cytotoxicity, though, in U251 silencing model, there was a minor, but significant decrease in the sensitivity to anti-PD1 therapy with the silencing of *HOXA9*, but this effect was not seen in the other GBM cell lines. This suggest that the effect of HOXA9 in anti-PD1 therapy is cell line dependent.

Anti-CTLA4 acts by activating anti-tumour immunity by promoting T-cell proliferation. Anti-PD1 blockade can induce T-cells proliferation and cytokine production. Also, it is described that, in melanoma, treatment with anti-CTLA4 can replace the numbers of effector and memory $CD4^+$ and $CD8^+$ T-cells (150). T-cell apoptosis was described as an important mechanism of cancer immune resistance, what can contribute to the decrease of T-cell number in the tumour microenvironment and lead to resistance to immunotherapies (151). In these co-cultures studies, ICIs therapy did not impact on T-cell survival and apoptosis; that could be explained by the percentage of apoptotic and dead T-cells which decrease the number of functional T-cells. It should be noted that the concentrations of anti-CTLA4 and of anti-PD1 used were based on the literature (152–154). As were not tested before in our assays, it is important to perform a dose-response curve, and evaluate the responses of tumour and activated T-cells. Importantly, including a positive control for the ICIs response in the co-culture assays, will confirm the efficacy of the ICIs in each assay, as a melanoma cell line, since it is described that melanomas respond well to ICIs therapy. Moreover, in the co-culture assays, could be tested a combination therapy, in which will be tested anti-CTLA4 and anti-PD1, since it is described that combination of these two ICIs improve the outcome in several cancer patients, namely in melanoma patients (150,155–158).

Preclinical studies in melanoma models show that, upon treatment with anti-CTLA4, the Teff/Treg ratio increases in the tumour microenvironment and treatment with anti-PD1 can overcome inhibition by Treg cells (150). Although, no differences were observed regarding HOXA9 effect in Treg cells population with the use of ICIs, but required further confirmation with the increase in the number of independent assays. Evaluate Treg cells phenotype, could give extra information in terms of the immune cells function, as is described that in gliomas, Treg cells expressing higher levels of PD1 show an exhausted phenotype that fails to suppress T-cells proliferation (150). Thus, PD1 expression is used to identify exhausted T-cells (139). To distinguish Treg exhausted cells form T-cell exhaustion, Tregs can be first sorted and then evaluate its exhaustion by RT-qPCR, analysing pathways/genes involved in the PD1/PDL1 axis (e.g. evaluating the recruitment of phosphatases like SHP2) (159).

To move forward in this study, murine models are of extreme importance, since allow the exploitation of the GBM microenvironment in an immunocompetent mouse. This model permits the evaluation of the infiltrating immune cells, namely T-cells, the identification of the different sub-populations, and the assessment of the ratio between effector and Treg cells. Moreover, allows the study of mice survival upon ICIs therapy, with all the complexity of an *in vivo* model and of the tumour. For that, being able to manipulate the *Hoxa9* expression levels in a murine GBM cell line would be essential, though this was a

goal not achieved in the context of this project. Nevertheless, human GBM cell lines can also be used in *in vivo* studies upon humanization of immunocompromised mice [such as NOD.Cg-*Prkdc*^{scid} Il2rg$^{tm1Wjl/SzJ}$ (NSG) mice] with human, pre-activated PBMCs (160,161). With this model, it is possible, also, to evaluate the infiltration of immune cells, using subcutaneous models, and to evaluate the survival of mice, using intracranial models, in naïve treatment conditions and upon treatment with ICIs. This approach has an advantage of use human cells, but in return this can lead to graft-vs-host disease and make impossible the development of a normal immune response since the PBMCs have to be engrafted already activated and, for example, memory T-cells are more prone to be activated (162).

6. Conclusions and Future Perspectives

Clinical evidences suggest that activation of some oncogenic pathways is associated with an immunosuppressive microenvironment and resistance to immunotherapy. Previous work showed that HOXA9, an oncogene in GBM, downregulates pathways associated with immune responses, suggesting that this gene may have a role in immune evasion and in the resistance to immunotherapy. However, no link was previously established between the expression of *HOXA9* and immune evasion and/or response to immunotherapies.

By using *in vitro* approaches and cell lines overexpressing or silenced for *HOXA9* expression, this work suggests that HOXA9 might increases immunosuppression in GBM, by modulating the expression of some cytokines and chemokines, namely *IL1B*, *IL8* and *CCL2*; and also, immune checkpoint ligands, PD-L1 and PD-L2. Moreover, suggests that GBM cells can escape to immune surveillance, although a partially effective immune response against GBM cell lines seems to exist and that *HOXA9* leads to a minor, but significant, increase in sensitivity to anti-PD1 therapy, in U251 cell line but not in other cell lines (U87 and GL18). Also, regarding the T-cell population, *HOXA9* expression and ICIs therapy did not impact in the survival, neither in its subpopulations.

In the future, perform a proteomic analysis to GBM cell lines with distinct *HOXA9* expression levels and *in vivo* approaches, as well evaluation of patient's samples should be used as important tools to discriminate about HOXA9 role in GBM immune evasion and in sensitivity to immunotherapies.

7. References

1. Bray F et al. Global cancer statistics 2018: GLOBOCAN estimates of incidence and mortality worldwide for 36 cancers in 185 countries. CA Cancer J Clin. 2018;68(6):394–424.
2. Thun MJ et al. The global burden of cancer: Priorities for prevention. Carcinogenesis. 2010;31(1):100–10.
3. Widschwendter M et al. Epigenome-based cancer risk prediction: Rationale, opportunities and challenges. Nat Rev Clin Oncol. 2018;15(5):292–309.
4. Wu S et al. Evaluating intrinsic and non-intrinsic cancer risk factors. Nat Commun. 2018;9(1).
5. Whiteman DC, Wilson LF. The fractions of cancer attributable to modifiable factors: A global review. Cancer Epidemiol. 2016;44:203–21.
6. Kasper DL et al. Harrison's Principles of Internal Medicine - 17ed - McGraw-Hill. 2008.
7. Astrin SM, Rothberg PG. Oncogenes and Cancer. Cancer Invest. 1983;1(4):355–64.
8. Gerstung M et al. The temporal order of genetic and pathway alterations in tumorigenesis. PLoS One. 2011;6(10).
9. Lee EYH., Muller WJ. Oncogenes and tumor suppressor genes. Cold Spring Harb Perspect Biol. 2010;2(1):1–18.
10. Hanahan D, Weinberg RA. Hallmarks of cancer: the next generation. Cell. 2011;144(5):646–74.
11. Huse JT, Holland EC. Targeting brain cancer: Advances in the molecular pathology of malignant glioma and medulloblastoma. Nat Rev Cancer. 2010;10(5):319–31.
12. Barnholtz-Sloan JS, Ostrom QT, Cote D. Epidemiology of Brain Tumors. Neurol Clin. 2018;36(3):395–419.
13. Furnari FB et al. Malignant astrocytic glioma: Genetics, biology, and paths to treatment. Genes Dev. 2007;21(21):2683–710.
14. Zong H et al. Cell of origin for malignant gliomas and its implication in therapeutic development. Cold Spring Harb Perspect Biol. 2015;7(5):1–12.

15. Backos DS et al. The Role of Glutathione and the Glutathione-Linked Enzyme Systems in Brain Tumor Drug Resistance. In: Tumors of the Central Nervous System. 2014. p. 277–90.

16. Heiland DH et al. Comprehensive analysis of PD-L1 expression in glioblastoma multiforme. Oncotarget. 2017;8(26):42214–25.

17. Louis DN et al. The 2016 World Health Organization Classification of Tumors of the Central Nervous System: a summary. Acta Neuropathol. 2016;131(6):803–20.

18. Louis DN et al. The 2007 WHO classification of tumours of the central nervous system. Acta Neuropathol. 2007;114(2):97–109.

19. Bralten LBC, French PJ. Genetic alterations in Glioma. Cancers (Basel). 2011;3(1):1129–40.

20. Ferris SP et al. Characterization of gliomas: from morphology to molecules. Virchows Arch. 2017;471(2):257–69.

21. Nørøxe DS et al. Hallmarks of glioblastoma: A systematic review. ESMO Open. 2016;1(6):1–9.

22. Nakada M et al. Aberrant signaling pathways in Glioma. Cancers (Basel). 2011;3(3):3242–78.

23. Erwin G. Van Meir et al. Exciting New Advances in Neuro-Oncology: The Avenue to a Cure for Malignant Glioma. CA Cancer J Clin. 2010;60(3):166–93.

24. Mao H et al. Deregulated signaling pathways in glioblastoma multiforme: molecular mechanisms and therapeutic targets. Cancer Invest. 2012;30(1):48–56.

25. Roel G.W. Verhaak et al. An integrated genomic analysis identifies clinically relevant subtypes of glioblastoma characterized by abnormalities in PDGFRA, IDH1, EGFR and NF1. Cancer Cell. 2010;17(1):38–46.

26. Patrick Y. Wen, Santosh Kesari. Malignant Gliomas in Adults. N Engl J Med. 2008;359(5):492–507.

27. McNeill KA. Epidemiology of Brain Tumors. Neurol Clin. 2016;34(3):981–98.

28. Ramirez YP et al. Glioblastoma multiforme therapy and mechanisms of resistance. Pharmaceuticals. 2013;6(12):1475–506.

29. Iacob G, Dinca EB. Current data and strategy in glioblastoma multiforme. J Med Life. 2009;2(4):386–93.

30. Weller M et al. Standards of care for treatment of recurrent. Neuro Oncol. 2013;15(1):4–27.

31. Hess C et al. Role of HOXA9 in leukemia: dysregulation, cofactors and essential targets. Oncogene. 2016;35(9):1090–8.

32. Goodman FR. Limb malformations and the human HOX genes. Am J Med Genet. 2002;112(3):256–65.

33. Duboule D, Dollé P. The structural and functional organization of the murine HOX gene family resembles that of Drosophila homeotic genes. EMBO J. 1989;8(5):1497–505.

34. Seifert A et al. Role of Hox genes in stem cell differentiation. World J Stem Cells. 2015;7(3):583.

35. Grier DG et al. The pathophysiology of HOX genes and their role in cancer. J Pathol. 2005;205(2):154–71.

36. Golub T et al. Molecular Classification of Cancer: Class Discovery and Class Prediction by Gene Expression monitoring. Science (80-). 1999;286(15):531–537.

37. Andreeff M et al. HOX expression patterns identify a common signature for favorable AML. Leukemia. 2008;22(11):2014–7.

38. Sun Y et al. HOXA9 Reprograms the Enhancer Landscape to Promote Leukemogenesis. Cancer Cell. 2018;34(4):1–16.

39. Bhatlekar S et al. HOX genes and their role in the development of human cancers. J Mol Med. 2014;92(8):811–23.

40. Ko SY, Naora H. HOXA9 promotes homotypic and heterotypic cell interactions that facilitate ovarian cancer dissemination via its induction of P-cadherin. Mol Cancer. 2014;13(1):1–13.

41. Abdel-Fattah R et al. Differential expression of HOX genes in neoplastic and non-neoplastic human astrocytes. J Pathol. 2006;209(1):15–24.

42. Song YK et al. HOXA9 promotes ovarian cancer growth by stimulating cancer-associated fibroblasts. J Clin Invest. 2012;122(10):3603–17.

43. Northcotta JM et al. Fighting the force: potential of homeobox genes for tumor microenvironment regulation. Biochim Biophys Acta. 2015;1855(2):248–53.

44. Ko SY et al. Expression of the homeobox gene HOXA9 in ovarian cancer induces peritoneal macrophages to acquire an M2 tumor-promoting phenotype. Am J Pathol. 2014;184(1):271–81.

45. Costa B et al. Reversing HOXA9 oncogene activation by PI3K inhibition: Epigenetic mechanism and prognostic significance in human glioblastoma. Cancer Res. 2010;70(2):453–62.

46. Pojo M et al. A transcriptomic signature mediated by HOXA9 promotes human glioblastoma initiation, aggressiveness and resistance to temozolomide. Oncotarget. 2015;6(10):7657–74.

47. Murat A et al. Stem cell-related 'self-renewal' signature and high epidermal growth factor receptor expression associated with resistance to concomitant chemoradiotherapy in glioblastoma. J Clin Oncol. 2008;26(18):3015–24.

48. Spranger S, Gajewski TF. Impact of oncogenic pathways on evasion of antitumour immune responses. Nat Rev Cancer. 2018;18(3):139–47.

49. Willy H et al. Genomic and Transcriptomic Features of Response to Anti-PD-1 Therapy in Metastatic Melanoma. Cell. 2016;165(1):35–44.

50. Jiménez-Sánchez A et al. Heterogeneous Tumor-Immune Microenvironments among Differentially Growing Metastases in an Ovarian Cancer Patient. Cell. 2017;170(5):927-938.e20.

51. Schreiber RD et al. Cancer immunoediting: Integrating the role of immunity in cancer suppression and promotion. Science (80-). 2011;331(6024):1565–70.

52. Burnet M. Cancer-A Biological Approach: III. Viruses Associated with Neoplastic Conditions. Br Med J. 1957;1(5023):841–7.

53. Goodnow CC, Sprent J, Barbara BF, Vinuesa CG. Cellular and genetic mechanisms of self tolerance and autoimmunity. Nature. 2005;435(7042):590–7.

54. Burnet M. Immunological Factors in the process of carcinogenesis. Brit med Bull. 1964;101(14):154–8.

55. Dunn GP et al. Cancer immunoediting: from immuno- surveillance to tumor escape. Nat Immunol. 2002;3(11):991–8.

56. Shankaran V et al. IFNγ, and lymphocytes prevent primary tumour development and shape tumour immunogenicity. Nature. 2001;410(6832):1107–11.

57. Heath WR, Carbone FR. Cross-Presentation in Viral Immunity and Self-Tolerance. Nature. 2001;1(1):126–35.

58. Chen DS, Mellman I. Oncology meets immunology: The cancer-immunity cycle. Immunity. 2013;39(1):1–10.

59. de Charette M, Houot R. Hide or defend, the two strategies of lymphoma immune evasion: Potential implications for immunotherapy. Haematologica. 2018;103(8):1256–68.

60. Dustin ML. The immunological synapse. Cancer Immunol Res. 2014;2(11):1023–33.

61. Bird CH et al. Selective Regulation of Apoptosis: the Cytotoxic Lymphocyte Serpin Proteinase Inhibitor 9 Protects against Granzyme B-Mediated Apoptosis without Perturbing the Fas Cell Death Pathway. Mol Cell Biol. 1998;18(11):6387–98.

62. Afshar-Sterle S et al. Fas ligand-mediated immune surveillance by T cells is essential for the control of spontaneous B cell lymphomas. Nat Med. 2014;20(3):283–90.

63. Sharpe AH, Freeman GJ. The B7-CD28 superfamily. Nat Rev Immunol. 2002;2(2):116–26.

64. Jacobs JFM et al. Regulatory T cells and the PD-L1/PD-1 pathway mediate immune suppression in malignant human brain tumors. Neuro Oncol. 2009;11(4):394–402.

65. See AP et al. The role of regulatory T cells and microglia in glioblastoma-associated immunosuppression. J Neurooncol. 2015;123(3):405–12.

66. Togashi Y et al. Regulatory T cells in cancer immunosuppression — implications for anticancer therapy. Nat Rev Clin Oncol. 2019;16(6):356–71.

67. Tanaka A, Sakaguchi S. Regulatory T cells in cancer immunotherapy. Cell Res. 2014;27(1):109–18.

68. Takeuchi Y, Nishikawa H. Roles of regulatory T cells in cancer immunity. Int Immunol. 2016;28(8):401–9.

69. Shitara K, Nishikawa H. Regulatory T cells: A potential target in cancer immunotherapy. Ann N Y Acad Sci. 2018;1417(1):104–15.

70. Weiner G, Makkouk A. Cancer Immunotherapy and Breaking Immune Tolerance-New Approaches to an Old Challenge. Cancer Res. 2015;75(1):5–10.

71. Martin-Liberal J et al. The expanding role of immunotherapy. Cancer Treat Rev. 2017;54(17):74–86.

72. Hathcock KS et al. Identification of an Alternative Ligand for T Cell Activation Costimulatory. Adv Sci. 2012;262(5135):905–7.

73. Freeman GJ et al. Cloning of B7-2: A CTLA-4 Counter-Receptor That Costimulates Human T Cell Proliferation. Science (80-). 1993;262(5):909–11.

74. Krummel, Matthew F. and Allison JP. CD28 and CTLA-4 Have Opposing Effects on the Response of T ceils to Stimulation. J Exp Med. 1995;182(1):459–65.

75. Wing K et al. CTLA-4 Control over Foxp3+ Regulatory T Cell Function. Am Assoc Adv Sci. 2008;322(5899):271–5.

76. Huang J, Liu F, Liu Z, Tang H, Wu H, Gong Q, et al. Immune checkpoint in glioblastoma: Promising and challenging. Front Pharmacol. 2017;8(MAY).

77. Khalil DN et al. The future of cancer treatment: immunomodulation, CARs and combination immunotherapy. Nat Rev Clin Oncol. 2016;13(5):273–90.

78. Greenwald RJ et al. the B7 Family Revisited. Annu Rev Immunol. 2005;23(1):515–48.

79. Razavi S-M et al. Immune Evasion Strategies of Glioblastoma. Front Surg. 2016;3(1):1–9.

80. Preusser M et al. Prospects of immune checkpoint modulators in the treatment of glioblastoma. Nat Rev Neurol. 2015;11(9):504–14.

81. Pardoll DM. The blockade of immune checkpoints in cancer immunotherapy. Nat Rev Cancer. 2016;12(4):252–64.

82. Chen L and, Han X. Anti–PD-1/PD-L1 therapy of human cancer: past, present, and future. J Clin Invest. 2015;125(9):3384–91.

83. Zhang H, Chen J. Current status and future directions of cancer immunotherapy. J Cancer. 2018;9(10):1773–81.

84. Sharma P et al. Primary, Adaptive and Acquired Resistance to Cancer Immunotherapy. Cell. 2017;168(4):707–723.

85. Zhang H, Chen J. Current status and future directions of cancer immunotherapy. J Cancer. 2018;9(10):1773–81.

86. Barbee MS et al. Current status and future directions of the immune checkpoint inhibitors ipilimumab, pembrolizumab, and nivolumab in oncology. Ann Pharmacother. 2015;1(31):907–37.

87. Swart M et al. Combination Approaches with Immune-Checkpoint Blockade in Cancer Therapy. Front Oncol. 2016;6(233):1–16.

88. Kates M et al. Immune checkpoint inhibitors: a new frontier in bladder cancer. World J Urol. 2015;34(1):49–55.

89. Marrone, KA and Brahmer J. Using Immune Checkpoint Inhibitors in Lung Cancer. Oncol J. 2016;30(8):1173–8.

90. Abril-Rodriguez G, Ribas A. SnapShot: Immune Checkpoint Inhibitors. Cancer Cell. 2017;31(6):848-848.e1.

91. Huang J et al. Immune checkpoint in glioblastoma: Promising and challenging. Front Pharmacol. 2017;8(242):1–10.

92. Brown NF et al. Harnessing the immune system in glioblastoma. Br J Cancer. 2018;119(10):1171–81.

93. Nduom EK et al. Immunosuppressive mechanisms in glioblastoma. Neuro Oncol. 2015;17:vii9–14.

94. Maganã-Maldonado R et al. Immunological Evasion in Glioblastoma. Biomed Res Int. 2016;2016:1–7.

95. Fecci PE et al. Increased regulatory T-cell fraction amidst a diminished CD4 compartment explains cellular immune defects in patients with malignant glioma. Cancer Res. 2006;66(6):3294–302.

96. Darrasse-Jèze G, Podsypanina K. How numbers, nature, and immune status of Foxp3+ regulatory T-cells shape the early immunological events in tumor development. Front Immunol. 2013;4(292):1–11.

97. Tomaszewski W et al. Brain Tumor Micro-environment and Host State - Implications for Immunotherapy. Clin Cancer Res. 2019;25(14):4202–10.

98. Jordan JT et al. Preferential migration of regulatory T cells mediated by glioma-secreted chemokines can be blocked with chemotherapy. Cancer Immunol Immunother. 2008;57(1):123–31.

99. Crane CA et al. Soluble factors secreted by glioblastoma cell lines facilitate recruitment, survival, and expansion of regulatory T cells: implications for immunotherapy. Neuro Oncol. 2012;14(5):584–95.

100. Reardon DA et al. Immunotherapy advances for glioblastoma. Neuro Oncol. 2014;16(11):1441–58.

101. Berghoff AS et al. Programmed death ligand 1 expression and tumor-infiltrating lymphocytes in glioblastoma. Neuro Oncol. 2015;17(8):1064–75.

102. Yue Q et al. The prognostic value of Foxp3+ tumor-infiltrating lymphocytes in patients with glioblastoma. J Neurooncol. 2014;116(2):251–9.

103. Han S et al. Tumour-infiltrating CD4 + and CD8 + lymphocytes as predictors of clinical outcome in glioma. Br J Cancer. 2014;110(10):2560–8.

104. Wei B et al. The upregulation of programmed death 1 on peripheral blood T cells of glioma is correlated with disease progression. Tumor Biol. 2014;35(4):2923–9.

105. Xue S et al. The prognostic significance of PD-L1 expression in patients with glioma: A meta-analysis. Sci Rep. 2017;7(4231):1–8.

106. Munoz L et al. Oncogenic Ras modulates p38 MAPK-mediated inflammatory cytokine production in glioblastoma cells. Cancer Biol Ther. 2016;17(4):355–63.

107. Grivennikov SI, Karin M. Inflammatory cytokines in cancer: Tumour necrosis factor and interleukin 6 take the stage. Ann Rheum Dis. 2011;70(1):104–8.

108. Zhu VF et al. Understanding the role of cytokines in Glioblastoma Multiforme pathogenesis. Cancer Lett. 2012;316(2):139–50.

109. Alfaro C et al. Interleukin-8 in cancer pathogenesis, treatment and follow-up. Cancer Treat Rev. 2017;60:24–31.

110. Lin W et al. A cytokine-mediated link between innate immunity , inflammation , and cancer. J Clin Invest. 2007;117(5):1175–83.

111. Fisher DT et al. The Two Faces of IL-6 in the Tumor Microenvironment. Semin Immunol. 2014;26(1):38–47.

112. Yeo AT, Charest A. Immune Checkpoint Blockade Biology in Mouse Models of Glioblastoma. J Cell Biochem. 2017;118(9):2516–27.

113. Tan AC, Heimberger AB, Khasraw M. Immune Checkpoint Inhibitors in Gliomas. Curr Oncol Rep. 2017;19(4).

114. Filley AC et al. Recurrent glioma clinical trial, CheckMate-143: the game is not over yet. Oncotarget. 2017;8(53):91779–94.

115. Livak KJ, Schmittgen TD. Analysis of relative gene expression data using real-time quantitative PCR and the 2-ΔΔCT method. Methods. 2001;25(4):402–8.

116. Yeung YT et al. Interleukins in glioblastoma pathophysiology: Implications for therapy. Br J Pharmacol. 2013;168(3):591–606.

117. Camarillo C et al. Comparison of microarray and quantitative real-time PCR methods for measuring microRNA levels in MSC cultures. Methods Mol Biol. 2011;698(8):419–29.

118. Kjartansdóttir KR et al. A combination of culture conditions and gene expression analysis can be used to investigate and predict hES cell differentiation potential towards male gonadal cells. PLoS One. 2015;10(12):1–23.

119. Kousidou OC et al. Expression of MMPs and TIMPs genes in human breast cancer epithelial cells depends on cell culture conditions and is associated with their invasive potential. Anticancer Res. 2004;24(6):4025–30.

120. Anaka M et al. Brief report: Stem cell media culture of melanoma results in the induction of a nonrepresentative neural expression profile. Stem Cells. 2012;30(2):336–43.

121. Kore RA, Abraham EC. Inflammatory cytokines, interleukin-1 beta and tumor necrosis factor-alpha, upregulated in glioblastoma multiforme, raise the levels of CRYAB in exosomes secreted by U373 glioma cells. Biochem Biophys Res Commun. 2014;453(3):326–31.

122. Qian J et al. The IFN-γ/PD-L1 axis between T cells and tumor microenvironment: Hints for glioma anti-PD-1/PD-L1 therapy. J Neuroinflammation. 2018;15(290):1–13.

123. Yao H et al. Cancer Cell-Intrinsic PD-1 and Implications in Combinatorial Immunotherapy. Front Immunol. 2018;9(1774):1–7.

124. Havel JJ et al. The evolving landscape of biomarkers for checkpoint inhibitor immunotherapy. Nat Rev Cancer. 2019;19(3):133–50.

125. Yi M et al. Biomarkers for predicting efficacy of PD-1/PD-L1 inhibitors. Mol Cancer. 2018;17(129):1–14.

126. Pross S and, Lefkowitz D. Cell-Mediated Immunity. In: Psychoneuroimmunology. 2007. p. 1–4.

127. C.M. N et al. Anti-CD3-Induced T-cell Activation in vivo - Flow Cytometric Analysis of Dose-Responsive , Time-Dependent, and Cyclosporin A-Sensitive Parameters of CD4+ and CD8+ Cells from the Draining Lymph nodes of C57B1/6 Mice. Int J bnmunopharmac. 1992;14(7):1295–304.

128. Glauben L et al. Chronic inflammation and cytokines in the tumor microenvironment. J Immunol Res. 2014;2014:1–14.

129. Noel PJ et al. CD28 costimulation prevents cell death during primary T cell activation. J Immunol. 1996;157(2):636–42.

130. Inui K et al. Effects of beta mercaptoethanol on the proliferation and differentiation of human osteoprogenitor cells. Cell Biol Int. 1997;21(7):419–25.

131. Kohlmeier JE et al. Costimulation of naive human CD4+ T cells through intercellular adhesion molecule-1 promotes differentiation to a memory phenotype that is not strictly the result of multiple rounds of cell division. Immunology. 2006;118(4):549–58.

132. Phillips NE et al. Costimulatory blockade induces hyporesponsiveness in T cells that recognize alloantigen via indirect antigen presentation. Transplantation. 2006;82(8):1085–92.

133. Overgaard NH et al. CD4 + /CD8 + double-positive T cells: more than just a developmental stage? J Leukoc Biol. 2015;97(1):31–8.

134. Ray S et al. Treatment Patterns, Survival, and Healthcare Costs of Patients with Malignant Gliomas in a Large US Commercially Insured Population. Am Heal Drug Benefits. 2014;7(3):140–9.

135. Broekman ML et al. Multidimensional communication in the microenvirons of glioblastoma. Nat Rev Neurol. 2018;14:1–14.

136. Tarassishin L et al. Aberrant expression of interleukin-1β and inflammasome activation in human malignant gliomas. PLoS One. 2014;9(7):1–14.

137. Han J et al. TGF-β signaling and its targeting for glioma treatment. Am J Cancer Res. 2015;5(3):945–55.

138. Jackson C et al. Challenges in immunotherapy presented by the glioblastoma multiforme microenvironment. Clin Dev Immunol. 2011;2011:1–10.

139. Crespo J et al. T cell anergy, exhaustion, senescence and stemness in the tumor microenvironment. Curr Opin Immunol. 2013;25(2):214–21.

140. Cao M et al. Hepatocellular carcinoma cell supernatants increase expansion and function of CD4+CD25+ regulatory T cells. Lab Investig. 2007;87(6):582–90.

141. Wei J et al. Glioblastoma cancer-initiating cells inhibit T cell proliferation and effector responses by the STAT3 pathway. Mol Cancer Ther. 2010;9(1):67–78.

142. Mangani D et al. The network of immunosuppressive pathways in glioblastoma. Biochem Pharmacol. 2016;130:1–9.

143. Flies DB, Chen L. Modulation of immune response by B7 family molecules in tumor microenvironments. Immunol Invest. 2006;35:395–418.

144. Foreman KE et al. Expression of Costimulatory Molecules CD80 and / or CD86 by a Kaposi ' s Sarcoma Tumor Cell Line Induces Differential T-cell Activation and Proliferation. Clin Immunol. 1999;91(3):345–53.

145. Wang Z liang et al. PD-L2 expression is correlated with the molecular and clinical features of glioma, and acts as an unfavorable prognostic factor. Oncoimmunology. 2019;8(2):1–9.

146. Abusamra A et al. Tumor exosomes expressing Fas ligand mediate CD8+ T-cell apoptosis. Blood Cells, Mol Dis. 2005;35(2):169–73.

147. Ricklefs FL. Immune evasion mediated by PD-L1 on glioblastoma-derived extracellular vesicles. Sci Adv. 2018;4(3):1–14.

148. Kaplanov I et al. Blocking IL-1β reverses the immunosuppression in mouse breast cancer and synergizes with anti–PD-1 for tumor abrogation. Proc Natl Acad Sci. 2018;116(4):1–9.

149. Garg AD et al. Preclinical efficacy of immune-checkpoint monotherapy does not recapitulate corresponding biomarkers-based clinical predictions in glioblastoma. Oncoimmunology. 2017;6(4):1–13.

150. Sasidharan Nair V, Elkord E. Immune checkpoint inhibitors in cancer therapy: A focus on T-regulatory cells. Immunol Cell Biol. 2018;96(1):21–33.

151. Zhu J et al. Apoptosis of tumor-infiltrating T lymphocytes: a new immune checkpoint mechanism. Cancer Immunol Immunother. 2018;68(5):835–47.

152. Rosignoli G et al. Programmed death (PD)-1 molecule and its ligand PD-L1 distribution among memory CD4 and CD8 T cell subsets in human immunodeficiency virus-1-infected individuals. Clin Exp Immunol. 2009;157(1):90–7.

153. Bennett F et al. Program Death-1 Engagement Upon TCR Activation Has Distinct Effects on Costimulation and Cytokine-Driven Proliferation: Attenuation of ICOS, IL-4, and IL-21, But Not CD28, IL-7, and IL-15 Responses. J Immunol. 2003;170(2):711–8.

154. Park J et al. Effect of combined anti-PD-1 and temozolomide therapy in glioblastoma. Oncoimmunology. 2018;8(1):1–11.

155. Rotte A. Combination of CTLA-4 and PD-1 blockers for treatment of cancer. J Exp Clin Cancer Res. 2019;38(255):1–12.

156. Das R et al. Combination therapy with anti-CTLA4 and anti-PD1 leads to distinct immunologic changes in-vivo. J Immunol. 2015;194(3):950–9.

157. Chae YK et al. Current landscape and future of dual anti-CTLA4 and PD-1/PD-L1 blockade immunotherapy in cancer; lessons learned from clinical trials with melanoma and non-small cell lung cancer (NSCLC). J Immunother Cancer. 2018;6(39):1–27.

158. Wolchok JD et al. Safety and clinical activity of combined PD-1 (nivolumab) and CTLA-4 (ipilimumab) blockade in advanced melanoma patients. N Engl J Med July. 2013;369(2):122–33.

159. Sharpe AH, Pauken KE. The diverse functions of the PD1 inhibitory pathway. Nat Rev Immunol. 2018;18(3):153–67.

160. Choi Y et al. Studying cancer immunotherapy using patient-derived xenografts (PDXs) in humanized mice. Exp Mol Med. 2018;50(99):1–9.

161. Gammelgaard OL et al. Human cancer evolution in the context of a human immune system in mice. Mol Oncol. 2018;12:1797–810.

162. Brehm MA et al. Overcoming Current Limitations in Humanized Mouse Research. J Infect Dis. 2013;208(suppl_2):S125–30.

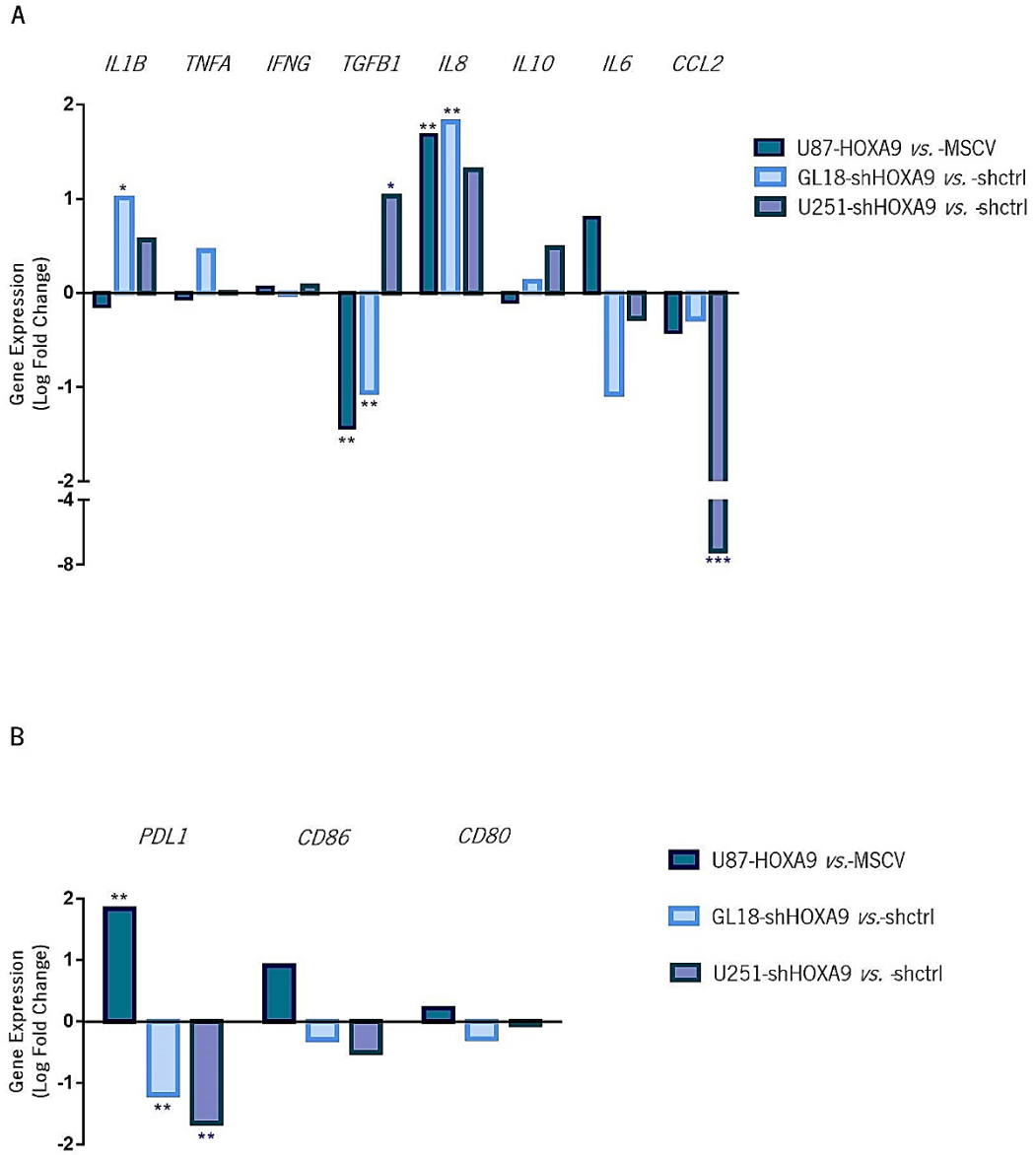

Supplementary figure 1 – Microarray data, regarding immune-related genes validated by RT-qPCR: cytokines, chemokines and immune checkpoint ligands. A) Expression of cytokines and chemokines: *IL1B*; *TNFA*; *IFNG*; *TGFB1*; *IL8*; *IL10*; *IL6* and *CCL2*. **B)** Expression of immune checkpoint ligands: *PDL1* (PD1 ligand) and *CD86* and *CD80* (CTLA4 ligands). The depicted data is from Pojo M. *et al.*, 2015 (46), but was analysed in the context of this thesis to evaluate the gene expression of these cytokines, chemokines and immune checkpoint ligands.

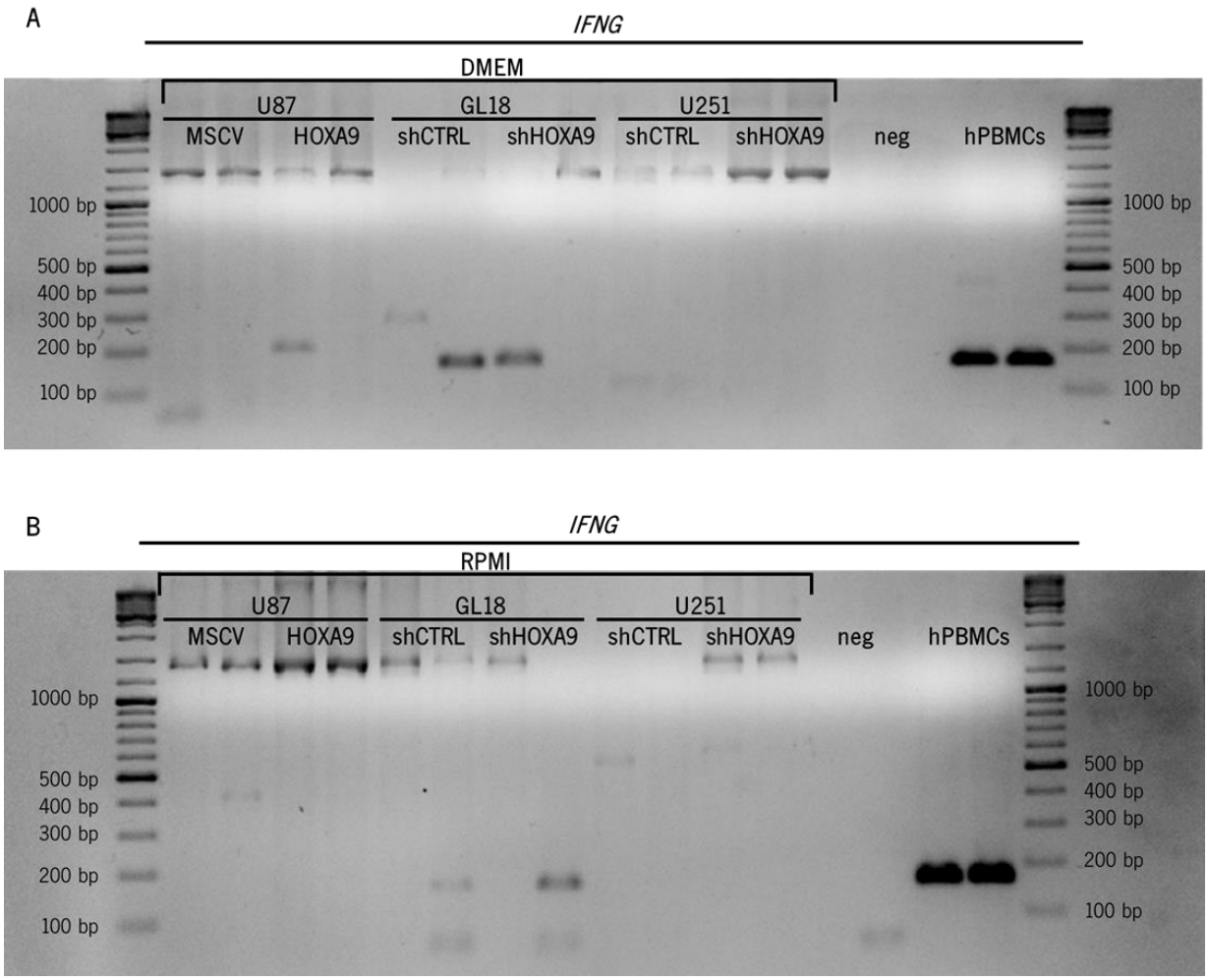

Supplementary figure 2 – *IFNG* is not detected in human GBM cell lines. Represented the agarose gel from expression of *IFNG* in human GBM cell lines cultured in **A)** DMEM and **B)** in RPMI; analysed by RT-qPCR. These human GBM cell lines were considered as negative for *IFNG* expression since the RT-qPCR was contaminated by several unspecific links, besides the presence of bands of interest, make it not possible to quantify the expression of *IFNG* in these cell lines. hPBMCs – positive control; neg – negative control for the RT-qPCR reaction (RT-qPCR mix without cDNA).

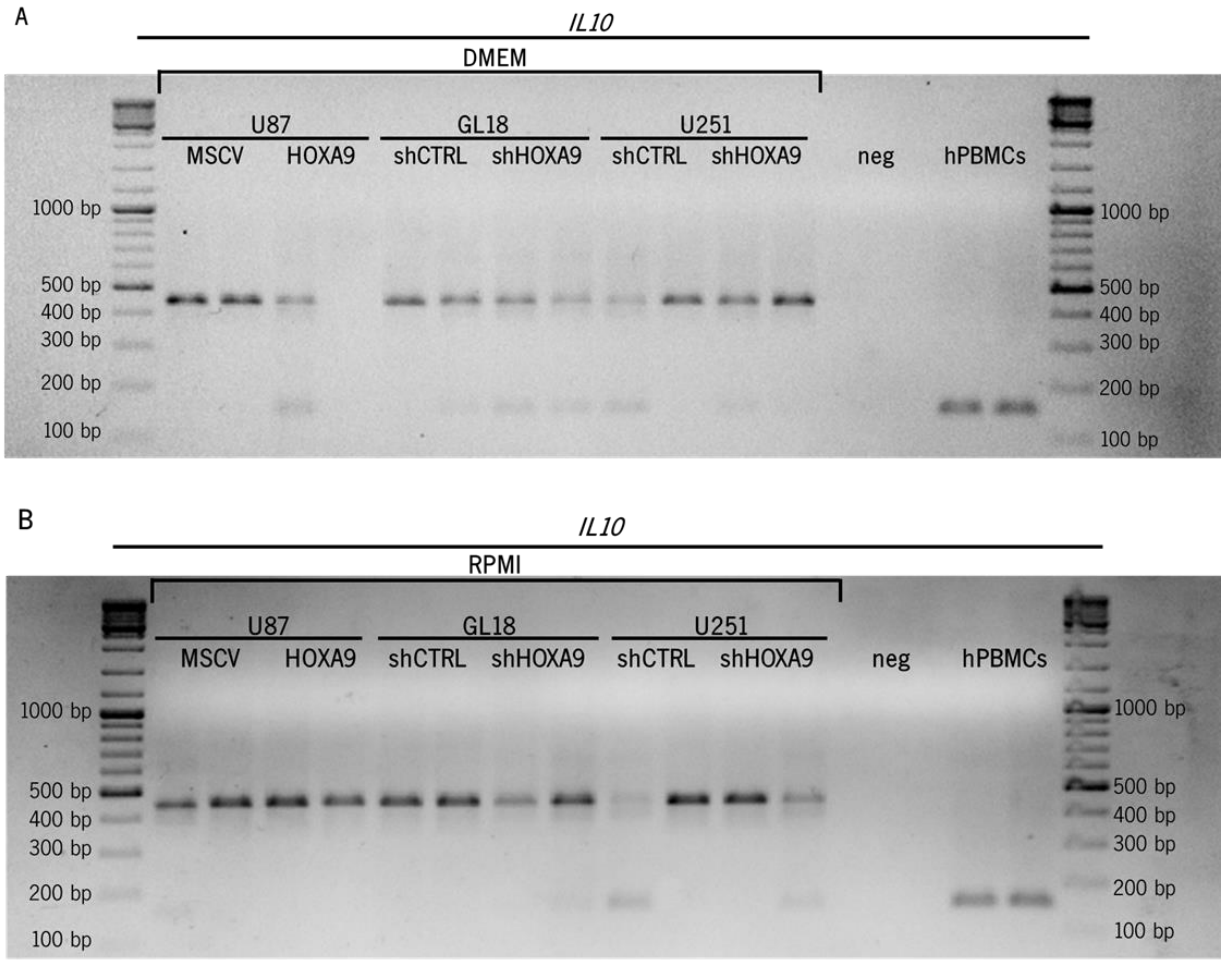

Supplementary figure 3 – *IL10* is not detected in human GBM cell lines. Represented the agarose gel from expression of *IL10* in human GBM cell lines cultured in **A)** DMEM and **B)** in RPMI; analysed by RT-qPCR. These human GBM cell lines were considered as negative for *IL10* expression since the RT-qPCR was contaminated by several unspecific links, besides the presence of bands of interest, make it not possible to quantify the expression of *IL10* in these cell lines. hPBMCs – positive control; neg – negative control for the RT-qPCR reaction (RT-qPCR mix without cDNA).

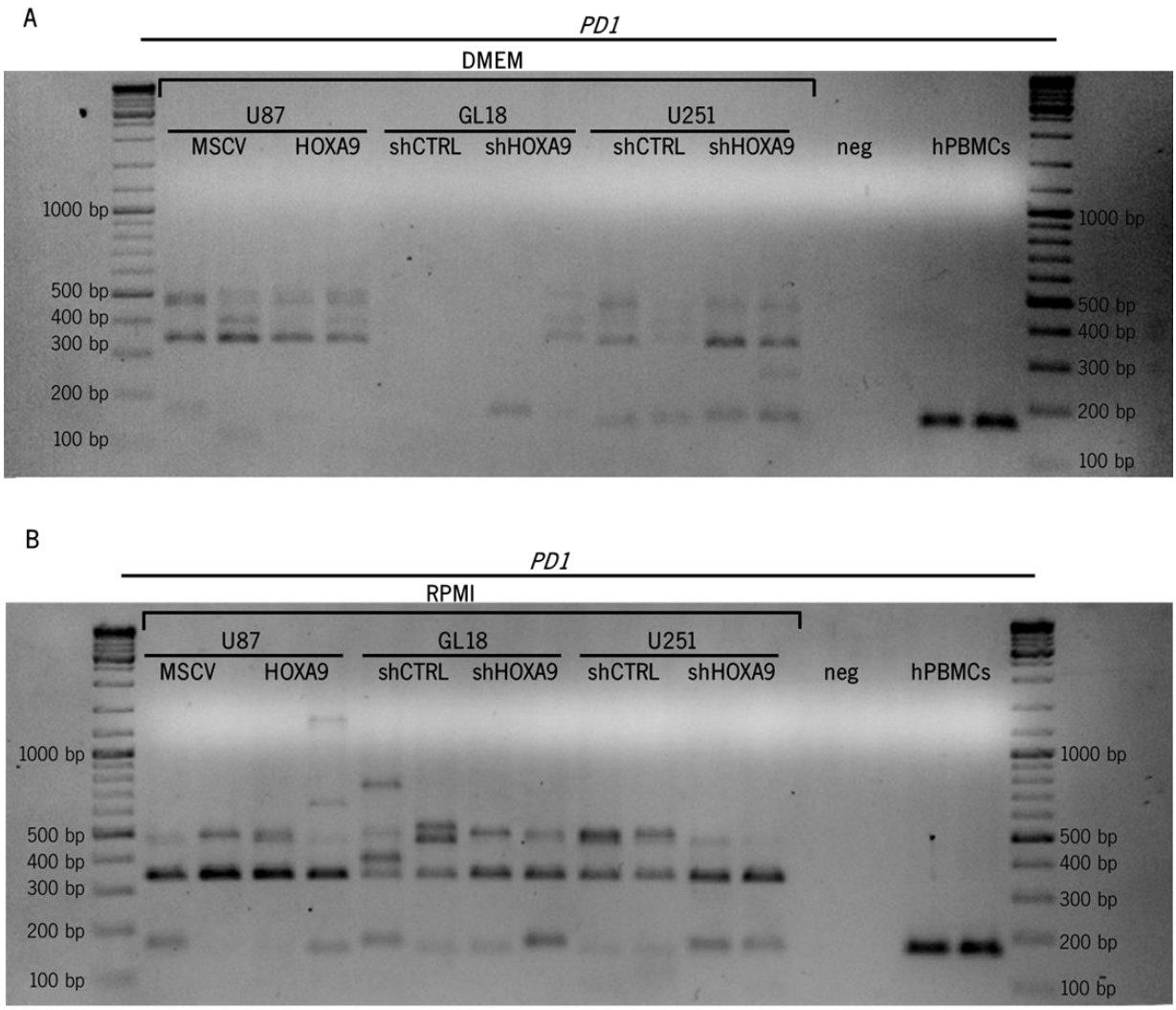

Supplementary figure 4 – *PD1* is not detected in human GBM cell lines. Represented the agarose gel from expression of *PD1* in human GBM cell lines cultured in **A)** DMEM and **B)** in RPMI; analysed by RT-qPCR. These human GBM cell lines were considered as negative for *PD1* expression since the RT-qPCR was contaminated by several unspecific links, besides the presence of bands of interest, make it not possible to quantify the expression of *PD1* in these cell lines. hPBMCs – positive control; neg – negative control for the RT-qPCR reaction (RT-qPCR mix without cDNA).

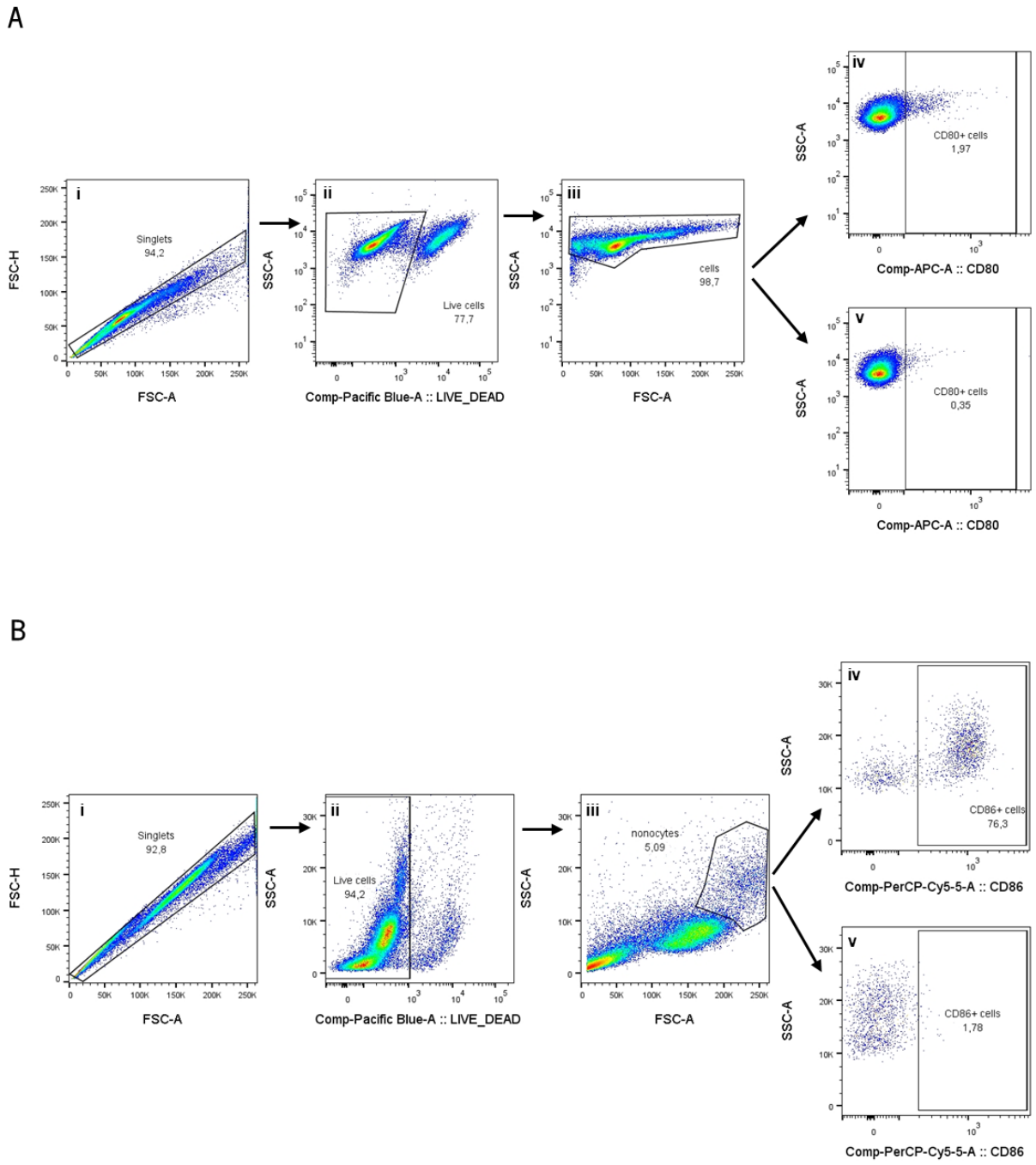

Supplementary figure 5 – Positive controls for staining with CD80 and CD86. A) CD80 positive control: activated T-cells were stained with CD80 antibody, according to surface stain for flow cytometry. **B)** CD86 positive control: fresh hPBMCs were stained with CD86 antibody, according to surface stain for flow cytometry. **A-B)** The doublets were excluded (i) and the live cells (ii) and the population of cells of interest were selected (iii). Lastly, was selected the population of cells positive for CD80 or CD86 (iv). (v) Represents the FMO (fluorescence minus one) of each antibody.

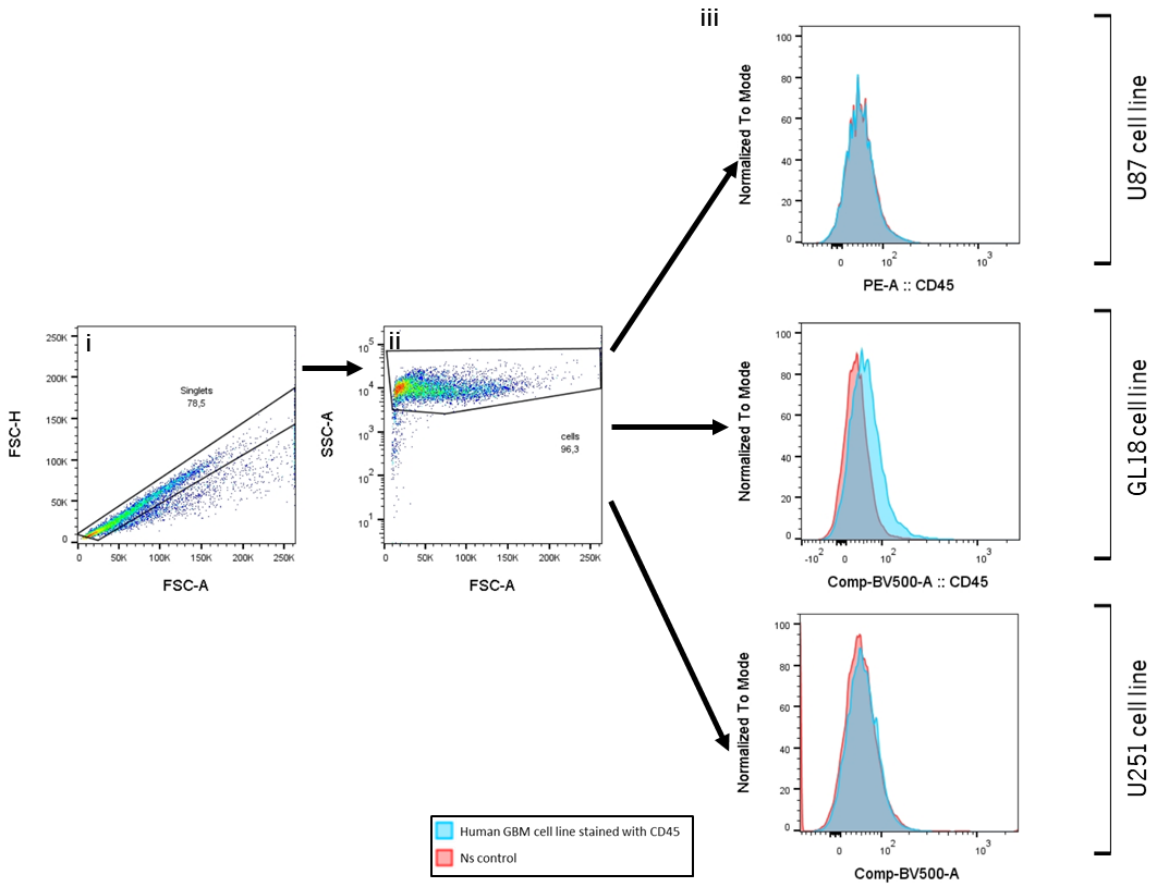

Supplementary figure 6 – Expression of CD45 in human GBM cell lines. The doublets were first excluded (i) and then selected the cell population of interest (ii). Histograms with the expression of CD45 in each human GBM cell line (U87, GL18 and U251 cell lines) are depicted (iii). Blue histograms represent the human GBM cell line stained with CD45 and the red histograms represent the non-stain (ns) control.

Supplementary Table 1 – Primers used for RT-qPCR, with the respective Tm and the length of the products.

	Gene	Primers	Primer Tm (°C)	Products lenght (bp)
Human genes	*IL1B**	Fwd (5'-3'): GCATCCAGCTACGAATCTCC Rv (3'-5'): TCGTTATCCCATGTGTCGAA	61 (power up) / 60 (Sybr green)	193/450
	*TNF**	Fwd (5'-3'): CGCTCCCCAAGAAGACAG Rv (3'-5'): GCCAGAGGGCTGATTAGAGA	61 (Power up) / 60 (Sybr green)	175
	*IFNG**	Fwd (5'-3'): GGCTTAATTCTCTCGGAAACG Rv (3'-5'): TCCGCTACATCTGAATGACCT	60 (Sybr green)	161
	*TGFB1**	Fwd (5'-3'): TCCTGTGACAGCAGGGATAA Rv (3'-5'): TGAAGCAATAGTTGGTGTCCA	59 (Sybr green)	190
	*IL8**	Fwd (5'-3'): AAGACATACTCCAAACCTTTCCA Rv (3'-5'): ACTTCTCCACAACCCTCTGC	59 (Sybr green)	163
	IL10	Fwd (5'-3'): CCAAGCTGAGAACCAAGACC Rv (3'-5'): AAGGCATTCTTCACCTGCTC	61 (Power up)	150
	IL6	Fwd (5'-3'): AAAGAGGCACTGGCAGAAAA Rv (3'-5'): AGCTCTGGCTTGTTCCTCAC	62 (Sybr green)	183
	CCL2	Fwd (5'-3'): TCTGTGCCTGCTGCTCATAG Rv (3'-5'): GCTTCTTTGGGACACTTGCT	60 (Sybr green)	168
	*CD86**	Fwd (5'-3'): GACGCGGCTTTTATCTTCAC Rv (3'-5'): GGTTGCCCAGGAACTTACAA	60 (Sybr green)	386/242
	*CD80**	Fwd (5'-3'): TCCATTGTGATCCTGGCTCT Rv (3'-5'): TTTTCCAACCAGGAGAGGTG	61 (Sybr green)	236
	*PDL1**	Fwd (5'-3'): CGAAGTCATCTGGACAAGCA Rv (3'-5'): ATTTGGAGGATGTGCCAGAG	61 (Power up) / 60 (Sybr green)	220/114
	*PD1**	Fwd (5'-3'): CTGGGCGGTGCTACAACT Rv (3'-5'): ACGAAGCTCTCCGATGTGTT	60 (Sybr green)	159
	HOXA9	Fwd (5'-3'): GCCCGTGCAGCTTCCAGTCC Rv (3'-5'): GAGCGCGCATGAAGCCAGTTG	61 (Sybr green)	287/460
	TBP	Fwd (5'-3'): GAGCTGTGATGTGAAGTTTCC Rv (3'-5'): TCTGGGTTTGATCATTCTGTAG	60 (Sybr green)	79/118
Mouse genes	*Hoxa9*	Fwd (5'-3'): ATCCTGCGGTTCTGGAACCAGATC Rv (3'-5'): CGCTGGAACTGGAGAAGGAGTTTCTG	60 (Sybr green)	124
	Tbp	Fwd (5'-3'): GGGAGAATCATGGACCAGAA Rv (3'-5'): TTGCTGCTGCTGTCTTTGTT	55 (Sybr green)	192

* Primers designed and optimized in the context of this thesis

Supplementary Table 2 – Antibodies panel for the molecular analysis by Flow Cytometry.

Antibody/ Dye	Fluorocrome	Clone	Dilution *	Company	Target specie	Target cells
Ann	Alexa Fluor 647	-	1/25	BioLegend	Human/ Mouse	Apoptotic cells
CD3	PB	OKT3	1/200	BioLegend	Human	T-cells
CD3	BV605	145-2C11	1/100	BioLegend	Mouse	T-cells
CD4	APC-Cy7	RPA-T4	1/100	BioLegend	Human	CD4 T-cells
CD4	APC-Cy7	RM4-5	1/100	BioLegend	Mouse	CD4 T-cells
CD8	PeCy7	RPA-T8	1/200	BioLegend	Human	CD8 T-cells
CD8	FITC	53-6.7	1/100	BioLegend	Mouse	CD8 T-cells
CD25	APC	BC96	1/66.67	BioLegend	Human	Treg cells
CD44	PeCy7	IM7	1/400	BioLegend	Mouse	Activated T-cells
CD45	BV510	HI30	1/66.67	BioLegend	Human	Leukocytes
CD45	PeCy7	I3/2.3	1/100	BioLegend	Mouse	Leukocytes
CD62L	PercPCy5.5	MEL-14	1/100	BioLegend	Mouse	Naïve T-cells
CD69	BV650	H1.2F3	1/100	BioLegend	Mouse	Activated T-cells
CD80	Alexa Fluor 647	2D10	1/100 **	BioLegend	Human	Tumour cells
CD86	Percp/Cy5.5	IT2.2	1/20 **	BioLegend	Human	Tumour cells
CD127	PercPCy5.5	AO19D5	1/20	BioLegend	Human	Treg cells
FOXP3	Pe	PCH101	1/66.67	eBiosciences	Human	
Live/Dead	Pacific Blue	-	1/1000	eBiosciences	Human	Live tumour cells
Live/Dead	FITC	-	1/1000	Invitrogen	Human	Live Leukocytes
Live/Dead	eFluor660	-	1/1000	eBiosciences	Mouse	Live T-cells
PD1	BV785	29F.1A12	1/100	BioLegend	Mouse	Activated/ Exhausted T-cells
PDL1	APC	29E.2A3	1/100 **	BioLegend	Human	Tumour cells
PDL2	PE	MIH18	1/20 **	BioLegend	Human	Tumour cells
PI	PercPCy5.5	-	1/50	Sigma	Human/ Mouse	Dead cells

* The optimal concentration of each antibody was determined by testing serial dilutions

** Antibodies titrated in the context of this thesis

Supplementary Table 3 – Relative expression of *IL1B* in human GBM cell lines, obtained by RT-qPCR.

	IL1B					
	Cell line	Relative expression (mean) *	Cell line	Relative expression (mean) *	Cell line	Relative expression (mean) *
DMEM	U87-MSCV n1	512,3810	GL18 shCTRL n1	0,8275	U251 shCTRL n1	0,0001
	U87-HOXA9 n1	9,7822	GL18 shHOXA9 n1	1,5542	U251 shHOXA9 n1	0,0005
	U87-MSCV n2	212,3529	GL18 shCTRL n2	0,0750	U251 shCTRL n2	0,0023
	U87-HOXA9 n2	30,1497	GL18 shHOXA9 n2	0,1655	U251 shHOXA9 n2	0,0020
	U87-MSCV n3	19,8763	GL18 shCTRL n3	0,0470	U251 shCTRL n3	0,0307
	U87-HOXA9 n3	15,6888	GL18 shHOXA9 n3	0,3300	U251 shHOXA9 n3	0,0745
RPMI	U87-MSCV n1	4800,2401	GL18 shCTRL n1	0,7842	U251 shCTRL n1	0,0021
	U87-HOXA9 n1	160,3304	GL18 shHOXA9 n1	3,8816	U251 shHOXA9 n1	1,2195
	U87-MSCV n2	826,3668	GL18 shCTRL n2	0,0134	U251 shCTRL n2	0,0003
	U87-HOXA9 n2	155,9087	GL18 shHOXA9 n2	0,4911	U251 shHOXA9 n2	0,0003
	U87-MSCV n3	51,8501	GL18 shCTRL n3	0,7541	U251 shCTRL n3	0,0002
	U87-HOXA9 n3	17,6293	GL18 shHOXA9 n3	18,2183	U251 shHOXA9 n3	0,0007

* The relative expression of *IL1B* was calculated to the housekeeping, *TBP*, of mean of two replicates for each cell line (in each RT-qPCR run). Data was analysed using the ΔΔCT method.

Supplementary Table 4 – Relative expression of *TNFA* in human GBM cell lines, obtained by RT-qPCR.

	TNFA					
	Cell line	Relative expression (mean) *	Cell line	Relative expression (mean) *	Cell line	Relative expression (mean) *
DMEM	U87-MSCV n1	0,2222	GL18 shCTRL n1	0,0026	U251 shCTRL n1	0,0089
	U87-HOXA9 n1	0,2811	GL18 shHOXA9 n1	0,0282	U251 shHOXA9 n1	0,0453
	U87-MSCV n2	0,1336	GL18 shCTRL n2	0,0623	U251 shCTRL n2	0,2008
	U87-HOXA9 n2	0,1956	GL18 shHOXA9 n2	0,1250	U251 shHOXA9 n2	0,1541
	U87-MSCV n3	0,2830	GL18 shCTRL n3	0,0564	U251 shCTRL n3	0,0513
	U87-HOXA9 n3	0,2160	GL18 shHOXA9 n3	0,0915	U251 shHOXA9 n3	0,1061
RPMI	U87-MSCV n1	0,0131	GL18 shCTRL n1	1,6930	U251 shCTRL n1	0,0427
	U87-HOXA9 n1	0,1876	GL18 shHOXA9 n1	3,3314	U251 shHOXA9 n1	0,0293
	U87-MSCV n2	0,1989	GL18 shCTRL n2	0,9789	U251 shCTRL n2	0,0377
	U87-HOXA9 n2	0,7240	GL18 shHOXA9 n2	1,0821	U251 shHOXA9 n2	0,1317
	U87-MSCV n3	0,0000	GL18 shCTRL n3	0,4160	U251 shCTRL n3	0,1895
	U87-HOXA9 n3	0,0000	GL18 shHOXA9 n3	0,0777	U251 shHOXA9 n3	0,0794

* The relative expression of *TNFA* was calculated to the housekeeping, *TBP*; of mean of two replicates for each cell line (in each RT-qPCR run). Data was analysed using the ΔΔCT method.

Supplementary Table 5 – Relative expression of *TGFB1* in human GBM cell lines, obtained by RT-qPCR.

	TGFB1					
	Cell line	Relative expression (mean) *	Cell line	Relative expression (mean) *	Cell line	Relative expression (mean) *
DMEM	U87-MSCV n1	55,8690	GL18 shCTRL n1	218,8588	U251 shCTRL n1	556,0508
	U87-HOXA9 n1	72,4259	GL18 shHOXA9 n1	86,4537	U251 shHOXA9 n1	400,4944
	U87-MSCV n2	0,1999	GL18 shCTRL n2	268,3388	U251 shCTRL n2	381,8816
	U87-HOXA9 n2	15,7450	GL18 shHOXA9 n2	118,4317	U251 shHOXA9 n2	199,3081
	U87-MSCV n3	245,6803	GL18 shCTRL n3	130,7674	U251 shCTRL n3	513,5214
	U87-HOXA9 n3	225,4997	GL18 shHOXA9 n3	30,1859	U251 shHOXA9 n3	291,1988
RPMI	U87-MSCV n1	185,3276	GL18 shCTRL n1	2648,2155	U251 shCTRL n1	263,9032
	U87-HOXA9 n1	129,0840	GL18 shHOXA9 n1	1158,2050	U251 shHOXA9 n1	238,2167
	U87-MSCV n2	446,5905	GL18 shCTRL n2	1323,4642	U251 shCTRL n2	262,2534
	U87-HOXA9 n2	251,2615	GL18 shHOXA9 n2	639,7354	U251 shHOXA9 n2	466,0725
	U87-MSCV n3	138,1325	GL18 shCTRL n3	148,9678	U251 shCTRL n3	177,4509
	U87-HOXA9 n3	147,0916	GL18 shHOXA9 n3	126,5757	U251 shHOXA9 n3	142,6822

* The relative expression of *TGFB1* was calculated to the housekeeping, *TBP*, of mean of two replicates for each cell line (in each RT-qPCR run). Data was analysed using the ΔΔCT method.

Supplementary Table 6 – Relative expression of *IL8* in human GBM cell lines, obtained by RT-qPCR.

	IL8					
	Cell line	Relative expression (mean) *	Cell line	Relative expression (mean) *	Cell line	Relative expression (mean) *
DMEM	U87-MSCV n1	5,2582	GL18 shCTRL n1	0,4832	U251 shCTRL n1	40,7734
	U87-HOXA9 n1	40,3381	GL18 shHOXA9 n1	19,9444	U251 shHOXA9 n1	50,9339
	U87-MSCV n2	25,9754	GL18 shCTRL n2	4,5975	U251 shCTRL n2	63,2088
	U87-HOXA9 n2	46,2110	GL18 shHOXA9 n2	15,1503	U251 shHOXA9 n2	117,6907
	U87-MSCV n3	43,1707	GL18 shCTRL n3	2,3534	U251 shCTRL n3	31,7151
	U87-HOXA9 n3	12,8176	GL18 shHOXA9 n3	11,5384	U251 shHOXA9 n3	65,2235
RPMI	U87-MSCV n1	1676,6417	GL18 shCTRL n1	16,7185	U251 shCTRL n1	11,9946
	U87-HOXA9 n1	33,4048	GL18 shHOXA9 n1	89,2062	U251 shHOXA9 n1	21,4820
	U87-MSCV n2	66,2045	GL18 shCTRL n2	7,0840	U251 shCTRL n2	0,6324
	U87-HOXA9 n2	59,2547	GL18 shHOXA9 n2	110,9753	U251 shHOXA9 n2	10,3665
	U87-MSCV n3	197,2628	GL18 shCTRL n3	0,8098	U251 shCTRL n3	0,3015
	U87-HOXA9 n3	62,3712	GL18 shHOXA9 n3	10,7490	U251 shHOXA9 n3	7,8129

* The relative expression of *IL8* was calculated to the housekeeping, *TBP*, of mean of two replicates for each cell line (in each RT-qPCR run). Data was analysed using the ΔΔCT method.

Supplementary Table 7 – Relative expression of *IL6* in human GBM cell lines, obtained by RT-qPCR.

	IL6					
	Cell line	Relative expression (mean) *	Cell line	Relative expression (mean) *	Cell line	Relative expression (mean) *
DMEM	U87-MSCV n1	3,6587	GL18 shCTRL n1	4,4565	U251 shCTRL n1	22,0209
	U87-HOXA9 n1	7,7230	GL18 shHOXA9 n1	1,8013	U251 shHOXA9 n1	11,7851
	U87-MSCV n2	1,9606	GL18 shCTRL n2	9,6027	U251 shCTRL n2	47,6981
	U87-HOXA9 n2	4,5474	GL18 shHOXA9 n2	1,6878	U251 shHOXA9 n2	17,0805
	U87-MSCV n3	5,4080	GL18 shCTRL n3	40,3203	U251 shCTRL n3	35,9439
	U87-HOXA9 n3	4,4194	GL18 shHOXA9 n3	4,9532	U251 shHOXA9 n3	34,6002
RPMI	U87-MSCV n1	98,9657	GL18 shCTRL n1	30,9994	U251 shCTRL n1	41,3943
	U87-HOXA9 n1	3,6398	GL18 shHOXA9 n1	33,8564	U251 shHOXA9 n1	43,8977
	U87-MSCV n2	10,4030	GL18 shCTRL n2	11,7847	U251 shCTRL n2	371,9421
	U87-HOXA9 n2	7,8643	GL18 shHOXA9 n2	22,2086	U251 shHOXA9 n2	208,8221
	U87-MSCV n3	7,8480	GL18 shCTRL n3	8,1334	U251 shCTRL n3	45,5510
	U87-HOXA9 n3	7,2634	GL18 shHOXA9 n3	11,5056	U251 shHOXA9 n3	42,5969

* The relative expression of *IL6* was calculated to the housekeeping, *TBP*, of mean of two replicates for each cell line (in each RT-qPCR run). Data was analysed using the ΔΔCT method.

Supplementary Table 8 – Relative expression of *CCL2* in human GBM cell lines, obtained by RT-qPCR.

	CCL2					
	Cell line	Relative expression (mean) *	Cell line	Relative expression (mean) *	Cell line	Relative expression (mean) *
DMEM	U87-MSCV n1	0,1084	GL18 shCTRL n1	663,5991	U251 shCTRL n1	353,5291
	U87-HOXA9 n1	0,1860	GL18 shHOXA9 n1	468,1603	U251 shHOXA9 n1	2,2745
	U87-MSCV n2	1,0489	GL18 shCTRL n2	508,8620	U251 shCTRL n2	402,3533
	U87-HOXA9 n2	1,7191	GL18 shHOXA9 n2	499,9657	U251 shHOXA9 n2	0,1382
	U87-MSCV n3	1,5576	GL18 shCTRL n3	606,3777	U251 shCTRL n3	1368,9377
	U87-HOXA9 n3	1,0951	GL18 shHOXA9 n3	346,0662	U251 shHOXA9 n3	0,2527
RPMI	U87-MSCV n1	0,1793	GL18 shCTRL n1	2240,2501	U251 shCTRL n1	550,5472
	U87-HOXA9 n1	0,2696	GL18 shHOXA9 n1	3013,6980	U251 shHOXA9 n1	0,0133
	U87-MSCV n2	0,1339	GL18 shCTRL n2	1012,0365	U251 shCTRL n2	100,4201
	U87-HOXA9 n2	0,8123	GL18 shHOXA9 n2	3840,2427	U251 shHOXA9 n2	0,0080
	U87-MSCV n3	0,1289	GL18 shCTRL n3	113,8565	U251 shCTRL n3	15,3361
	U87-HOXA9 n3	0,2121	GL18 shHOXA9 n3	351,9632	U251 shHOXA9 n3	0,0196

* The relative expression of *CCL2* was calculated to the housekeeping, *TBP*, of mean of two replicates for each cell line (in each RT-qPCR run). Data was analysed using the ΔΔCT method.

Supplementary Table 9 – Relative expression of *CD86* in human GBM cell lines, obtained by RT-qPCR.

	CD86					
	Cell line	Relative expression (mean) *	Cell line	Relative expression (mean) *	Cell line	Relative expression (mean) *
DMEM	U87-MSCV n1	0,0095	GL18 shCTRL n1	0,0001	U251 shCTRL n1	0,2167
	U87-HOXA9 n1	0,0213	GL18 shHOXA9 n1	0,0080	U251 shHOXA9 n1	0,2009
	U87-MSCV n2	0,0060	GL18 shCTRL n2	0,0004	U251 shCTRL n2	0,3065
	U87-HOXA9 n2	0,1231	GL18 shHOXA9 n2	0,0179	U251 shHOXA9 n2	0,1943
	U87-MSCV n3	0,0124	GL18 shCTRL n3	0,0056	U251 shCTRL n3	0,0495
	U87-HOXA9 n3	0,0411	GL18 shHOXA9 n3	0,0072	U251 shHOXA9 n3	0,0001
RPMI	U87-MSCV n1	0,0003	GL18 shCTRL n1	0,1719	U251 shCTRL n1	0,1378
	U87-HOXA9 n1	0,0434	GL18 shHOXA9 n1	0,0623	U251 shHOXA9 n1	0,0625
	U87-MSCV n2	0,0141	GL18 shCTRL n2	0,1964	U251 shCTRL n2	0,1076
	U87-HOXA9 n2	0,0999	GL18 shHOXA9 n2	0,0258	U251 shHOXA9 n2	0,0006
	U87-MSCV n3	0,0108	GL18 shCTRL n3	0,7468	U251 shCTRL n3	0,1759
	U87-HOXA9 n3	0,0180	GL18 shHOXA9 n3	0,2808	U251 shHOXA9 n3	0,0741

* The relative expression of *CD86* was calculated to the housekeeping, *TBP*, of mean of two replicates for each cell line (in each RT-qPCR run). Data was analysed using the ΔΔCT method.

Supplementary Table 10 – Relative expression of *CD80* in human GBM cell lines, obtained by RT-qPCR.

	CD80					
	Cell line	Relative expression (mean) *	Cell line	Relative expression (mean) *	Cell line	Relative expression (mean) *
DMEM	U87-MSCV n1	0,2654	GL18 shCTRL n1	0,0839	U251 shCTRL n1	0,2856
	U87-HOXA9 n1	0,3652	GL18 shHOXA9 n1	0,1782	U251 shHOXA9 n1	0,8134
	U87-MSCV n2	1,3297	GL18 shCTRL n2	0,0641	U251 shCTRL n2	0,5185
	U87-HOXA9 n2	0,6888	GL18 shHOXA9 n2	0,1137	U251 shHOXA9 n2	0,6020
	U87-MSCV n3	0,1129	GL18 shCTRL n3	0,0491	U251 shCTRL n3	0,8349
	U87-HOXA9 n3	0,1306	GL18 shHOXA9 n3	0,1098	U251 shHOXA9 n3	1,1045
RPMI	U87-MSCV n1	0,3911	GL18 shCTRL n1	0,5628	U251 shCTRL n1	0,0889
	U87-HOXA9 n1	0,2481	GL18 shHOXA9 n1	0,7109	U251 shHOXA9 n1	0,1664
	U87-MSCV n2	0,8774	GL18 shCTRL n2	0,7198	U251 shCTRL n2	0,0168
	U87-HOXA9 n2	0,9787	GL18 shHOXA9 n2	1,5397	U251 shHOXA9 n2	0,0223
	U87-MSCV n3	0,1448	GL18 shCTRL n3	0,0448	U251 shCTRL n3	0,0211
	U87-HOXA9 n3	0,3376	GL18 shHOXA9 n3	0,0874	U251 shHOXA9 n3	0,0419

* The relative expression of *CD80* was calculated to the housekeeping, *TBP*, of mean of two replicates for each cell line (in each RT-qPCR run). Data was analysed using the ΔΔCT method.

Supplementary Table 11 – Relative expression of *PDL1* in human GBM cell lines, obtained by RT-qPCR.

	PDL1					
	Cell line	Relative expression (mean) *	Cell line	Relative expression (mean) *	Cell line	Relative expression (mean) *
DMEM	U87-MSCV n1	61,6605	GL18 shCTRL n1	1,9383	U251 shCTRL n1	169,4181
	U87-HOXA9 n1	12,1641	GL18 shHOXA9 n1	1,9471	U251 shHOXA9 n1	37,7729
	U87-MSCV n2	118,1688	GL18 shCTRL n2	2,0652	U251 shCTRL n2	129,2339
	U87-HOXA9 n2	58,3106	GL18 shHOXA9 n2	1,3004	U251 shHOXA9 n2	38,7149
	U87-MSCV n3	85,0455	GL18 shCTRL n3	1,6324	U251 shCTRL n3	143,5196
	U87-HOXA9 n3	91,7797	GL18 shHOXA9 n3	0,9644	U251 shHOXA9 n3	53,5191
RPMI	U87-MSCV n1	314,9402	GL18 shCTRL n1	25,2171	U251 shCTRL n1	70,2421
	U87-HOXA9 n1	70,0078	GL18 shHOXA9 n1	19,0955	U251 shHOXA9 n1	26,0853
	U87-MSCV n2	176,0820	GL18 shCTRL n2	4,7202	U251 shCTRL n2	34,3960
	U87-HOXA9 n2	135,6374	GL18 shHOXA9 n2	6,1926	U251 shHOXA9 n2	5,6675
	U87-MSCV n3	141,4902	GL18 shCTRL n3	1,8431	U251 shCTRL n3	44,6350
	U87-HOXA9 n3	107,5666	GL18 shHOXA9 n3	2,6852	U251 shHOXA9 n3	7,2520

* The relative expression of *PDL1* was calculated to the housekeeping, *TBP*, of mean of two replicates for each cell line (in each RT-qPCR run). Data was analysed using the ΔΔCT method.

Supplementary Table 12 – Mean fluorescence intensities (MFIs) of CD86 in the human GBM cell lines, obtained by flow cytometry. The fold change was not determined, when the MFI of the ns (non-stain) was equal or superior to the MFI of the samples stained. In these cases, cells were considered as negatives for this marker.

CD86					
Cell line	MFI	Cell	MFI	Cell line	MFI
U87 NS n1	33,9	GL18 NS n1	27,5	U251 NS n1	54,1
U87-MSCV n1	31,2	GL18 shCTRL n1	23,4	U251 shCTRL n1	43,4
U87-HOXA9 n1	43,3	GL18 shHOXA9 n1	38,0	U251 shHOXA9 n1	51,6
U87 NS n2	34,2	GL18 NS n2	18,4	U251 NS n2	51,2
U87-MSCV n2	30,6	GL18 shCTRL n2	27,4	U251 shCTRL n2	37,3
U87-HOXA9 n2	31,1	GL18 shHOXA9 n2	39,3	U251 shHOXA9 n2	57,7
U87 NS n3	30,8	GL18 NS n3	29,1	U251 NS n2	47,3
U87-MSCV n3	24,4	GL18 shCTRL n3	21,3	U251 shCTRL n3	29,4
U87-HOXA9 n3	28,2	GL18 shHOXA9 n3	31,7	U251 shHOXA9 n3	51,6

Supplementary Table 13 – MFIs of CD80 in the human GBM cell lines, obtained by flow cytometry. The fold change was not determined, when the MFI of the ns (non-stain) was equal or superior to the MFI of the samples stained. In these cases, cells were considered as negatives for this marker.

CD80					
Cell line	MFI	Cell line	MFI	Cell line	MFI
U87 NS n1	26,9	GL18 NS n1	33,0	U251 NS n1	37,8
U87-MSCV n1	23,8	GL18 shCTRL n1	21,8	U251 shCTRL n1	18,3
U87-HOXA9 n1	33,7	GL18 shHOXA9 n1	34,3	U251 shHOXA9 n1	25,0
U87 NS n2	27,5	GL18 NS n2	37,0	U251 NS n2	19,4
U87-MSCV n2	21,8	GL18 shCTRL n2	29,6	U251 shCTRL n2	8,5
U87-HOXA9 n2	26,8	GL18 shHOXA9 n2	48,8	U251 shHOXA9 n2	15,9
U87 NS n3	29,6	GL18 NS n3	25,1	U251 NS n3	39,3
U87-MSCV n3	22,2	GL18 shCTRL n3	35,1	U251 shCTRL n3	30,7
U87-HOXA9 n3	24,9	GL18 shHOXA9 n3	49,3	U251 shHOXA9 n3	38,3
-	-	GL18 NS n4	32,6	U251 NS n4	32,6
-	-	GL18 shCTRL n4	20,6	U251 shCTRL n4	22,9
-	-	GL18 shHOXA9 n4	36,9	U251 shHOXA9 n4	34,0

Supplementary Table 14 – MFIs of PDL1 in human GBM cell lines, obtained by flow cytometry. NS – non-stain

PDL1					
Cell line	MFI	Cell line	MFI	Cell line	MFI
U87 NS n1	26,3	GL18 NS n1	33,0	U251 NS n1	36,1
U87-MSCV n1	2409,0	GL18 shCTRL n1	131,0	U251 shCTRL n1	1555,0
U87-HOXA9 n1	1498,0	GL18 shHOXA9 n1	176,0	U251 shHOXA9 n1	898,0
U87 NS n2	27,2	GL18 NS n2	35,2	U251 NS n2	33,1
U87-MSCV n2	1174,0	GL18 shCTRL n2	124,0	U251 shCTRL n2	1117,0
U87-HOXA9 n2	1021,0	GL18 shHOXA9 n2	126,0	U251 shHOXA9 n2	644,0
U87 NS n3	26,4	GL18 NS n3	25,1	U251 NS n3	18,5
U87-MSCV n3	1062,0	GL18 shCTRL n3	375,0	U251 shCTRL n3	303,0
U87-HOXA9 n3	1004,0	GL18 shHOXA9 n3	158,0	U251 shHOXA9 n3	168,0
-	-	GL18 NS n4	30,9	-	-
-	-	GL18 shCTRL n4	122,0	-	-
-	-	GL18 shHOXA9 n4	122,0	-	-
-	-	GL18 NS n5	15,3	-	-
-	-	GL18 shCTRL n5	113,0	-	-
-	-	GL18 shHOXA9 n5	52,1	-	-

Supplementary Table 15 – MFIs of PDL2 in human GBM cell lines, obtained by flow cytometry. NS – non-stain

PDL2					
Cell line	MFI	Cell line	MFI	Cell line	MFI
U87 NS n1	39,0	GL18 NS n1	29,3	U251 NS n1	46,0
U87-MSCV n1	291,0	GL18 shCTRL n1	66,9	U251 shCTRL n1	86,1
U87-HOXA9 n1	278,0	GL18 shHOXA9 n1	88,7	U251 shHOXA9 n1	157,0
U87 NS n2	40,5	GL18 NS n2	37,8	U251 NS n2	41,1
U87-MSCV n2	214,0	GL18 shCTRL n2	29,7	U251 shCTRL n2	83,8
U87-HOXA9 n2	209,0	GL18 shHOXA9 n2	82,8	U251 shHOXA9 n2	155,0
U87 NS n3	38,7	GL18 NS n3	36,0	U251 NS n3	38,7
U87-MSCV n3	232,0	GL18 shCTRL n3	27,9	U251 shCTRL n3	102,0
U87-HOXA9 n3	148,0	GL18 shHOXA9 n3	45,7	U251 shHOXA9 n3	132,0